

COORDINATION CHEMISTRY OF NONCYCLIC AND
MACROCYCLIC THIOETHER-DIAZINE POLYDENTATE LIGANDS

CENTRE FOR NEWFOUNDLAND STUDIES

**TOTAL OF 10 PAGES ONLY
MAY BE XEROXED**

(Without Author's Permission)

LIQIN CHEN





National Library
of Canada

Acquisitions and
Bibliographic Services Branch

395 Wellington Street
Ottawa, Ontario
K1A 0N4

Bibliothèque nationale
du Canada

Direction des acquisitions et
des services bibliographiques

395, rue Wellington
Ottawa (Ontario)
K1A 0N4

Author: Librarian

Title: Acquisition

NOTICE

The quality of this microform is heavily dependent upon the quality of the original thesis submitted for microfilming. Every effort has been made to ensure the highest quality of reproduction possible.

If pages are missing, contact the university which granted the degree.

Some pages may have indistinct print especially if the original pages were typed with a poor typewriter ribbon or if the university sent us an inferior photocopy.

Reproduction in full or in part of this microform is governed by the Canadian Copyright Act, R.S.C. 1970, c. C-30, and subsequent amendments.

AVIS

La qualité de cette microforme dépend grandement de la qualité de la thèse soumise au microfilmage. Nous avons tout fait pour assurer une qualité supérieure de reproduction.

S'il manque des pages, veuillez communiquer avec l'université qui a conféré le grade.

La qualité d'impression de certaines pages peut laisser à désirer, surtout si les pages originales ont été dactylographiées à l'aide d'un ruban usé ou si l'université nous a fait parvenir une photocopie de qualité inférieure.

La reproduction, même partielle, de cette microforme est soumise à la Loi canadienne sur le droit d'auteur, SRC 1970, c. C-30, et ses amendements subséquents.

**Coordination Chemistry of Noncyclic and Macrocyclic
Thioether-diazine Polydentate Ligands**

by

© Liqin Chen, B.Sc., M.Sc.

A thesis submitted to the
School of Graduate Studies
in partial fulfilment of the
requirements for the degree of
Doctor of Philosophy

Department of Chemistry
Memorial University of Newfoundland

August 1993

St. John's

Newfoundland

Abstract

This thesis describes studies of noncyclic and macrocyclic thioether-diazine polydentate ligands and their coordination chemistry with Cu(II), Cu(I) and Ag(I). In chapter 1, The magnetic interactions in polynuclear copper(II) complexes involving diazine (N-N) bridges are briefly reviewed. The synthesis and properties of a series of polynuclear Cu(II), and Cu(I) complexes of three noncyclic tetradentate (N₄) thioether-diazine ligands are described. The Cu(II) complexes are generally synthesized by the reaction of Cu(II) salts with ligands while some of them are synthesized by oxidation of Cu(I) complexes with air *in situ*. The X-ray structures of eight complexes were determined. The dinuclear Cu(I) complex is bridged by the diazine group only and dinuclear and tetranuclear Cu(II) complexes are bridged by the diazine and a hydroxide or halogen. Variable-temperature magnetic studies on the Cu(II) complexes indicate moderately strong antiferromagnetic coupling ($-2J = 35-537 \text{ cm}^{-1}$). Cyclic voltammetry on the Cu(II) complexes in DMF shows single, essentially nonreversible, redox waves at positive potentials ($E_{1/2} = 0.41-0.48 \text{ V vs. SCE}$) associated with two electron reduction to produce rearranged dinuclear Cu(I) species. In chapter 2, the synthesis, structural, electrochemical, esr and magnetic properties of a series of

dinuclear Cu(II) complexes of a potentially octadentate (N_8) ligand PTAPY (PTAPY = 3,6-bis-N,N,N',N'-tetrakis(pyridine-2-ylmethyl)-aminoethanethiolato-pyridazine) are discussed. The X-ray structures of two complexes were determined. In each case the ligand is hexadentate with the pyridazine group remaining uncoordinated and there is no magnetic interaction between the distant copper centres. In chapter 3, five novel thioether-pyridazine macrocycles containing one, two or three pyridazine subunits were synthesized. A series of mononuclear, dinuclear, trinuclear and polymeric polynuclear Cu(II) complexes were isolated. The X-ray structures of six of these complexes were determined. The macrocycles generally act as nitrogen donors with the copper centres in square planar geometries. The esr spectra of these complexes were studied in detail and interpreted according to their structures. The presence of very weak intradimer antiferromagnetic exchange ($-2J < 18 \text{ cm}^{-1}$), with even weaker interdimer exchange ($-zJ' < 0.51 \text{ cm}^{-1}$) was observed. In chapter 4, a series of Cu(I) and Ag(I) complexes with two macrocycles containing one pyridazine or phthalazine subunit and a S_4 linkage were prepared. The X-ray structures of one ligand and four complexes were determined. The complexes have most unusual polynuclear structures including double stranded chains and crosslinked polymers with the ligands acting predominantly as sulfur donors.

Acknowledgements

I am greatly indebted to my supervisor, professor Laurence K. Thompson, for his outstanding supervision, encouragement, and financial support throughout the course of this research and for his help with variable temperature magnetic studies. His assistance and patience in the preparation of this thesis are also gratefully acknowledged.

Special acknowledgement is extended to Dr. J.N. Bridson for the X-ray structural determinations, to Dr. C.P. Jablonski and Ms. N. Brunet for nmr spectroscopic measurements, to Dr. B. Gregory and Ms. M. Baggs for mass spectrometry and Dr. S.S. Tandon for his advice and help with chemistry in the lab.

I would like to thank Dr. C.R. Lucas for his kindness and the loan of some chemicals from his lab. and for his kind advice and discussion with my work, to Dr. J.N. Burnell for discussion on organic synthesis and to Dr. N.J. Gogan for help and discussion on esr spectroscopy.

Many thanks are also extended to my fellow students and the staff of the Chemistry Department for making the years in chemistry at MUN enjoyable.

I wish to thank the Department of Chemistry and School of Graduate Studies of Memorial University of Newfoundland for their fellowship support.

I would like to thank my wife for her understanding, patience, encouragement and love and for her dedicated care of our son.

To My Parents

Table of Contents

Title	i
Abstract	ii
Acknowledgements	iv
Dedication	vi
Table of Contents	vii
List of Tables	xi
List of Figures	xiv
List of Abbreviations	xx
Chapter 1 Dinuclear and Tetranuclear Copper(II) and Dinuclear Copper(I) Complexes of the tetradentate (N₄) Thio-diazine Ligands ..	1
1.1. Introduction	1
1.1.1. Magnetic exchange in dinuclear copper(II) complexes	1
1.1.2. Diazine bridged dinuclear copper(II) complexes	13
1.2. The tetradentate (N ₄) thio-diazine ligands involved in this study	31
1.3. Experimental	33
1.3.1. Synthesis of the ligands	34
1.3.2. Synthesis of the complexes	36

1.4.	Results and discussion	40
1.4.1.	Ligands	40
1.4.2.	Structures	41
1.4.3.	Reactions	67
1.4.4.	Spectroscopy	72
1.4.5.	Magnetism	78
1.4.6.	Electrochemistry	90
1.5.	Conclusion	93
Chapter 2	Dinuclear and Tetranuclear Copper(II) Complexes of 3,6-Bis-	
	(N,N,N',N'-tetrakis-(pyridine-2-ylmethyl)-aminoethanethiolato-	
	pyridazine (PTAPY) - a Modified N₆ Diazine Ligand Exhibiting	
	Hexadentate Coordination Behaviour	96
2.1.	Introduction	96
2.2.	Experimental	98
2.2.1.	Synthesis of the ligands	98
2.2.2.	Synthesis of the complexes	100
2.3.	Results and discussion	102
2.3.1.	Ligands	102
2.3.2.	Structures	104

2.3.3.	Spectroscopy	112
2.3.4.	Magnetism	120
2.3.5.	Electrochemistry	120
2.4.	Conclusion	123
Chapter 3	Mononuclear, Dinuclear, Trinuclear and Polymeric Polynuclear Copper(II) Complexes of Thioether-pyridazine Macrocycles	125
3.1.	Introduction	125
3.2.	Experimental	140
3.2.1.	Synthesis of the macrocycles	140
3.2.2.	Synthesis of the complexes	142
3.3.	Results and discussion	147
3.3.1.	Synthesis	147
3.3.2.	Structures	149
3.3.3.	Spectroscopy	167
3.3.4.	Magnetism	179
3.4.	Conclusion	184
Chapter 4	Polymeric, Polynuclear Cu(I) and Ag(I) Complexes of Pyri- dazinophane and Phthalazinophane Macrocycles. Unusual Extended Metallo-cyclic Structures	186

4.1.	Introduction	186
4.2.	Experimental	187
4.2.1.	Synthesis of the macrocycles	187
4.2.2.	Synthesis of the complexes	188
4.3.	Results and discussion	190
4.3.1.	Synthesis	190
4.3.2.	Structures	190
4.3.3.	Spectroscopy	209
4.4.	Conclusion	211
References	212
Appendix	232

List of Tables

Table	Page
1-1. Magnetic and structural data of doubly diazine bridged dinuclear copper(II) (Cu_2N_4) complexes	20
1-2. Structural, magnetic and electrochemical data for dinuclear copper(II) complexes of polydentate diazine ligands	21
1-3. Selected bond distances (\AA) and angles (deg) for $[\text{Cu}_2(\text{PTPH})\text{Cl}_4] \cdot 2\text{CH}_3\text{OH}$ (1)	43
1-4. Selected bond distances (\AA) and angles (deg) for $[\text{Cu}_2(\text{DPTD})\text{Br}_4]$ (4)	45
1-5. Selected bond distances (\AA) and angles (deg) for $[\text{Cu}_2(\text{PTPH})(\text{OH}) \cdot (\text{NO}_3)_3(\text{H}_2\text{O})_2]_2$ (5)	49
1-6. Selected bond distances (\AA) and angles (deg) for $[\text{Cu}_2(\text{PTPH})(\text{OH}) \cdot (\text{NO}_3)_2(\text{H}_2\text{O})_2](\text{NO}_3)$ (6)	53
1-7. Selected bond distances (\AA) and angles (deg) for $[\text{Cu}_2(\text{PTPH})(\text{OH})\text{Cl}_3] \cdot 1.5\text{CHCl}_3$ (9)	57
1-8. Selected bond distances (\AA) and angles (deg) for $[\text{Cu}_2(\text{PTP})(\text{OH})\text{Cl}_3] \cdot 2\text{CH}_3\text{CN}$ (11)	60

1-9. Selected bond distances (Å) and angles (deg) for $[\text{Cu}_2(\text{PTPH})_2](\text{ClO}_4)_2 \cdot 2\text{CH}_3\text{CN}$ (12)	63
1-10. Selected bond distances (Å) and angles (deg) for $[\text{Cu}(\text{PTPO})_2(\text{H}_2\text{O})][\text{CuCl}_4] \cdot [\text{Cu}(\text{PTPO})\text{Cl}_2]$ (13)	66
1-11. Spectral and electrochemical data of copper complexes of PTPH, PTP, DPTD	74
1-12. Magnetic and structural data of dinuclear copper(II) complexes of PTPH, PTP, DPTD	80
1-13 Comparison of structural parameters of $[\text{Cu}_2(\text{PTPH})(\text{OH})\text{Cl}_3] \cdot 1.5\text{CHCl}_3$ (9) and $[\text{Cu}_2(\text{PTP})(\text{OH})\text{Cl}_3] \cdot 2\text{CH}_3\text{CN}$ (11)	87
2-1. Selected bond distances (Å) and angles (deg) for $[\text{Cu}_2(\text{PTAPY})\text{Br}_4] \cdot 2\text{DMF}$ (15)	106
2-2. Selected bond distances (Å) and angles (deg) for $[\text{Cu}_2(\text{PTAPY})(\text{NO}_3)_2(\text{N}_3) \cdot (\text{H}_2\text{O})_2]_2(\text{NO}_3)_2 \cdot 1.2\text{CH}_3\text{OH}$ (17)	110
2-3. Magnetic, spectral, conductance and electrochemical data of dinuclear copper(II) complexes of PTAPY	114
3-1. Selected bond distances (Å) and angles (deg) for $[\text{Cu}_3(\text{L1})_2\text{Cl}_4] \cdot 2\text{CHCl}_3$ (18)	152
3-2. Selected bond distances (Å) and angles (deg) for $[\text{Cu}(\text{L2})\text{Cl}_2]$ (19)	153

3-3. Selected bond distances (Å) and angles (deg) for [Cu(L2) ₂](ClO ₄) ₂ ·CH ₃ CN·CHCl ₃ (22)	158
3-4. Selected bond distances (Å) and angles (deg) for [Cu ₂ (L3)Cl] _x (23)	161
3-5. Selected bond distances (Å) and angles (deg) for [Cu(L3)Cl] ₂ (24)	164
3-6. Selected bond distances (Å) and angles (deg) for [Cu(L3)(NO ₃) ₂] (25)	166
3-7. Infrared and electronic spectral data of Cu(II) complexes with thioether-pyridazine macrocycles	168
3-8. Magnetic and esr data of Cu(II) complexes with thioether-pyridazine macrocycles	176
4-1. Selected bond distances (Å) and angles (deg) for L6	194
4-2. Selected bond distances (Å) and angles (deg) for [Cu(L5)Cl] _x (29)	197
4-3. Selected bond distances (Å) and angles (deg) for [Cu(L5)Br] _x (30)	201
4-4. Selected bond distances (Å) and angles (deg) for [Cu _{1.5} (L6)Cl _{1.5}] _x (31)	203
4-5. Selected bond distances (Å) and angles (deg) for [Ag(L5)(ClO ₄)] _x (32)	208
4-6. Infrared spectral data of Cu(I) and Ag(I) complexes of L5 and L6 .	209

List of Figures

Figure	page
1-1. Comparison of the temperature dependence of magnetic susceptibility for paramagnetic (a), ferromagnetic (b), and antiferromagnetic (c) dinuclear copper(II) complexes	6
1-2. Map of the overlap density between the magnetic orbitals in planar bridged copper(II) dimer	10
1-3. Structural representation of $[\text{Cu}_2(\text{PTPH})\text{Cl}_4] \cdot 2\text{CH}_3\text{OH}$ (1), with hydrogen atoms omitted (40% probability ellipsoids)	42
1-4. Structural representation of $[\text{Cu}_2(\text{DPTD})\text{Br}_4]$ (4), with hydrogen atoms omitted (40% probability ellipsoids)	45
1-5. Structural representation of $[\text{Cu}_2(\text{PTPH})(\text{OH})(\text{NO}_3)_3(\text{H}_2\text{O})]_2$ (5), with hydrogen atoms omitted (40% probability ellipsoids)	48
1-6. Structural representation of $[\text{Cu}_2(\text{PTPH})(\text{OH})(\text{NO}_3)_2(\text{H}_2\text{O})](\text{NO}_3)$ (6), with hydrogen atoms omitted (40% probability ellipsoids)	52
1-7. Structural representation of $[\text{Cu}_2(\text{PTPH})(\text{OH})\text{Cl}_3] \cdot 2\text{CHCl}_3$ (9), with hydrogen atoms omitted (40% probability ellipsoids)	56

1-8. Structural representation of $[\text{Cu}_2(\text{PTP})(\text{OH})\text{Cl}_3] \cdot 2\text{CH}_3\text{CN}$ (11), with hydrogen atoms omitted (40% probability ellipsoids)	59
1-9. Structural representation of $[\text{Cu}_2(\text{PTPH})_2](\text{ClO}_4)_2 \cdot 2\text{CH}_3\text{CN}$ (12), with hydrogen atoms omitted (40% probability ellipsoids)	62
1-10. Structural representation of $[\text{Cu}(\text{PTPO})_2(\text{H}_2\text{O})][\text{CuCl}_4][\text{Cu}(\text{PTPO})\text{Cl}_2]$ (12), with hydrogen atoms omitted	65
1-11. Magnetic data for $[\text{Cu}_2(\text{PTPH})\text{Cl}_4] \cdot 2\text{CH}_3\text{OH}$ (1). The solid line was calculated from eq. 2 with $g = 2.10(3)$, $-2J = 124(2) \text{ cm}^{-1}$, $\rho = 0.003$, $N\alpha = 60 \times 10^{-6} \text{ cgsu}$ ($R = 0.59$)	79
1-12. Cyclic voltammogram for $[\text{Cu}_2(\text{PTPH})\text{Cl}_4] \cdot 2\text{H}_2\text{O}$ (1) in DMF ($3 \times 10^{-3} \text{ M}$, 0.1 M TEAP , GC, SCE; 100 mVs^{-1})	91
1-13. Cyclic voltammograms for $[\text{Cu}_2(\text{PTPH})\text{Cl}_4] \cdot 2\text{H}_2\text{O}$ (1) in DMF ($3 \times 10^{-3} \text{ M}$, 0.1 M TEAP , GC, SCE; $50 - 500 \text{ mVs}^{-1}$)	92
2-1. Structural representation of $[\text{Cu}_2(\text{PTAPY})\text{Br}_4] \cdot 2\text{DMF}$ (15), with hydrogen atoms omitted (40% probability ellipsoids)	105
2-2. Structural representation of the monomeric, dinuclear unit of $[\text{Cu}_2(\text{PTAPY})(\text{NO}_3)_2(\text{N}_3)(\text{H}_2\text{O})]$ (17), with hydrogen atoms and nitrates omitted (40% probability ellipsoids)	108

2-3.	Structural representation of the dimeric tetranuclear complex $[\text{Cu}_2(\text{PTAPY})(\text{NO}_3)_2(\text{N}_3)(\text{H}_2\text{O})]_2$ (17), with hydrogen atoms and nitrates omitted (40% probability ellipsoids)	109
2-4.	Solid state esr spectrum for a powdered sample of $[\text{Cu}_2(\text{PTAPY})(\text{NO}_3)_4] \cdot \text{H}_2\text{O}$ (14) (9.76 GHz; 295 K)	116
2-5.	Solid state esr spectrum for a powdered sample of $[\text{Cu}_2(\text{PTAPY})\text{Br}_4] \cdot 2\text{DMF}$ (15) (9.77 GHz; 295 K)	118
2-6.	Solid state esr spectrum for a powdered sample of $[\text{Cu}_2(\text{PTAPY})(\text{NO}_3)_2 \cdot (\text{N}_3)(\text{H}_2\text{O})]_2(\text{NO}_3)_2 \cdot 1.2\text{CH}_3\text{OH}$ (17) (9.77 GHz; 295 K)	119
2-7.	Cyclic voltammograms for $[\text{Cu}_2(\text{PTAPY})\text{Br}_4] \cdot 2\text{H}_2\text{O}$ (15) in DMF (3×10^{-3} M, 0.1 M TEAP, GC, SCE; A - D: 100 - 500 mVs^{-1})	121
2-8.	Cyclic voltammograms for $[\text{Cu}_2(\text{PTAPY})(\text{NO}_3)_2(\text{N}_3)(\text{H}_2\text{O})]_2(\text{NO}_3)_2 \cdot 1.2\text{CH}_3\text{OH}$ (17) in DMF (3×10^{-3} M, 0.1 M TEAP, GC, SCE; A - D: 100 - 500 mVs^{-1})	122
3-1.	Structural representation of $[\text{Cu}_3(\text{L1})_2\text{Cl}_4] \cdot 2\text{CHCl}_3$ (18), with hydrogen atoms omitted (40% probability ellipsoids)	151
3-2.	Structural representation of $[\text{Cu}(\text{L2})\text{Cl}_2]$ (19), with hydrogen atoms omitted (40% probability ellipsoids)	154

3-3.	Structural representation of $[\text{Cu}(\text{L}2)_2]^{2+}$ (22), with hydrogen atoms omitted (40% probability ellipsoids)	156
3-4.	Packing diagram for $[\text{Cu}(\text{L}2)_2](\text{ClO}_4)_2 \cdot \text{CH}_3\text{CN} \cdot \text{CHCl}_3$ (22)	157
3-5.	Structural representation of $[\text{Cu}_2(\text{L}3)\text{Cl}_4]_x$ (23) showing a single dinuclear fragment, with hydrogen atoms omitted (40% probability ellipsoids)	159
3-6.	Structural representation of $[\text{Cu}_2(\text{L}3)\text{Cl}_4]_x$ (23) illustrating the single stranded polymer, with hydrogen atoms omitted	160
3-7.	Structural representation of $[\text{Cu}(\text{L}3)\text{Cl}_2]$ (24), with hydrogen atoms omitted (40% probability ellipsoids)	163
3-8.	Structural representation of $[\text{Cu}(\text{L}3)(\text{NO}_3)_2]$ (25), with hydrogen atoms omitted (40% probability ellipsoids)	165
3-9.	Solid state esr spectrum for a powdered sample of $[\text{Cu}_3(\text{L}1)_2\text{Cl}_6] \cdot 2\text{CHCl}_3$ (18) (9.77 GHz; 295 K)	175
3-10.	Solid state esr spectrum for a powdered sample of $[\text{Cu}(\text{L}2)_2](\text{ClO}_4)_2 \cdot \text{CH}_3\text{CN} \cdot \text{CHCl}_3$ (22) (9.76 GHz; 295 K)	177
3-11.	Frozen glass (nitromethane) esr spectrum of $[\text{Cu}(\text{L}2)_2](\text{ClO}_4)_2 \cdot \text{CH}_3\text{CN} \cdot \text{CHCl}_3$ (22) (9.52 GHz, 77 K)	178

3-12. Magnetic data for $[\text{Cu}(\text{L}5)\text{Cl}_2]_x$ (27). The solid line was calculated from eqs. [4], [5], [6] and [7] with $g = 2.061(3)$, $-2J = 17.77(7) \text{ cm}^{-1}$, $zJ' = -0.51(5) \text{ cm}^{-1}$, $\rho = 0.045$, $N\alpha = 60 \times 10^6 \text{ cgsu}$ ($R = 0.22$)	181
4-1. Structural representation of L6, with hydrogen atoms omitted (40% probability ellipsoids)	193
4-2. Structural representation of $[\text{Cu}(\text{L}5)\text{Cl}]_x$ (29) illustrating the double stranded polymer, with hydrogen atoms omitted	196
4-3. Structural representation of fragment of $[\text{Cu}(\text{L}5)\text{Cl}]_x$ (29), with hydrogen atoms omitted (40% probability ellipsoids)	197
4-4. Structural representation of fragment of $[\text{Cu}(\text{L}5)\text{Br}]_x$ (30), with hydrogen atoms omitted (40% probability ellipsoids)	199
4-5. Structural representation of $[\text{Cu}(\text{L}5)\text{Br}]_x$ (30) showing cross-linking, with hydrogen atoms omitted	200
4-6. Structural representation of fragment of $[\text{Cu}_{1.5}(\text{L}6)\text{Cl}_{1.5}]_x$ (31), with hydrogen atoms omitted (40% probability ellipsoids)	202
4-7. Structural representation of fragment of $[\text{Ag}(\text{L}5)(\text{ClO}_4)]_x$ (32), with hydrogen atoms omitted (40% probability ellipsoids)	206
4-8. Structural representation of $[\text{Ag}(\text{L}5)(\text{ClO}_4)]_x$ (32) illustrating the 2-dimensional polymeric arrangement, with hydrogen atoms omitted .	207

List of Abbreviations

AAMT:	4-amino-3,5-bis(aminomethyl)-1,2,4-triazole
APHP:	1,4-dihydrazinophthalazine-bis(2'-pyridine)acetalimine
BDPDZ:	3,6-bis(di-2-pyridylmethyl)-pyridazine
BLEPH:	3,5-bis(4'-pyridyl-2'-thiabut-1'-yl)pyrazole
BLMPH:	3,5-bis(3'-pyridyl-2'-thioprop-1'-yl)-pyrazole
BPTH:	3,5-bis(pyridin-2-yl)-1,2,4-triazole
BPYPZ:	3,5-bis(pyridin-2-yl)pyrazole
DHPH:	1,4-dihydrazinophthalazine
DMF:	N,N-dimethylformamide
DPAP:	3,5-bis[(2-diethylamino)propylaminomethyl]-pyrazole
DPPN:	3,6-bis-(2'-pyridyl)-pyridazine
DPTD:	2,5-di-(2'-pyridylthio)-thiadiazole
DPYH:	3,6-dialdoxime-pyridazine
HBAMPZ:	3,5-bis(aminomethyl)pyrazole
HPHAP:	1,4-dihydrazinophthalazine-bis(2'-pyridine)aldaldimine
IMPH:	1,4-dihydrazinophthalazine-bis(1-methyl-2-imidazolyl)aldaldimine
L1:	28,29,30,31,32,33-hexaaza-2,6,11,15,20,24-hexathiatetra-cyclo[23.2. 2.2 ^{7,10} .2 ^{16,19}]tritriaconta-1(28),7(33),8,10(21),16(31),17,19(30),25(29),

- 26-nonaene
- L2: 19,20,21,22-tetraaza-2,6,11,15-tetrathiatricyclo[14.2.2.2^{7,10}]docosa-1(19),8,10(21),16(20),17-hexaene
- L3: 23,24,25,26-tetraaza-2,5,8,13,16,19-hexathiatricyclo[18.2.2.2^{9,12}]-hexacosa-1(23),9(26),10,12(25),20(24),21-hexaene
- L4: 29,30,31,32-tetraaza-2,5,8,11,16,19,22,25-octathiatricyclo[24.2.2.2^{12,15}]dotriaconta-1(29),12(32),13,15(31),26(30),27-hexaene
- L5: 16,17-diaza-2,5,9,12-tetrathiabicyclo[11.2.2]heptadeca-1(16),13(17),14-triene
- L6: 20,21-diaza-2,5,9,12-tetrathiatricyclo[11.4.2^{1,13}.0^{14,19}]hencicosa-1(20),13(21),14(19),15,17-pentaene
- MIP: 1,4-bis(1-methyl-2-imidazolyl)phthalazine
- PAP: 1,4-bis(2-pyridylamino)phthalazine
- PAP4Me: 1,4-bis((4-methyl-2-pyridyl)amino)-phthalazine
- PAP46Me: 1,4-bis-((4,6-dimethyl-2-pyridyl)amino)-phthalazine
- PHP6Me: 1,4-dihydrazinophthalazine-bis(6-methyl-2-pyridyl)aldaldimine
- PPD: 3,6-bis(1-pyrazolyl)pyridazine
- PTA: 3,6-di-(aminoethanethiolato)-pyridazine
- PTAPY: 3,6-bis(N,N,N',N'-tetrakis-(pyridine-2-ylmethyl-aminoethanethiolato)-pyridazine

PTP:	3,6-di-(2'-pyridylthio)-pyridazine
PTPH:	1,4-di-(2'-pyridylthio)-phthalazine
PZEN:	3,5-bis[(3-dimethylamino)propylaminomethyl]-pyrazole
RBITP:	3,6-bis(N-R-2-benzimidazolylthio)-pyridazine
SCE:	aqueous saturated calomel electrode
TEAP:	tetraethylammonium perchlorate
THF:	tetrahydrofuran

Chapter 1

Dinuclear and Tetranuclear Copper(II) and Dinuclear Copper(I) Complexes of the Tetradentate (N₄) Thio-diazine Ligands

1.1. Introduction

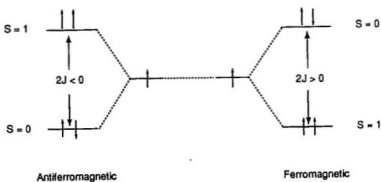
1.1.1. Magnetic Exchange in Dinuclear Copper(II) Complexes

Dinuclear copper(II) complexes with metal centres in close proximity have been the subject of recent extensive investigations since dinuclear copper units are involved in a variety of important biochemical processes, especially oxygen transport and oxygen activation, e.g. in hemocyanin and tyrosinase [1 - 6]. Magnetic interactions between copper centres have been detected in these systems and in some cases are large enough to render copper esr silent [3].

Cu(II) ion has only one unpaired electron ($S = 1/2$) and dinuclear copper(II) complexes are simple model complexes for studying the magnetic properties of copper containing proteins and enzymes. Spin-coupled dinuclear copper(II) complexes can be divided into two categories; ferromagnetic and antiferromagnetic, depending on the mode of spin interaction between the metal centres [7, 8]. In dinuclear copper(II) complexes in which the metal centres have

no spin interaction, the magnetic properties of the complexes are essentially the same as the paramagnetic monomer. In dinuclear copper(II) complexes which involve very strong copper-copper antiferromagnetic interactions, essentially complete spin pairing of the two unpaired electrons can occur and the complexes will effectively display simple diamagnetic behaviour. In dinuclear complexes which involve weak to moderate antiferromagnetic copper-copper interactions, partial spin pairing will occur. Antiferromagnetic coupling involves a spin singlet ground state ($S = 0$) and a spin triplet excited state ($S = 1$) (Scheme 1-1). Ferromagnetic coupling involves a spin triplet ground state ($S=1$) and a spin singlet excited state ($S = 0$) (Scheme 1-1) and is quite uncommon (approx. 5% reported spin coupled cases).

Scheme 1-1.

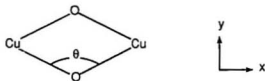


The singlet-triplet energy gap is conventionally denoted by $2J$ [7 - 9]. The $2J$ value is negative when the interaction is antiferromagnetic, and positive when the interaction is ferromagnetic. Spin exchange in complexes of this sort usually occurs through the intervening ligands, with large copper-copper separations (3 - 5Å), and is known as superexchange [10].

The net measured exchange (J_T) in a spin-coupled copper(II) dimer is, in reality, the sum of any antiferromagnetic (J_{AF}) and ferromagnetic (J_F) components, i.e.

$$J_T = J_{AF} + J_F$$

J_F is usually small and is weakly sensitive to small structural changes, while J_{AF} is found to vary dramatically as a function of e.g. bridge angle at the superexchange bridge. In a simple dimer of the type shown below



which involves d_{xy} type metal orbitals, J_{AF} varies as $-\Delta^2$, where Δ is the energy gap between the two singly occupied molecular orbitals in the low-lying triplet state [11]. The overlap density is given by

$$\rho(i) = \phi_A^{(0)}(i)\phi_B^{(0)}(i)$$

where $\phi_A^{(0)}$ and $\phi_B^{(0)}$ are the two natural (nonorthogonalized) magnetic orbitals in the copper(II) dimer. The overlap integral S and the two-electron exchange integral j are given by

$$S = \int_{space} \rho(i) dV(i)$$

$$j = \int_{space} \rho(i) \rho(j) \frac{dV(i) dV(j)}{r_{ij}}$$

J_{AF} varies as a function of $-S^2$ and J_F as a function of j . With d_{xy} type magnetic orbitals the overlap density ($\rho^{(xy, xy)}$) creates two positive lobes along the x axis and

two negative lobes along the y axis at each bridge. For a bridge angle (θ) around 90° the positive and negative lobes compensate each other and the overlap integrals effectively become zero and $J_T = J_F$. With increasing θ the positive lobes increase at the expense of the negative lobes (S^2 increase) leading to an increase in J_{AF} and net antiferromagnetism [12].

For antiferromagnetically coupled dinuclear copper(II) complexes, the magnetic susceptibility (χ_m) decreases at low temperatures with decreasing temperature (Fig. 1-1(c)). The critical temperature for the onset of antiferromagnetism is called the **Néel temperature** (T_N) [13]. For ferromagnetically coupled dinuclear copper(II) complexes, the magnetic susceptibility (χ_m) increases with decreasing temperature (Fig. 1-1(b)). The critical temperature for the onset of ferromagnetism is called the **Curie temperature** (T_C).

There are several factors which can affect spin interactions in dinuclear copper(II) complexes:

- 1). Geometry at the copper centres (i.e. magnetic ground state).
- 2). Angle at the bridge.
- 3). Number of atoms in the bridge (distance between the copper centres).
- 4). Electronegativity effects of the bridging and non-bridging atoms bound to copper.

- 5). The presence or absence of orthogonal bridge interactions.
- 6). Spin polarization effects.

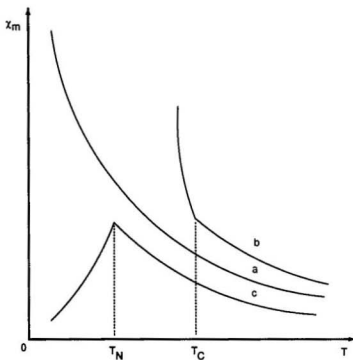


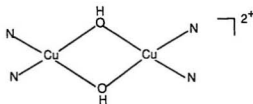
Fig. 1-1. Comparison of the temperature dependence of magnetic susceptibility for paramagnetic (a), ferromagnetic (b), and antiferromagnetic (c) dinuclear copper(II) complexes.

The geometries of copper(II) complexes are quite varied. The copper(II) ion can be four, five or six-coordinate in square planar, tetrahedral, square-pyramidal, trigonal-bipyramidal or octahedral geometries. The magnetic orbital for copper(II) centres in square planar, square pyramidal and octahedral geometries is $d_{x^2-y^2}$, while the magnetic orbital for copper(II) centres in trigonal bipyramidal geometries is d_z^2 . The interaction of the magnetic orbitals of each copper ion with the single atom bridging ligands will generally result in antiferromagnetic interactions for bridge angles $> 90^\circ$ [12], while the interaction of the magnetic orbital of one copper ion with a non-magnetic orbital of another ion and the interaction of two non-magnetic copper orbitals via the bridging ligands (orthogonal interactions) cannot result in antiferromagnetic coupling, but leads to ferromagnetic coupling.

The effect of Cu(II)-L-Cu(II) bridge angle (L = single atom bridge) on the exchange interaction has been extensively studied. The qualitative calculation by R. Hoffmann and coworkers [10] for some singly bridged and doubly bridged copper(II) dimers predicts a large antiferromagnetic coupling for a 180° bond angle when the metal orbitals can interact with a bridging ligand orbital of the same symmetry, and a weak ferromagnetic coupling for a 90° bond angle. These results are consistent with the experimental results of Hatfield, Hodgson and coworkers [14, 15], who have carefully studied a series of dihydroxy-bridged copper(II) dimers with regard to their crystal structures and magnetic properties.

The copper centres generally have $d_{x^2-y^2}$ magnetic ground states (Scheme 1-2) bridged by two hydroxide oxygen atoms. The antiferromagnetic coupling ($-2J$) varies as a function of the hydroxide bridge angle (θ) (eq. 1).

Scheme 1-2.



$$2J = 74.53\theta \text{ (cm}^{-1}\text{deg}^{-1}) - 7270 \text{ cm}^{-1} \dots\dots [1]$$

$$(\theta = 95.6 - 104.4^\circ)$$

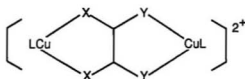
The number of atoms in the bridge affects the magnetic interaction between the two copper centres by effectively changing the copper-copper distance. The spin exchange will diminish with increased copper-copper separation. The ligand 1,2,4,5-tetrakis(4,5-dihydroimidazol-2-yl) benzene (BTIM) forms a dinuclear copper(II) complex that involves very weak antiferromagnetic exchange between the metal centres ($-2J = 1.8(1) \text{ cm}^{-1}$) [16], which are separated by 7.610 Å.

The electronegativity of the bridging and non-bridging atoms bound to the

copper centres will affect the spin exchange by affecting the electron density on the bridging atoms and the copper(II) ions. The antiferromagnetic interaction decreases as electron density is removed from the bridging atoms and copper(II) ions. Conversely, an increase in electron density on the bridging atoms and copper(II) ions enhances the antiferromagnetic coupling [10]. These results are consistent with experimental results of O. Kahn and coworkers [9] who studied a series of dinuclear copper(II) complexes in which two copper(II) ions are bridged by ligands of the type $C_2X_2Y_2^{2-}$, where the X and Y atoms bound to the metal ions may be oxygen, nitrogen or sulfur (Scheme 1-3).

As oxygen is more electronegative than nitrogen and sulfur, the complex is less strongly coupled when a ligand contains more oxygen atoms.

Scheme 1-3.



C_2O_4	(X=Y=O)	$-2J = 384.5 \text{ cm}^{-1}$
$C_2O_2N_2$	(X=O, Y=N)	$-2J = 581 \text{ cm}^{-1}$
$C_2S_2N_2$	(X=S, Y=N)	$-2J = 594 \text{ cm}^{-1}$

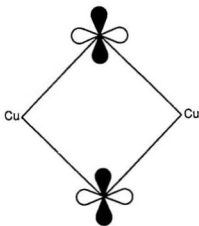


Fig. 1-2. Map of the overlap density between the magnetic orbitals in planar bridged copper(II) dimer.

Orthogonal interactions result from the overlapping of unsymmetrical magnetic orbitals [10], or with bridge angles close to 90° as we just discussed [12, 17], since positive lobes of overlap density exactly compensate the negative lobes (Fig. 1-2). The orthogonality generally results in ferromagnetism, not antiferromagnetism in the complexes.

The spin polarization effects were demonstrated very well by azide bridged dinuclear copper(II) complexes. The azide group can act as a 1,1- or a 1,3- bridge in its dinuclear complexes. It contains two unpaired electrons, one at one each of

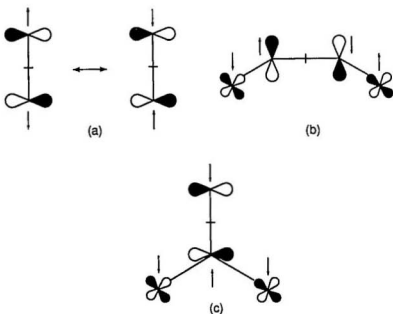
the two terminal nitrogens with spins antiparallel (Scheme 1-4(a)) [17]. It can polarize the spin of the unpaired electrons on two copper(II) centres to favour either the singlet or the triplet state depending on which way it bridges the two copper(II) ions. When N_3^- bridges in the 1,3 fashion (Scheme 1-4(b)), the two spin antiparallel electrons localized on the two terminal nitrogen atoms will polarize the electron spin on the two copper(II) ions in the opposite direction, with resulting antiparallel spin of the two unpaired electrons on the copper(II) ions. Consequently copper complexes with azide bridging in a 1,3 fashion are generally strongly antiferromagnetically coupled ($-2J > 800 \text{ cm}^{-1}$) [6]. If N_3^- bridges two copper(II) ions in the 1,1 fashion (Scheme 1-4(c)), the electron on the bridging nitrogen will polarize the electron spin on the two copper(II) ions with the result that the two unpaired electrons on the two copper(II) ions have parallel spins. So the dinuclear complexes with azide bridging in the 1,1 fashion are generally strongly ferromagnetically coupled ($2J > 200 \text{ cm}^{-1}$) [17].

The molar magnetic susceptibility of dinuclear copper(II) complexes can be calculated from Bleaney-Bowers expression (eq.2) [18], using the isotropic (Heisenberg) exchange Hamiltonian ($\hat{H} = -2JS_1S_2$) for two interacting $S = 1/2$ centres. In this expression $2J$ is the singlet-triplet splitting or exchange integral, χ_m is expressed per mole of copper atoms and other symbols have their usual

meaning (ρ represents the fraction of a possible magnetically dilute copper(II) impurity, $N\alpha$ is the temperature-independent paramagnetism, and θ is a corrective term for interdimer interactions [19, 20]).

$$\chi_m = \frac{N\beta^2 g^2}{3k(T-\theta)} [1 + 1/3 \exp(-2J/kT)]^{-1} (1-\rho) + \frac{[N\beta^2 g^2] \rho}{4kT} + N\alpha \dots \dots [2]$$

Scheme 1-4.

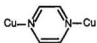


1.1.2. Diazine-bridged Dinuclear Copper(II) Complexes

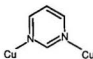
The study of dinuclear copper complexes containing bridging heterocyclic ligands has been the subject of much recent attention, since they are of great significance as models for some biological systems [1 - 6, 21]. The magnetic communication between the two copper centres via the π system of the heterocyclic ligand varies with the identity of the ligand. In the dinuclear copper complexes involving pyrazine bridges, where the heterocyclic nitrogen donor centres are arranged at the 1,4 ring positions [22, 23] and in the dinuclear copper complexes involving pyrimidine bridges, where the heterocyclic nitrogen donor centres are arranged at the 1,3 ring positions [24 - 27] (Scheme 1-5), only weak intramolecular antiferromagnetic interactions were observed. However, in the dinuclear copper complexes involving pyridazine bridges and its diazine analogues (Scheme 1-6), where the heterocyclic nitrogen donor centres are arranged at the 1,2 ring positions, the two copper centres are bridged by the diazine groups and in many cases by additional exogenous bridges e.g. Cl, Br, OH, N₃, NO₃, SO₄, IO₃, [28 - 79]. The two copper ions are bound in close proximity and usually experience moderate to strong antiferromagnetic [28 - 80] or ferromagnetic [80] coupling. Typical ligands of this type (Scheme 1-7, 1-8) have created an ideal framework for several magneto-structural studies. In particular spin coupling in

dinuclear copper(II) complexes was extensively investigated and related to structural features, bridge groups, bridge angle (especially when the bridge is hydroxide), chelate ring sizes and the polarizing nature of the nonbridging ligands.

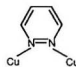
Scheme 1-5.



Pyrazine



Pyrimidine



Pyridazine

Scheme 1-6.



Phthalazine



4-Amino-1,2,4-triazole



1,2,4-Triazol-5-olate



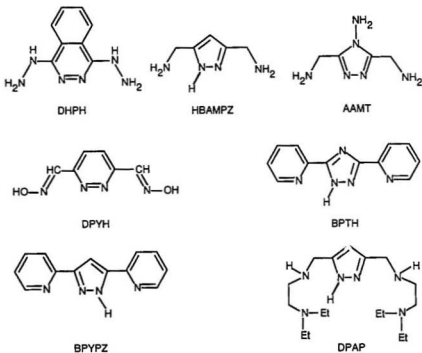
Pyrazolate



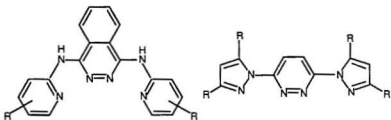
Thiadiazole

Phthalazines [62], pyridazines [67], pyrazoles [72 - 74, 76, 78], and 1,2,4-triazoles [68 - 71] form a family of bridging ligands (Scheme 1-7) which can combine two copper ions with only diazine (N_2) groups and have a general coordination environment of Cu_2N_8 (Scheme 1-9).

Scheme 1-7.

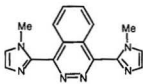


Scheme 1-8.

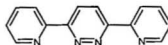


PAPR (R = H, 3Me, 4Me, 5Me, 6Me, 46Me)

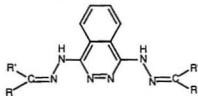
R = H (PPD), Me(PPDMe)



MIP

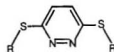


DPPN



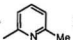
HPHAP

(R = H, R' = )



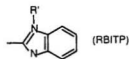
R =  (PTP)

PHP6Me

(R = H, R' = )

APHP

(R = CH₃, R = )



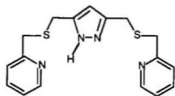
(RBITP)

IMPH

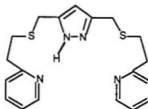
(R = H, R' = )

(R' = H, Me, Et, ⁱPr, nBu)

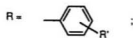
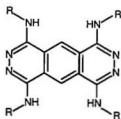
Scheme 1-8 (continued)



BLMPH

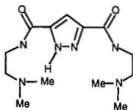


BLEP

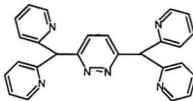


R' = H (TNL), 4Me (TNL4),

5Me (TNL5), 4Et (TNL4E)

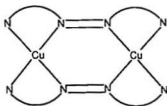


PZEN



BDPDZ

Scheme 1-9.

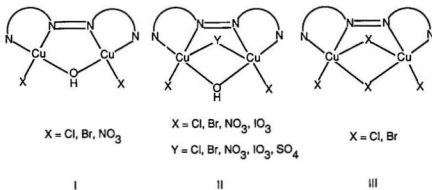


A large number of tetradentate (N_4) [37 - 55], hexadentate (N_6) [36, 55, 59, 66] and octadentate (N_8) [81, 82] ligands involving diazine groups shown in Scheme 1-8 usually form a series of dinuclear copper(II) complexes in which the dinuclear copper centres are bridged by diazine and also by additional exogenous groups. The complexes usually have one of three kinds of structure as illustrated in Scheme 1-10. The copper centres in these complexes usually have distorted square planar, square pyramidal or octahedral geometries with $d_{x^2-y^2}$ magnetic orbitals bridged by the diazine group and an exogenous group, which in most cases is hydroxide, but in some cases can be halides (Cl^- or Br^-).

The copper-copper separation in dinuclear complexes only bridged by diazine groups is in the range of 3.70 - 4.44 Å (Table 1-1 & 1-2), while the copper-copper separations for the complexes with the structures shown in Scheme 1-10 are in the range of 3.00 - 3.8 Å. The hydroxide bridge angles fall in the range of 102 - 128° (Table 1-2). The Cu-O (hydroxide) distances are in the range

1.88 - 2.16 Å and the Cu-N (diazine) distances are in the range of 1.88 - 2.10 Å [34, 35, 37, 39, 40, 43, 45, 51, 52, 56].

Scheme 1-10.



There are several factors which will affect the copper-copper separations and hydroxide bridge angles in these complexes. Changing the chelate ring size from five (MIP, PPD, DPPN) to six (PAPR, PTP) will result in greater ligand flexibility and allow a reduction in the intermetallic separations (Table 1-2). Thus the five-membered chelate ring systems typically form doubly bridged dicopper complexes with intermetal separations between 3.30 and 3.50 Å. The large copper-

Table 1-1. Magnetic and structural data of doubly diazine bridged dinuclear copper(II) (Cu_2N_2) complexes

Complex	$-2J$ (cm^{-1})	Cu...Cu (\AA)	Cu-N (\AA) (diazine)	Cu-N (\AA) (peripheral)	Cu-O (\AA) (axial)	Ref.
$[\text{Cu}_2(\text{DPYH})_2(\text{H}_2\text{O})_2(\text{ClO}_4)_2]$	536(2)	3.760(2)	2.027(5) 2.014(6)	1.977(7) 1.974(6)	2.310(6) 2.554(6)	67
$[\text{Cu}_2(\text{DHPH})_2(\text{H}_2\text{O})_2(\text{ClO}_4)_2](\text{ClO}_4)_2$	489(1)	3.729	1.981(7) 1.965(8)	1.966(8) 2.019(7)	2.351(7) 2.615(12)	62
$[\text{Cu}_2(\text{DPAP})_2](\text{BPh}_4)_2$	428	3.903(2)	1.929(4) 1.906(3)	2.028(3) 2.108(4)		76
$[\text{Cu}_2(\text{BAMPZ})_2\text{Br}_2]$	384.0	3.947(4)	1.88(2) 1.96(1)	2.07(1)		78
$[\text{Cu}_2(\text{BPYPZ})_2(\text{H}_2\text{O})_2(\text{NO}_3)_2 \cdot 2\text{H}_2\text{O}]$	361.8	4.044	1.954(5) 1.942(5)	2.074(5) 2.092(5)	2.22	72
$[\text{Cu}_2(\text{BPT})_2(\text{CF}_3\text{SO}_3)_2(\text{H}_2\text{O})_2]$	236(20)	4.085(1)	1.942(3) 1.936(3)	2.082(3) 2.087(3)	2.376(3) 2.802(4)	69
$[\text{Cu}_2(\text{AAMT})_2(\text{H}_2\text{O})_2\text{Br}_2]$	220(2)	4.069(7)	1.950(3) 1.937(3)	2.032(3) 2.043(2)	2.647(3)	68

Table 1-2. Structural, magnetic and electrochemical data for dinuclear copper(II) complexes of polydentate diazine ligands

Compound	Cu...Cu (Å)	Cu-OH-Cu (°)	μ_{eff} (RT)	-2J (cm ⁻¹)	$E_{1/2}$ (V) ^a (vs. SCE)	Ref.
[Cu ₂ (DPPN)(μ_2 -OH)Cl ₃ (H ₂ O)]	3.376	126.5(3)				39
[Cu ₂ (DPPN)(μ_2 -OH)Cl ₂ (H ₂ O)(NO ₃)]	3.361(4)	124.0(5)				43
[Cu ₂ (DPPN)(μ_2 -OH)(μ_2 -NO ₃)Cl ₂]	3.346(3)	123.2(5)				43
{[Cu ₂ (DPPN)(μ_2 -OH)Cl ₂ (H ₂ O)]Cl} _n	3.387(3)	122.5(6)				40
[Cu ₂ (DPPN)(μ_2 -OH)Br ₃] _n	3.398(8)	128.1(17)				45
[Cu ₂ (DPPN)(μ_2 -Cl)Cl ₃ (H ₂ O)]	3.51					42
[Cu ₂ (DPPN)(μ_2 -Cl)Cl ₃ (H ₂ O)]	3.566(2)					44
[Cu ₂ (PAP46Me)(μ_2 -Cl) ₂ Cl ₂]	3.251(1)		1.72	55.2(1)		56
[Cu ₂ (PTP)(μ_2 -Cl) ₂ Cl ₂] · CH ₃ CH ₂ OH	3.198(1)		1.61	131(0.4)	0.48	53
[Cu ₂ (PTP)(μ_2 -Br) ₂ Br ₂]	3.318(3)		1.43	244(0.5)		57
[Cu ₂ (EtBITP)(μ_2 -OH)(μ_2 -Cl)Cl ₂] · DMF	3.017(1)	104.7(1)	1.38	260(1)	0.43	52
[Cu ₂ (PAP)(μ_2 -OH)(μ_2 -Br)Br ₂] · 1.5H ₂ O	3.010(2)	102.9(3)	1.66	190		35

Table 1-2. Structural, magnetic and electrochemical data for dinuclear copper(II) complexes of polydentate diazine ligands (continued)

Compound	Cu...Cu (Å)	Cu-OH-Cu (°)	μ_{eff} (RT)	-2J (cm ⁻¹)	$E_{1/2}$ (V) ^a (vs. SCE)	Ref.
[Cu ₂ (PAP)(μ_2 -OH)(μ_2 -Cl)Cl ₂] · 1.5H ₂ O	3.001(2)	101.8(2)	1.60	200		35
[Cu ₂ (PAP)(μ_2 -OH)(μ_2 -IO ₃)(IO ₃) ₂]	3.165(1)	113.8(2)	1.49	290		35
[Cu ₂ (PAP)(μ_2 -OH)(μ_2 -SO ₄)Cl] · 2H ₂ O	3.211(1)	115.5(1)	1.01	516		37
[Cu ₂ (PAP6Me)(μ_2 -OH)(μ_2 -Cl)Cl ₂] · 3H ₂ O	3.137(2)	112.2(4)	1.10	432(5)	0.41	54
[Cu ₂ (PAP4Me)(μ_2 -OH)(μ_2 -NO ₃)(NO ₃)(H ₂ O) ₂](NO ₃)	3.138(1)	115.3(1)	1.02	497		35
[Cu ₂ (PAP6Me)(μ_2 -OH)(μ_2 -NO ₃)(NO ₃) ₂]	3.134(2)	114.1(5)	0.98	501(4)	0.86	56
[Cu ₂ (PAP46Me)(μ_2 -OH)(NO ₃) ₂ (H ₂ O) ₂](NO ₃) ₂	3.156(2)	113.7(3)	1.02	597(5)	0.89	37
[Cu ₂ (PPDMe)(μ_2 -OH)(NO ₃) ₂ (H ₂ O) ₂](NO ₃)	3.338(1)	119.3(2)	1.03	750(50)		37
[Cu ₂ (PPD)(μ_2 -OH)Cl ₃ (H ₂ O)] · 0.8H ₂ O	3.454(1)	116.4(1)	0.55	898(13)	0.41	51
[Cu ₂ (PPD)(μ_2 -OH)Br ₃ (H ₂ O)] · 0.6H ₂ O	3.413(2)	118.9(1)	Dia.	1304	0.47	51

Table 1-2. Structural, magnetic and electrochemical data for dinuclear copper(II) complexes of polydentate diazine ligands (continued)

Compound	Cu...Cu (Å)	Cu-OH-Cu (°)	μ_{eff} (RT)	-2J (cm ⁻¹)	E _{1/2} (V)* (vs. SCE)	Ref.
[Cu ₂ (MIP)(μ ₂ -OH)Cl ₃ (H ₂ O)] · H ₂ O	3.425(1)	126.3(2)	0.62	800(40)		35
[Cu ₂ (MIP)(μ ₂ -OH)Br ₃ (H ₂ O)] · H ₂ O	3.420(2)	124.9(4)	0.43	992	0.44	51
[Cu ₂ (BDPDZ)(μ ₂ -Cl) ₂ Cl ₂ (H ₂ O)] · 3.5H ₂ O	3.511(1)			79.6		66
[Cu ₂ (BDPDZ)(μ ₂ -Br) ₂ Br ₂] · 2CH ₃ CN	3.673(2)			98.1		66
[Cu ₂ (BLEP)(μ ₂ -Cl)Cl(H ₂ O)]	3.652(2)		1.68			79
[Cu ₂ (BLEMP)(μ ₂ -Br)Br ₃]	3.789(2)		1.33			79
[Cu ₂ (PZEN)(OH)(H ₂ O) ₂]	4.440		1.63			79
[Cu ₂ (APHP-H)(μ ₂ -OH)(H ₂ O) ₂](ClO ₄) ₂ · H ₂ O	3.295(2)	117.3(3)	0.34	990(50)	0.50	55
[Cu ₄ (TNL4)(μ ₂ -OH) ₂ (H ₂ O) ₄](CF ₃ SO ₃) ₆ · 6H ₂ O	3.202(2)	116.3(3)	1.24	334(6)		81
[Cu ₄ (TNL)](μ ₂ -OH) ₂ (H ₂ O) ₆ (EtOH) ₂](CF ₃ SO ₃) ₆	3.190(2)	116.0(5)	1.06	436(8)		81

*Scan rate 50 - 200 mV/sec. 3×10^{-3} to 5×10^{-4} M complex in DMF or acetonitrile, 0.1 M tetraethylammonium perchlorate, glassy carbon working electrode, and saturate calomel reference electrode.

copper separation makes it impossible for a third bridge group to bind to two metal centres simultaneously. The complexes involving hydroxide bridges usually have a larger bridge angle (122 - 126°) [35, 39, 42, 43, 51]. The six-membered chelate system however usually forms triply bridged complexes with shorter copper-copper separations (3.0 - 3.2 Å) and smaller Cu-OH-Cu angles (101 - 116°) [35, 37, 51, 52, 55, 81].

Replacement of the central six-membered diazine (phthalazine and pyridazine) rings by a five-membered heterocycle (pyrazole, 1,2,4-triazole) results in an increase in the intermetallic separation. The pyrazolato, triazolato and triazole bridged dinuclear complexes (Cu_2N_3) (Table 1-1) usually have larger copper-copper separation (>3.90 Å) than pyridazine and phthalazine bridged analogous (<3.80 Å). When the phthalazine group in APHP is replaced by pyrazole in a series of similar ligands such as BLEPH (3,5-bis-(4'-pyridyl-2'-thiabut-1'-yl)pyrazole), BLMPH (3,5-bis-(3'-pyridyl-2'-thiapropr-1'-yl)pyrazole) and PZEN (Scheme 1-8), the copper-copper separations become much larger (>3.65 Å) (Table 1-2), while in $[\text{Cu}_2(\text{APHP-H})(\mu_2\text{-OH})(\text{H}_2\text{O})_2]^{2+}$ the copper-copper separation is only 3.190 Å with a Cu-OH-Cu angle of 116.0° [37]. Apparently the replacement of the hydroxide group by halide (Cl, Br) in BLEPH and BLMPH complexes [79] is not the major reason which makes the copper-copper separation so different. The extremely large copper-copper separation in

$[\text{Cu}_2(\text{PZEN})(\text{OH})(\text{H}_2\text{O})_2]$ (4.440 Å) [79] makes it impossible for the hydroxide to bridge two copper centres simultaneously and only binds to one copper atom terminally.

The copper-copper separations and hydroxide bridge angles will also increase when the third bridge group (Y in II, Scheme 1-10) becomes larger. It is very clear by comparing the analogous complexes of PAP (Table 1-2). The copper-copper separations and hydroxide bridge angles in $[\text{Cu}_2(\text{PAP})(\mu_2\text{-OH})(\mu_2\text{-SO}_2)\text{Cl}]$ (3.211 Å, 115.5°) and $[\text{Cu}_2(\text{PAP})(\mu_2\text{-OH})(\mu_2\text{-IO}_3)(\text{IO}_3)_2]$ (3.165 Å, 113.8°) are much larger than that in $[\text{Cu}_2(\text{PAP})(\mu_2\text{-OH})(\mu_2\text{-X})\text{X}_2]$ (3.010 Å, 102.9° for X = Br; 3.001 Å, 101.8° for X = Cl) due to replacement of the smaller halide by the larger three atom bridge groups SO_4 and IO_3 .

Dinuclear copper(II) complexes only bridged by diazine groups are rare (Scheme 1-9). The planarity of the complexes of the ligands illustrated in Scheme 1-7 results from the formation of terminal five-membered chelate rings in all cases, which makes a very efficient overlap between the copper magnetic orbitals and the diazine bridges. All these complexes show moderately strong antiferromagnetic interactions (Table 1-1) and spin-coupling between the two copper centres occurs only through a superexchange mechanism involving the diazine bridges. These complexes allow a direct comparison to be made on the effects of the diazine bridges themselves on the spin coupling between two copper(II) ions.

The structural and magnetic properties of dinuclear copper(II) complexes of DHPH (1,4-dihydrazinophthalazine) [62] and DPYH (3,6-dialdoxime-pyridazine) [67] (Table 1-1) provide a very realistic comparison between the exchange capacities of the phthalazine and pyridazine bridges. The complexes have planar, dinuclear six-coordinate structures, with four in-plane nitrogen donors per metal, with comparable in-plane Cu-N distances, angles, and axial contacts to a water and perchlorate and Cu...Cu separations. Antiferromagnetic coupling in the DHPH complex ($-2J = 489 \text{ cm}^{-1}$) is significantly less than that occurring in DPYH complex ($-2J = 536 \text{ cm}^{-1}$). The close structural comparison between the complexes of DHPH and DPYH, involving almost identical, distorted six-coordinate copper ion chromophores, clearly suggests that the presence of the fused benzene ring, with its capacitor-like action for delocalized metal unpaired spin, results in less efficient antiferromagnetic interaction between the two copper(II) centres. The recent structural and magnetic studies on TNLr systems (Scheme 1-8) in our group [81, 82] have shown significant cross-ring coupling ($-J = 36 - 210 \text{ cm}^{-1}$) in their tetranuclear complexes, which involve benzodipyridazine groups linking four copper centres, clearly indicating that copper charge has been delocalized into the fused benzene ring, some of which is coupled antiferromagnetically, and some may be capacitively stored in the aromatic system, as is the case in the phthalazine derivatives.

In a series of structurally related complexes of BPYPZ (3,5-bis(pyridin-2-yl)-pyrazole) [72], HBAMPZ (3,5-bis(aminomethyl)-pyrazole) [78], and DPAP (3,5-bis[(2-diethylamino)ethylaminomethyl]-pyrazole) [76] involving bis(μ -pyrazolato)-bridged dinuclear copper(II) centres, exchange integrals ($-2J$) fall in the range 362 - 428 cm^{-1} , indicating much weaker antiferromagnetic exchange than that occurring in complexes of DHPH and DPYH. This is due to the fact that the pyrazolato ring has an extra electron and a negative charge would probably inhibit accumulation of more charge from the two coppers and larger Cu...Cu distances (Table 1-1) resulting from the five-membered pyrazole ring, which would have the effect of reducing antiferromagnetic coupling.

For the related di- μ -(1,2,4-triazole) dicopper(II) complexes of AAMT (4-amino-3,5-bis(aminomethyl)-1,2,4-triazole) [68], the exchange integrals were determined to be around 220 cm^{-1} . For the di- μ -(1,2,4-triazolato) dicopper(II) complex of BPT (3,5-bis(2-pyridyl)-1,2,4-triazolato) [69] an exchange integral of 236 cm^{-1} was observed. The antiferromagnetic coupling in dinuclear copper(II) complexes doubly bridged by 1,2,4-triazole groups is much lower than in corresponding pyrazolato bridged analogues, due to the presence of one more nitrogen atom within the triazole group which has the ability to polarize spin within the triazole ring itself and thus limit exchange.

From these studies it is clear that for structurally related planar dinuclear

copper(II) complexes with different diazine bridges, the neutral pyridazine is more effective in mediating antiferromagnetic coupling than phthalazine which is more effective than other five-membered diazine groups. Of the five-membered ring diazine bridges, the pyrazolate bridge is a stronger mediator than 1,2,4-triazolate and 1,2,4-triazole bridges in conducting antiferromagnetic spin-coupling between two copper(II) ions.

The polydentate ligands in Scheme 1-8 usually form a series of copper(II) complexes in which the dinuclear centres have multiple bridges which are involved in superexchange between the copper atoms (Table 1-2) [35, 37, 40, 42, 45, 51, 52, 66, 81]. The diazine (N=N) fragment is the common focus of these polynucleating ligands and additional bridging groups include hydroxide, halide and some bidentate anions e.g. nitrate, sulfate, and iodate. The effects of changing hydroxide bridge angle (Cu-OH-Cu), chelate ring size, and electronegativity of bridging and nonbridging ligands on superexchange can be illustrated by comparing the magnetic properties of these complexes.

For a series of hydroxide bridged dinuclear copper(II) complexes of PAPR, which contain an 'essentially constant' dinuclear centre involving the two copper atoms and the diazine group, with $d_{x^2-y^2}$ ground state copper ions, a reasonably linear relationship (eq. 3) was observed between the exchange integral ($-2J$) and the Cu-OH-Cu bridge angle (α) [56], a study which complemented the earlier,

classical study of Hatfield and coworkers on dihydroxy bridged dicopper(II) complexes (eq. 1) [15].

$$-2J = 23.06\alpha - 2143 \text{ cm}^{-1} \dots\dots [3]$$

The antiferromagnetic coupling between the two copper(II) centres is proportional to the hydroxide bridge angle (α) when $\alpha > 92.9^\circ$ ($\alpha = 92.9^\circ$, $-2J = J_F + J_{AF} = 0$). The two copper centres in $[\text{Cu}_2(\text{PAP})(\mu_2\text{-OH})(\mu_2\text{-SO}_4)\text{Cl}] \cdot 2\text{H}_2\text{O}$ ($\alpha = 115.5^\circ$, $-2J = 516 \text{ cm}^{-1}$) are much more strongly coupled than in $[\text{Cu}_2(\text{PAP})(\mu_2\text{-OH})(\mu_2\text{-X})\text{X}_2] \cdot 2\text{H}_2\text{O}$ ($\alpha = 101.8^\circ$, $-2J = 200 \text{ cm}^{-1}$ for $\text{X} = \text{Cl}$, and $\alpha = 102.9^\circ$, $-2J = 190 \text{ cm}^{-1}$ for $\text{X} = \text{Br}$) [37, 56] (Table 1-2).

The chelate ring size, the presence of a third bridge group (other than diazine and hydroxide) and the identity of the central diazine group will affect magnetic exchange by changing the copper-copper separation and hydroxide bridge angle. The presence of five-membered chelate rings, larger third bridge group (SO_4 , IO_3) and five-membered diazine group (pyrazole) will result in increases in copper-copper separation and hydroxide bridge angles and thus result in an increase in antiferromagnetic coupling (Table 1-2), assuming the hydroxide bridge is the dominant variable pathway for superexchange [56].

The electronegativity of the peripheral donors (X in Scheme 1-10) has a

significant influence on antiferromagnetic coupling between two copper(II) centres [35, 42, 44, 51, 53, 56, 57]. For dinuclear complexes of MIP, PTP, BDPDZ (Scheme 1-8), a marked increase in exchange (Table 1-2) is observed when bromide replaces chloride, even though structural studies suggest that the halide complexes of each ligand have the same effective pathway for magnetic interaction. The axially bound halogen atoms are not expected to have any significant influence on the copper magnetic interaction as they usually bridge the two copper centres through equatorial-axial interactions and have weak axial bonding contacts ($> 2.5 \text{ \AA}$) to the copper centres [37, 49, 56, 57]. However, the shorter in-plane halogen contacts ($< 2.4 \text{ \AA}$) will influence the copper magnetic orbital. As they are bound terminally, their major influence can be considered in terms of how they would polarize the electron density in the copper centres. The more electronegative chloride atom will polarize the electron density in the copper magnetic orbitals which participates in the exchange process, effectively localizing it to some degree at the copper centre, with smaller resulting magnetic exchange.

Electrochemical studies have shown that in general negative reduction potentials (V vs. SCE) prevail for dinuclear copper(II) complexes involving oxygen atoms bridges [83 - 89], even though in many cases strong antiferromagnetic exchange is observed. However positive reduction potentials ($E_{1/2} = 0.23 - 0.89 \text{ V vs SCE}$), comparable with those of type III copper protein centres found in

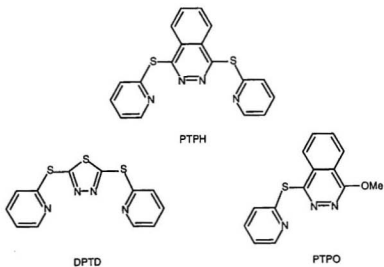
certain oxidases and oxygenases (e.g. fugal laccase, $E_{1/2} = +0.78$ V [90]; tree laccase, $E_{1/2} = 0.434$ V [90]; tyrosinase $E_{1/2} = 0.360$ V [91] (vs SHE)), were observed for some antiferromagnetically coupled, hydroxide bridged, dinuclear copper(II) complexes of polydentate diazine ligands [46, 48, 51, 52 - 54] (Table 1-2) and involved sequential two-electron transfer at the same potential to give dinuclear copper(I) species. Stable dinuclear copper(I) complexes with some of these ligands have also been isolated [53, 64]. The redox processes observed for many of these systems, which contain six-membered chelate ring, are reversible or quasi-reversible due to the flexibility imparted to the systems by the ligands. The complexes of PAPR (Scheme 1-8) are a small group of such systems [35, 54, 56]. The lack of electrochemical reversibility associated with ligands which generate five-membered chelate rings, for example, the complexes of PPD and MIP (Scheme 1-8) [51], can be attributed in part to their rigid, planar structures which would not accommodate the likely geometrical change to form copper(I) species easily.

1.2. The Tetradentate (N_4) Thio-diazine Ligands Involved in This Study

This chapter presents a study of a series dinuclear copper complexes of the thio-diazine ligands PTPH (PTPH = 1,4-di-(2'-pyridylthio)phthalazine), DPTD (DPTD = 2,5-di-(2'-pyridylthio)thiadiazole) (Scheme 1-11), and PTP (PTP = 3,5-

di-(2'-pyridylthio)pyridazine) (Scheme 1-8). These three ligands are all N_4 tetradentate ligands and will form six-membered chelate ring when coordinated to copper ions, but the diazine bridges are different. The isostructural complexes of these ligands will create an ideal framework for magneto-structural studies, in which the effect of the diazine bridge on magnetic exchange can be investigated.

Scheme 1-11.



1.3. Experimental

Commercially available reagents (Aldrich) were used without further purification. Tetrahydrofuran (THF) was distilled from sodium/benzophenone.

Infrared spectra were recorded as Nujol mulls using a Mattson Polaris FT-IR instrument. Electronic spectra were recorded as mulls using a Cary 5E spectrometer. ESR spectra were recorded with a Bruker 300 X-band spectrometer at room temperature and 77K. Mass spectra were obtained using a VG micromass 7070 HS spectrometer and nmr spectra using a GE 300 MHz instrument. X-ray diffraction data were collected using a Rigaku AFC6S instrument. Room temperature magnetic moments were measured using a Cahn 7600 Faraday magnetic balance and variable temperature magnetic data (5-300K) were obtained using an Oxford Instruments superconducting Faraday susceptometer with a Sartorius 4432 microbalance. A main solenoid field of 1.5T and a gradient field of 10Tm^{-1} were employed and $\text{Hg}[\text{Co}(\text{NCS})_4]$ was used as a calibration standard.

Electrochemical measurements were performed at room temperature in dimethylformamide (DMF) (spectro-quality grade dried over molecular sieves) under O_2 free conditions, using a BAS CV-27 voltammograph and a Hewlett-Packard X-Y recorder. For cyclic voltammetry a three electrode system was used in which the working electrode was glassy-carbon or platinum, the counter electrode platinum and with a saturated calomel (SCE) or silver wire reference

electrode. For constant potential electrolysis (CPE) a three component 'H' cell was used with a central 5 mL working compartment separated from auxiliary and reference compartments by medium porosity sintered glass frits. The working electrode was a platinum mesh 'flag', the auxiliary electrode a platinum wire, with a silver wire reference electrode. The supporting electrolyte was 0.1 M tetraethylammonium perchlorate (TEAP). All potentials ($E_{1/2}$ values) are reported versus the standard calomel electrode (SCE). For cyclic voltammetry all solutions were 10^{-3} - 10^{-4} M in complex.

Elemental analyses were carried out by Canadian Microanalytical Laboratories, Delta, Canada. Melting points were measured on a Fisher-John's melting point apparatus and are uncorrected.

1.3.1. Synthesis of the Ligands

1,4-di-(2'-pyridylthio)-phthalazine (PTPH)

The synthesis of PTPH was previously reported [48]. However it was prepared by using the following modified method: Sodium metal (0.46 g, 0.02 mmol) was dissolved in degassed absolute ethanol (50 mL) under N_2 and the solution refluxed for 30 min. A solution of pyridine-2-thiol (2.23 g, 0.02 mmol) in warm degassed absolute ethanol (50 mL) was then added. The reaction mixture was stirred at 60-70 °C for 30 min and a solution of 1,4-dichlorophthalazine (2.0

g, 0.01 mmol) in degassed absolute THF (50 mL) added dropwise, with stirring, over a period of 1 h. The reaction mixture was refluxed for 6 h and left at room temperature overnight and the solvents were evaporated to dryness. The residue was extracted with CHCl_3 , and dried with anhydrous Na_2SO_4 . The volume of the CHCl_3 solution was reduced to 10 mL and put in the refrigerator, until yellow crystals formed. Yield: 2.71 g (78%). The compound has the same melting point and mass spectrum as reported before.

3,6-di-(2'-pyridylthio)-pyridazine (PTP)

The synthesis of PTP was reported earlier [48] and was prepared by using the modified method similar to that for PTPH and was obtained as pale yellow crystals.

2,5-di-(2'-pyridylthio)-thiadiazole (DPTD)

Sodium metal (1.15 g, 0.050 mol) was dissolved in 50 mL absolute EtOH under N_2 . 2,5-dimercapto-1,3,4-thiadiazole (3.76 g, 0.025 mol) was added and refluxed for 0.5 h. 2-Bromopyridine (7.90 g, 0.050 mol) dissolved in 50 mL EtOH was then added dropwise over a period of 1 h with continued refluxing. The mixture was further refluxed for 0.5 h and cooled to room temperature. The solvent was evaporated to dryness and the residue was extracted with CHCl_3 . The CHCl_3 was washed with deionized water and dried over Na_2SO_4 . The volume of

the CHCl_3 solution was reduced to 25 mL, and 25 mL EtOH was added. A pale yellow crystalline compound was isolated. Yield: 3.20 g (42%). Mass spectrum, major mass peaks (m/e (relative intensity)): 304 (5) P, 168 (91), 136 (5), 110 (10), 78 (100). $^1\text{H NMR}$ (CDCl_3) (δ (relative intensity)): 7.25 (multiplet, 2H, py), 7.43 (multiplet, 2H, py), 7.67 (multiplet, 2H, py), 8.55 (multiplet, 2H, py).

1.3.2. Synthesis of the Complexes

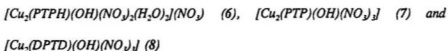
[Cu₂(PTPH)Cl₄·2H₂O (1), [Cu₂(DPTD)Cl₄] (2), [Cu₂(PTPH)Br₄]·1.5H₂O (3) and [Cu₂(DPTD)Br₄] (4)

PTPH (0.35 g, 1.0 mmol) was dissolved in boiling MeOH (40 mL) and a solution of 0.35 g of $\text{CuCl}_2 \cdot 2\text{H}_2\text{O}$ (2.0 mmol) in 10 mL H_2O added. The resulting mixture was allowed to stir at room temperature for 2 h. Green crystals formed, which were filtered off, washed with methanol and dried under vacuum. Yield: 0.46 g (70%). Anal. Calcd for $\text{C}_{18}\text{H}_{20}\text{N}_4\text{O}_2\text{S}_2\text{Cl}_4\text{Cu}_2$ (1): C 33.09, H 2.47, N 8.57; Found: C 33.15, H 2.25, N 8.22. The crystals for X-ray diffraction were obtained by diffusing diethyl ether into a methanol solution of the complex, and have the formula $[\text{Cu}_2(\text{PTPH})\text{Cl}_4] \cdot 2\text{CH}_3\text{OH}$. $[\text{Cu}_2(\text{DPTD})\text{Cl}_4]$ (2), $[\text{Cu}_2(\text{PTPH})\text{Br}_4] \cdot 1.5\text{H}_2\text{O}$ (3) and $[\text{Cu}_2(\text{DPTD})\text{Br}_4]$ (4) were prepared in a similar manner using CuCl_2 and CuBr_2 . 2 was obtained as a green crystalline compound. Yield: 0.34 g (60%).

Anal. Calcd for $C_{12}H_{10}N_4S_3Cl_4Cu_2$ (2): C 25.14, H 1.41, N 9.77; Found: C 24.82, H 1.45, N 9.92. **3** was obtained as brown crystals. Yield: 0.70 g (84%). Anal. Calcd for $C_{18}H_{13}N_4O_{1.5}S_2Br_4Cu_2$ (3): C 26.30, H 1.84, N 6.82; Found: C 26.15, H 1.61, N 7.20. **4** was obtained as greenish brown crystals. Yield: 0.52 g (69%). Anal. Calcd for $C_{12}H_{10}N_4S_3Br_4Cu_2$ (4): C 19.19, H 1.07, N 7.46; Found: C 19.11, H 1.17, N 7.94.



PTPH (0.35 g, 1.0 mmol) was dissolved in $CHCl_3$ (5 mL) and a solution of $Cu(NO_3)_2 \cdot 3H_2O$ (0.48 g, 2.0 mmol) in 30 mL CH_3CN added. The light blue coloured solution was kept at room temperature overnight. Light blue crystals formed, which were filtered off, washed with acetonitrile and dried under vacuum. Yield: 0.63 g (90%). Anal. Calcd for $C_{18}H_{15}O_{11}N_7S_2Cu_2$: C 31.04, H 2.17, N 14.08; Found: C 31.36, H 2.22, N, 14.44.



PTPH (0.35 g, 1.0 mmol) was dissolved in $CHCl_3$ (5 mL) and a solution of $Cu(NO_3)_2 \cdot 3H_2O$ (0.48 g, 2.0 mmol) in 35 mL H_2O/CH_3CN mixture (1:6) was added. The deep blue solution was kept at room temperature overnight. Dark blue crystals formed, which were filtered off and dried under vacuum. Yield: 0.46 g

(65%). Anal. Calcd for $C_{18}H_{13}N_7O_{11}S_2Cu_2$ (**6**): C 31.04, H 2.17, N 14.08; Found: C 31.43, H 2.28, N 14.44. Although two water molecules show up in the X-ray structure of **6**, the elemental analysis clearly shows one water molecule is lost on drying. $[Cu_2(PTP)(OH)(NO_3)_3]$ (**7**) and $[Cu_2(DPTD)(OH)(NO_3)_3]$ (**8**) were prepared in a similar manner and were obtained only as dark blue crystals. Yield: 0.51 g (75%) for **7** and 0.40 g (63%) for **8**. Anal. Calcd for $C_{14}H_{11}N_7O_{10}S_2Cu_2$ (**7**): C 26.76, H 1.77, N 15.60; Found: C 26.83, H 1.80, N 15.64. Anal. Calcd for $C_{12}H_{11}N_7O_{10}S_3Cu_2$ (**8**): C 22.71, H 1.43, N 15.48; Found: C 22.90, H 1.53, N 15.72.

$[Cu_2(PTPH)(OH)Cl] \cdot 1.5CHCl_3$ (**9**), $[Cu_2(PTPH)(OH)Br] \cdot CHCl_3 \cdot H_2O$ (**10**) and $[Cu_2(PTP)(OH)Cl] \cdot 2CH_3CN$ (**11**)

Copper powder (0.19 g, 3.0 mmol) was added to a solution of $CuCl_2 \cdot 2H_2O$ (0.17 g, 1.0 mmol) in CH_3CN (20 mL), the mixture was stirred under a nitrogen atmosphere until the solution became colourless, and then filtered into a solution of PTPH (0.175 g, 0.50 mmol) in $CHCl_3$ (20 mL) under a nitrogen atmosphere. The resulting dark red solution was allowed to stand at room temperature and oxidized slowly by air for several weeks. The colour of the solution changed from red to brown and finally to green. After leaving this green solution for a few days, dark green crystals formed which were filtered off, washed with CH_3CN and

CHCl_3 and air dried. Yield: 0.10 g (28%). The crystals lost solvent slowly in the air. Anal. Calcd for $\text{C}_{19.2}\text{H}_{14.2}\text{N}_4\text{OS}_2\text{Cl}_{4.6}\text{Cu}_2$ (9) (partially lost solvent): C 31.76, H 1.82, N 7.80; Found: C 31.04, H 2.04, N 7.63. $[\text{Cu}_2(\text{PTPH})(\text{OH})\text{Br}_3] \cdot \text{CHCl}_3 \cdot \text{H}_2\text{O}$ (10) and $[\text{Cu}_2(\text{PTP})(\text{OH})\text{Cl}_3] \cdot 2\text{CH}_3\text{CN}$ (11) were prepared in a similar manner and were obtained as dark green crystals. Yield: 0.10 g (25%) for 10 and 0.16 g (57%) for 11. Anal. Calcd for $\text{C}_{19}\text{H}_{16}\text{N}_4\text{O}_2\text{S}_2\text{Cl}_3\text{Br}_3\text{Cu}_2$ (10): C 26.24, H 1.85, N 6.44; Found C 26.07, H 1.66, N 6.26. Anal. Calcd for $\text{C}_{14}\text{H}_{13}\text{N}_4\text{OS}_2\text{Cl}_3\text{Cu}_2$ (11) (two molecules of CH_3CN were lost when dried under vacuum): C 30.64, H 1.84, N 10.21; Found C 30.56, H 2.03, N 10.20.

$[\text{Cu}_2(\text{PTPH})_2(\text{ClO}_4)_2 \cdot 2\text{CH}_3\text{CN}$ (12)

Copper powder (0.19 g, 3.0 mmol) was added to a solution of $\text{Cu}(\text{ClO}_4)_2 \cdot 6\text{H}_2\text{O}$ (0.15 g, 0.4 mmol) in CH_3CN (40 mL). The mixture was stirred under a nitrogen atmosphere until the solution became colourless, and then filtered into a solution of PTPH (0.175 g, 0.50 mmol) in CHCl_3 (10 mL) under a nitrogen atmosphere. The resulting deep red solution was allowed to stand at room temperature for several days. Red crystals formed, which were filtered off, washed with CH_3CN and CHCl_3 and air dried. Yield: 0.15 g (53%). Anal. calcd for $\text{C}_{40}\text{H}_{30}\text{N}_{10}\text{O}_8\text{S}_4\text{Cl}_2\text{Cu}_2$: C 43.48, H 2.74, N 12.68; Found: C 43.27, H 2.55, N 12.40.

$\{[Cu(PTPO)_2(H_2O)]\{CuCl_2\}[Cu(PTPO)Cl_2]\} \cdot 2.8H_2O$ (13) (PTPO = 1-methoxy-4-(2'-pyridylthio)phthalazine (Scheme 1-11))

PTPH (0.175 g, 0.50 mmol) was dissolved in hot methanol (40 mL) and triethylamine (1.26 g, 1.25 mmol) was added. This solution was added to a solution of $CuCl_2 \cdot 2H_2O$ (0.213 g, 1.25 mmol) in H_2O (10 mL). The resulting green solution was refluxed for 30 minutes and filtered. The yellowish green filtrate was allowed to stand at room temperature for several days. A deep green crystalline complex formed which was filtered off, washed with ethanol. Dark green crystals suitable for X-ray diffraction were obtained by diffusing ether into a CH_3OH/H_2O (4:1) solution of the complex. Yield: 0.062 g (29%). The composition of the complex was confirmed by X-ray crystallography.

1.4. Results and Discussion

1.4.1. Ligands

The diazine moiety in tetradentate 1,4-disubstituted phthalazines, 3,6-disubstituted pyridazines and 2,5-disubstituted thiadiazoles has been shown to be an effective dinucleating centre, bridging the metal ions (in most cases copper) in close proximity [35, 37, 47 - 49, 51 - 54, 56, 58, 80], with the formation of halogen-bridged and hydroxo-bridged complexes. Ligands of this sort have been

synthesized by nucleophilic displacement from halogenated pyridazines and phthalazines or by ring expansion of disubstituted isoindolines. In most of the previously reported cases the ligands have involved nitrogen donor substituents (e.g. pyridines, imidazoles, pyrazoles) bound directly to the diazine moiety or *via* an intervening secondary amine centre. In this work the ligand syntheses are based on the very effective nucleophilic displacement of chloride from 3,6-dichloropyridazine (PTP) and 1,4-dichlorophthalazine (PTPH) or bromide from 2-bromopyridine (for DPTD) by thiolate derivatives. The ligand PTPO (Scheme 1-11) was formed when we tried to prepare a hydroxide bridged CuCl_2 complex of PTPH in a $\text{NEt}_3/\text{MeOH}/\text{H}_2\text{O}$ mixture. The structures of the three thio-diazine ligands are shown in Schemes 1-8 & 1-11.

1.4.2. Structures

$[\text{Cu}_2(\text{PTPH})\text{Cl}_4] \cdot 2\text{CH}_3\text{OH}$ (1)

The molecular structure of $[\text{Cu}_2(\text{PTPH})\text{Cl}_4] \cdot 2\text{CH}_3\text{OH}$ (1) is shown in Fig. 1-3 and consists of two distorted square-pyramidal copper centres bound to the tetradentate ligand, PTPH and bridged by the diazine nitrogen atoms ($\text{N}2, \text{N}2'$) and two chlorine atoms. Interatomic distances and angles relevant to the copper coordination spheres are given in Table 1-3. The copper-nitrogen and copper-

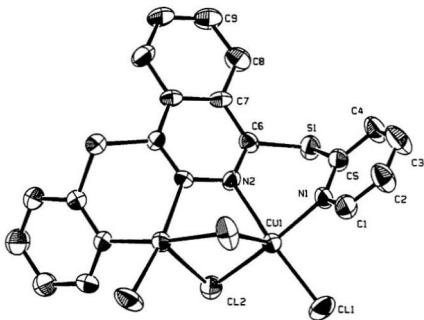


Fig. 1-3. Structural representation of [Cu₂(PTPH)Cl₄]·2CH₃OH (1), with hydrogen atoms omitted (40% probability ellipsoids).

Table 1-3. Selected bond distances (Å) and angles (deg) for $[\text{Cu}_2(\text{PTPH})\text{Cl}_4] \cdot 2\text{CH}_3\text{OH}$ (1)

Cu(1)-N(1)	2.017(5)	Cu(1)-N(2)	2.076(4)
Cu(1)-Cl(1)	2.236(2)	Cu(1)-Cl(2)	2.266(2)
Cu(1)-Cl(2)a	2.666(2)	Cu(1)-Cu(1)a	3.119(2)
Cl(1)-Cu(1)-Cl(1)	93.27(7)	Cl(1)-Cu(1)-N(1)	91.1(1)
Cl(1)-Cu(1)-N(2)	169.0(1)	Cl(2)-Cu(1)-N(1)	173.2(2)
Cl(2)-Cu(1)-N(2)	87.2(1)	N(1)-Cu(1)-N(2)	87.6(2)
Cu(1)-Cl(2)-Cu(1)a	80.35(9)		

chloride distances are close to those found for the analogous complex, $[\text{Cu}_2(\text{PTP})\text{Cl}_4] \cdot \text{CH}_3\text{CH}_2\text{OH}$ [49], which has the same triply bridged structure, but the Cu-N (phthalazine) distance (2.076(4) Å) is slightly longer than the Cu-N (pyridine) distance (2.017(5) Å), which is contrary to the situation in $[\text{Cu}_2(\text{PTP})\text{Cl}_4] \cdot \text{CH}_3\text{CH}_2\text{OH}$ (Cu-N (pyridazine) (av.) 2.072 Å, Cu-N (pyridine) (av.) 2.005 Å). The two chloride bridges are bound asymmetrically with respect to the two square-pyramidal copper centres, with each one occupying an axial and an equatorial ligand position. The axial interaction is weak with a long copper-chloride bond (2.666(2) Å), while the equatorial ligands are much more strongly

bound (2.236(2), 2.266(2) Å). The copper-copper separation (3.119(2) Å) is shorter than that for $[\text{Cu}_2(\text{PTP})\text{Cl}_4] \cdot \text{CH}_3\text{CH}_2\text{OH}$ (3.198(1) Å). The Cu-Cl-Cu (80.35(9)°) angles are very close to those found for $[\text{Cu}_2(\text{PTP})\text{Cl}_4] \cdot \text{CH}_3\text{CH}_2\text{OH}$ (80.67° (av.)). The ligand in **1** adopts a pronounced *anti* twist, creating an angle of 56.5° between the copper square-planes and angles of 53.1° between the copper planes and the phthalazine plane. The copper centre is displaced slightly from the N_2Cl_2 least-squares plane by 0.154(5) Å and the pyridine mean planes are twisted by 52.7° with respect to the phthalazine mean plane.

$[\text{Cu}_2(\text{DPTD})\text{Br}_4]$ (**4**)

The structure of $[\text{Cu}_2(\text{DPTD})\text{Br}_4]$ (**4**) is shown in Fig. 1-4, and interatomic distances and angles relevant to the copper coordination sphere are given in Table 1-4. Compounds **4** and **1** have very similar structures. The molecule has a two-fold symmetry axis which bisects the dinuclear centre. The copper centres are bound in a triple bridged arrangement involving two bromo-bridges and a thiadiazole diazine bridge. The angle at the bromine bridge is 84.34(4)°, with a copper-copper separation of 3.556(2) Å. The copper-copper separation and Cu-Br-Cu angle are significantly larger than those found for the analogous doubly bromo-bridged complex $[\text{Cu}_2(\text{PTP})\text{Br}_4]$ (3.318(3) Å, 79.28(2)°) [57] and can be attributed to the replacement of a six-membered pyridazine ring by a five-membered thiadiazole

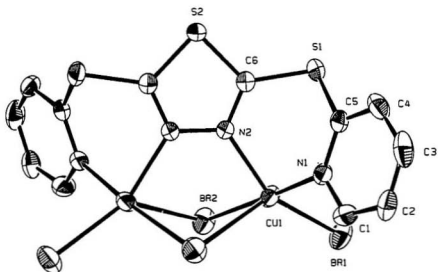


Fig. 1-4. Structural representation of $[\text{Cu}_2(\text{DPTD})\text{Br}_2]$ (**4**), with hydrogen atoms omitted (40% probability ellipsoids).

Table 1-4. Selected bond distances (Å) and angles (deg) for $[\text{Cu}_2(\text{DPTD})\text{Br}_2]$ (**4**)

Br(1)-Cu(1)	2.376(1)	Br(2)-Cu(1)	2.412(1)
Cu(1)-N(1)	2.034(5)	Cu(1)-N(2)	2.043(4)
Cu(1)-Br(2)	2.861(1)	Cu(1)-Cu(1)a	3.556(2)
Br(1)-Cu(1)-Br(2)	94.88(4)	Br(1)-Cu-N(1)	90.8(1)
Br(1)-Cu(1)-N(2)	150.5(1)	Br(2)-Cu-N(1)	173.6(2)
Br(2)-Cu(1)-N(2)	90.3(1)	N(1)-Cu(1)-N(2)	86.1(2)
Cu(1)-Br(2)-Cu(1)a	84.34(4)		

ring, which has the effect of forcing the metal centres further apart. The increased copper-copper separation in **4** is also accompanied by an increased Cu-N-N (diazine) angle ($122.6(1)^\circ$ in **4**, $117.5(9)^\circ$ in $[\text{Cu}_2(\text{PTP})\text{Br}_4]$) (This angle falls in the range $113.1 - 118.0^\circ$ in other related diazine bridged complexes [57]). The Cu-N (thiadiazole) distances ($2.043(4) \text{ \AA}$) are significantly shorter than those observed for similar complexes of BMPTD (BMPTD = 2,5-di-(methylpyridylthio)-thiadiazole) ($2.21 - 2.27 \text{ \AA}$) [80] which forms seven-membered chelate ring, and can be attributed to the difference in the chelate ring size. The Cu-N (pyridine) distances ($2.034(5) \text{ \AA}$) are quite normal for ligands of this sort.

The stereochemistry at each copper atom can best be described as a distorted square pyramid in which the copper atom is displaced by $0.241(3) \text{ \AA}$ from the mean plane of the basal donor set (N(1), N(2), Br(1), Br(2)) towards the axial bromine atom. The two bridged bromides are bound asymmetrically with respect to the two square-pyramidal copper centres, with each one occupying an axial and equatorial ligand position. The equatorial Cu-Br distances ($2.376(1)$, $2.412(1) \text{ \AA}$) are comparable with those in $[\text{Cu}_2(\text{PTP})\text{Br}_4]$ ($2.375(3) - 2.4139(25) \text{ \AA}$), but the axial Cu-Br distance ($2.861(1) \text{ \AA}$) is longer than those in $[\text{Cu}_2(\text{PTP})\text{Br}_4]$ ($2.766(3)$, $2.801(3) \text{ \AA}$) [57].



The structure of $[\text{Cu}_2(\text{PTPH})(\text{OH})(\text{NO}_3)_3(\text{H}_2\text{O})]_2$ (5) is shown in Fig. 1-5, and interatomic distances and angles relevant to the copper coordination spheres are given in Table 1-5. The two copper(II) centres (Cu(1), Cu(2)) are bridged by the phthalazine group (N(2)N(3)), and a hydroxide group. Three sites per copper in the basal plane are provided by phthalazine and pyridine nitrogens and the hydroxide oxygen. The fourth site at Cu(1) is occupied by a terminal water molecule (O(2)) while at Cu(2) an oxygen (O(3)) atom from a nitrate completes the basal plane. Somewhat longer, but nevertheless significant, contacts with the oxygen atoms from nitrates and a hydroxide of a neighbouring molecule (Cu(1)-O(8) 2.426(4) Å; Cu(2)-O(10) 2.336(4) Å; Cu(1)-O(1)' 2.440(3) Å) indicate additional ligands to Cu(1) and Cu(2). The second symmetry related Cu(1)-O(1)' contact clearly indicates that the molecule is a dimer, with a most unusual fusion of two dinuclear centres to form a tetranuclear structure. This is very rare for ligands of this sort. Only one other example was found in the $\text{Cu}(\text{NO}_3)_2$ complex with DPPN (DPPN = 3,6-bis-(2'-pyridyl)-pyridazine (Scheme 1-8)) [43] in which two copper(II) centres are triply bridged by a pyridazine diazine group, a hydroxide group and a bidentate nitrate group with one copper centre also bound to the oxygen of the bridging hydroxide group belonging to the another molecule

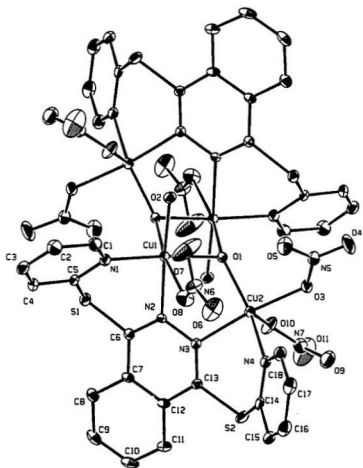


Fig. 1-5. Structural representation of $[\text{Cu}_2(\text{PTPH})(\text{OH})(\text{NO}_3)_2(\text{H}_2\text{O})_2]_2$ (**5**), with hydrogen atoms omitted (40% probability ellipsoids).

Table 1-5. Selected bond distances (Å) and angles (deg) for $[\text{Cu}_2(\text{PTPH})(\text{OH}) \cdot (\text{NO}_3)_3(\text{H}_2\text{O})_2] \cdot (5)$

Cu(1)-O(1)	1.938(3)	Cu(1)-O(2)	1.971(3)
Cu(1)-N(1)	2.007(4)	Cu(1)-N(2)	2.084(4)
Cu(1)-O(8)	2.426(4)	Cu(1)-O(1)	2.440(3)
Cu(2)-O(1)	1.940(3)	Cu(2)-O(3)	1.977(3)
Cu(2)-N(3)	2.060(4)	Cu(2)-N(4)	1.993(4)
Cu(2)-O(10)	2.336(4)	Cu(1)-Cu(2)	3.215(1)
Cu(1)-Cu(1) _a	3.269(1)		
O(1)-Cu(1)-O(2)	90.7(1)	O(1)-Cu(1)-N(1)	174.9(1)
O(1)-Cu(1)-N(2)	86.4(1)	O(2)-Cu(1)-N(1)	91.9(1)
O(2)-Cu(1)-N(2)	177.1(1)	O(8)-Cu(1)-O(1)	86.0(1)
O(8)-Cu(1)-O(2)	99.5(1)	O(8)-Cu(1)-N(1)	89.3(1)
O(8)-Cu(1)-N(2)	80.3(1)	O(1)-Cu(2)-O(3)	94.5(1)
O(1)-Cu(2)-N(3)	89.1(1)	O(1)-Cu(2)-N(4)	156.1(2)
O(3)-Cu(2)-N(3)	167.1(1)	O(3)-Cu(2)-N(4)	91.9(1)
N(3)-Cu(2)-N(4)	89.8(2)	O(10)-Cu(2)-N(4)	111.0(1)
O(10)-Cu(2)-O(3)	86.2(1)	O(10)-Cu(2)-O(1)	92.4(1)
O(10)-Cu(2)-N(3)	81.3(1)	Cu(1)-O(1)-Cu(2)	112.0(1)
Cu(1)-O(1)-Cu(1) [*]	95.9(1)	Cu(1) [*] -O(1)-Cu(2)	132.6(1)

of the same kind. Cu(2) is square-pyramidal, while Cu(1) is a tetragonally distorted octahedron. The hydroxide O(1) bridges Cu(1) and Cu(2) in the traditional manner, but also acts as a bridge between two symmetry related Cu(1) centres, thus acting as a μ_3 -hydroxide. The solid angle at O(1) (340.5°) indicates substantial pyramidal distortion at the μ_3 -hydroxide bridge. The Cu(1)-Cu(1)' distance is quite short (3.269(1) Å) and comparable with the Cu(1)-Cu(2) separation (3.215(1) Å). The four copper centres are therefore linked through both the diazine and hydroxide bridges, involving the fusion of the two five-membered Cu₂N₂O rings to the central Cu₂O₂ ring. O(1) links Cu(1) and Cu(2) equatorially, whereas the dimer linkage involves a combination of axial and equatorial bonds to Cu(1).

The conformation of the ligand contrasts sharply with that in **1**, with a *syn* arrangement of the pyridine rings, leading to the mutual equatorial bridging arrangement of the hydroxide. The pyridine rings (defined by N(1) and N(4)) have dihedral angles of 56.4° and 50.5° respectively with respect to the mean phthalazine plane. The Cu(1)N₂O₂ square plane has a substantial tetrahedral distortion, with a mean deviation from the plane of 0.253(4) Å. The CuN₂O₂ least-squares planes are inclined by 97.1° . The large copper-copper distance (3.215(1) Å) and Cu(1)-O(H)-Cu(2) angle ($112.0(1)^\circ$) is comparable with some triply bridged dinuclear copper(II) complexes of PAPR (Scheme 1-8) in which the two

copper centres are equatorially bridged by the phthalazine and hydroxide groups like the situation in **5**, and in addition bridged by an axial, bidentate bridging anions e.g. SO₄, IO₃, NO₃ (Table 1-2). Such a bulky third bridge has the effect of forcing the metal centres apart and leads to a larger copper-copper separation and Cu-OH-Cu angle. The absence of such a group in this case is unusual, but parallels the situation found for the tetranuclear copper complexes [Cu₄(TNL₄)(μ₂-OH)₂(H₂O)₄](CF₃SO₃)₆, [Cu₄(TNL)(μ₂-OH)₂(H₂O)₆(EtOH)₂] · (CF₃SO₃)₆ (Ligand = 1,4,6,9-tetrakis-(R-2-pyridyl)amino-benzodipyridazine (Scheme 1-8)), which have large Cu-O(H)-Cu angles (116.0(5)° and 116.0(5)° respectively) and only the diazine and hydroxide groups bridge the copper pairs in an equatorial fashion [81, 82].



The structure of [Cu₂(PTPH)(OH)(NO₃)₂(H₂O)₂](NO₃) (**6**) is shown in Fig. 1-6, and selected bond distances and angles relevant to the copper coordination spheres are given in Table 1-6. Superficially **6** and **5** appear to be very similar, but their marked colour difference and differences in their electronic spectra indicate that there must be significant structural differences. **6** involves the same *syn* ligand conformation. The two copper ions are bridged by the phthalazine diazine group and by a hydroxide oxygen (O(1)). Cu(1) has a tetragonally distorted octahedral

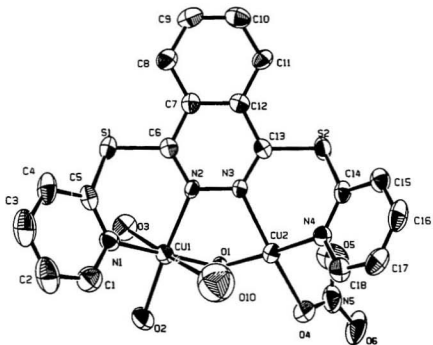


Fig. 1-6. Structural representation of $[\text{Cu}_2(\text{PTPH})(\text{OH})(\text{NO}_3)_2(\text{H}_2\text{O})_2](\text{NO}_3)$ (**6**), with hydrogen atoms omitted (40% probability ellipsoids) (O(2) and O(3) from two water molecules, O(10) from the distorted nitrate N(7)).

Table 1-6. Selected bond distances (Å) and angles (deg) for $[\text{Cu}_2(\text{PTPH})(\text{OH}) \cdot (\text{NO}_3)_2(\text{H}_2\text{O})_2](\text{NO}_3)_2$ (6)

Cu(1)-O(1)	1.918(5)	Cu(1)-O(2)	1.973(5)
Cu(1)-N(1)	2.008(7)	Cu(1)-N(2)	2.046(6)
Cu(1)-O(3)	2.360(6)	Cu(1)-O(10)	2.676(9)
Cu(2)-O(1)	1.591(5)	Cu(2)-O(4)	1.993(6)
Cu(2)-N(3)	2.031(6)	Cu(2)-N(4)	1.990(6)
Cu(2)-O(13)	2.59(2)	Cu(1)-Cu(2)	3.101(2)
O(1)-Cu(1)-O(2)	90.1(2)	O(1)-Cu(1)-N(1)	172.2(3)
O(1)-Cu(1)-N(2)	86.7(2)	O(2)-Cu(1)-N(1)	92.4(3)
O(2)-Cu(1)-N(2)	175.9(3)	N(1)-Cu(1)-N(2)	90.5(3)
O(3)-Cu(1)-O(1)	96.1(2)	O(3)-Cu(1)-O(2)	88.3(2)
O(3)-Cu(1)-N(1)	91.6(2)	O(3)-Cu(1)-N(2)	94.7(2)
O(10)-Cu(1)-O(1)	83.0(3)	O(10)-Cu(1)-O(2)	94.7(3)
O(10)-Cu(1)-N(1)	89.3(3)	O(10)-Cu(1)-N(2)	82.2(3)
O(1)-Cu(2)-O(4)	92.8(2)	O(1)-Cu(2)-N(3)	86.0(2)
O(1)-Cu(2)-N(4)	174.1(2)	O(4)-Cu(2)-N(3)	171.6(3)
O(4)-Cu(2)-N(3)	91.3(3)	N(3)-Cu(2)-N(4)	90.5(3)
O(13)-Cu(2)-O(1)	84.3(4)	O(13)-Cu(2)-O(4)	66.5(5)
O(13)-Cu(2)-N(3)	121.4(5)	Cu(1)-O(1)-Cu(2)	109.0(3)

geometry, with one water molecule and one nitrate bound axially (Cu(1)-O(3) 2.360(6) Å, Cu(1)-O(10) 2.676(9) Å), and another water molecule bound equatorially (Cu(1)-O(2) 1.973(5) Å). The N(7) nitrate is disordered (Fig. 1-6). O(10) has been refined at unit occupancy, but the other nitrate oxygens O(11), O(12), O(13) and O(14) have been refined at half occupancy. Cu(2) has a pseudo square-planar geometry, with one nitrate bound equatorially (Cu(2)-O(4) 1.993(6) Å). The in-plane ligand distances of **6** compare very closely with those observed for **5**, but the Cu-O (hydroxide) distances in **6** (1.918(5), 1.891(5) Å) are shorter than those found in **5** (1.938(3), 1.940(3) Å). The copper-copper separation (3.101(2) Å) and Cu-OH-Cu angle (109.0(3)°) are slightly smaller than those found in **5**, but there is no indication that a dimeric structure exists in **6** and a simpler dinuclear entity exists, typical for the ligands of this sort [43, 54, 56]. A similar dinuclear structure was found in [Cu₂(PAP46Me)(OH)(NO₃)₂(H₂O)](NO₃) (PAP46Me = 1,4-di-(4',6'-dimethylpyridin-2'-ylamino)phthalazine) [54]. The two copper centres are doubly bridged by hydroxide and phthalazine diazine groups with each nitrate group bound in a bidentate fashion to the copper centres. The copper-copper separation (3.156(2) Å) and Cu-OH-Cu angle (113.7(3)°) are slightly larger than those in **6**. A similar dinuclear structure was also found in [Cu₂(PPDMe)(OH)(NO₃)₂(H₂O)₂](NO₃) (PPDMe = 3,6-bis-(3,5-dimethyl-1-

pyrazolyl)- pyridazine), with a copper-copper separation 3.338(1) Å and Cu-OH-Cu angle 119.3(2)°, which are much larger than those in 6, due to the presence of five-membered chelate rings [47].

[Cu₂(PTPH)(OH)Cl₃] \cdot 2CHCl₃ (9)

A perspective view of [Cu₂(PTPH)(OH)Cl₃] \cdot 2CHCl₃ (9) is shown in Fig. 1-7, and selected bond distances and angles relevant to the copper coordination spheres are given in Table 1-7. The two copper(II) centres have distorted square-pyramidal geometries and are bound in a triple bridged arrangement involving a chloro-bridge, a hydroxo-bridge and a pyridazine diazine bridge. The angle at the hydroxo-bridge is 104.0(2)°, while that at chlorine is 69.87(5)°, with a copper-copper separation of 3.019(1) Å. The bridging copper-chlorine bonds are fairly long (Cu(1)-Cl(2) 2.636(2) Å, Cu(2)-Cl(2) 2.637(2) Å) while the two equatorial copper-chlorine bonds are much shorter (Cu(1)-Cl(1) 2.248(2) Å, Cu(2)-Cl(3) 2.256(2) Å). The Cu-O (hydroxide) bond lengths and Cu-N bond distances fall within the ranges established for other related dicopper complexes [35, 39, 43, 28, 51, 52, 54]. The copper atoms are displaced slightly from the basal N₂ClO mean planes (Cu(1) 0.250(4) Å, Cu(2) 0.282(4) Å) towards Cl(2), with a dihedral angle of 134.4° between the mean basal planes. Structurally 9 resembles the analogous

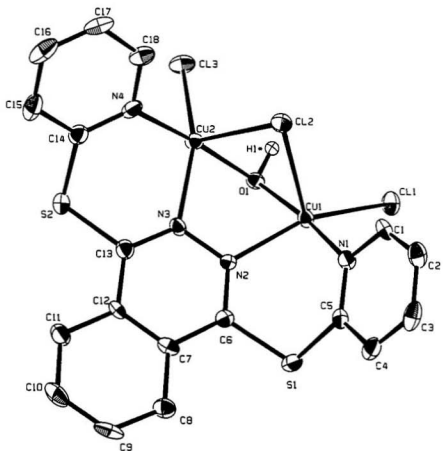


Fig. 1-7. Structural representation of $[\text{Cu}_2(\text{PTPH})(\text{OH})\text{Cl}_3] \cdot 1.5\text{SCHCl}_3$ (9), with hydrogen atoms omitted (40% probability ellipsoids).

Table 1-7. Selected bond distances (Å) and angles (deg) for $[\text{Cu}_2(\text{PTPH})(\text{OH}) \cdot \text{Cl}_3] \cdot 1.5\text{CHCl}_3$ (9)

Cu(1)-Cl(1)	2.248(2)	Cu(1)-O(1)	1.915(4)
Cu(1)-N(1)	1.994(5)	Cu(1)-N(2)	2.057(5)
Cu(2)-Cl(3)	2.256(2)	Cu(2)-O(1)	1.916(4)
Cu(2)-N(3)	2.059(5)	Cu(2)-N(4)	2.006(6)
Cu(1)-Cl(2)	2.636(2)	Cu(1)-Cu(2)	3.019(1)
Cu(2)-Cl(2)	2.637(2)		
Cl(1)-Cu(1)-O(1)	95.0(1)	Cl(1)-Cu(1)-N(1)	93.2(2)
Cl(1)-Cu(1)-N(2)	156.4(2)	O(1)-Cu(1)-N(1)	171.8(2)
O(1)-Cu(1)-N(2)	83.3(2)	N(1)-Cu(1)-N(2)	89.2(2)
Cl(3)-Cu(2)-O(1)	94.7(1)	Cu(1)-O(1)-Cu(2)	104.0(2)
Cl(3)-Cu(2)-N(3)	153.7(2)	Cl(3)-Cu(2)-N(4)	92.6(2)
O(1)-Cu(2)-N(3)	83.7(2)	O(1)-Cu(2)-N(4)	172.6(2)
N(3)-Cu(2)-N(4)	89.7(2)	Cu(1)-Cl(2)-Cu(2)	69.87(5)

complexes $[\text{Cu}_2(\text{EtBITP})(\text{OH})\text{Cl}_3] \cdot \text{DMF}$ (EtBITP = 3,6-bis-(N-ethyl-2-benzimidazolylthio)pyridazine) [52] and $[\text{Cu}_2(\text{PAP})(\text{OH})\text{Cl}_3] \cdot 1.5\text{H}_2\text{O}$ [35] (PAP = 1,4-di-(2'-pyridylamino)phthalazine), which involve two almost identical copper

square-pyramids bridged in the same fashion. The Cu-Cu separation and Cu-OH-Cu angle in **9** are very close to those in $[\text{Cu}_2(\text{EtBITP})(\text{OH})\text{Cl}_3] \cdot \text{DMF}$ (3.017(1) Å, 104.65(11)°), but are slightly longer and larger than those in $[\text{Cu}_2(\text{PAP})(\text{OH})\text{Cl}_3] \cdot 1.5\text{H}_2\text{O}$ (3.001(2) Å, 101.8(2)° (average 100.9° in PAP complexes)). The 'bite' of each ligand is clearly comparable, and the slight differences between **9** and $[\text{Cu}_2(\text{PAP})(\text{OH})\text{Cl}_3] \cdot 1.5\text{H}_2\text{O}$ in dinuclear centre dimensions can be attributed to the longer C-S bonds in PTPH compared with the C-N bonds in PAP. A unique feature of **9**, rarely seen in systems of this sort, is the hydroxide proton, located in a difference map. The angles subtended by the two coppers and the hydrogen atom at O(1) are closer to the tetrahedral angle than 120°, associated with a trigonal planar oxygen, and the solid angle (312°) implies little rehybridization, typical of so many alkoxy- and phenoxy- bridged dinuclear copper(II) complexes.

*$[\text{Cu}_2(\text{PTP})(\text{OH})\text{Cl}_3] \cdot 2\text{CH}_3\text{CN}$ (**11**)*

The structure of **11** is shown in Fig. 1-8, and selected bond distances and angles relevant to the copper coordination spheres are given in Table 1-8. The structures of **11** and **9** are very similar. The two square-pyramidal copper(II) centres are again bound in a triple bridged arrangement involving an axial chloro-bridge, and equatorial hydroxo- and phthalazine bridges. The angle at the hydroxo-

bridge is $106.2(1)^\circ$, the angle at the chlorine bridge is $72.38(4)^\circ$, and the copper-copper separation is $3.0514(8)$ Å. The two equatorial copper-chlorine bonds are relatively short (Cu(1)-Cl(2) $2.249(1)$ Å, Cu(2)-Cl(3) $2.259(1)$ Å), but the apical chlorine distances are quite long (Cu(1)-Cl(1) $2.560(1)$ Å, Cu(2)-Cl(2) $2.607(1)(2)$ Å). The two copper atoms are displaced slightly from their basal N_2ClO mean planes (Cu(2) 0.3623 Å, Cu(1) $0.380(2)$ Å) towards Cl(1), with a dihedral

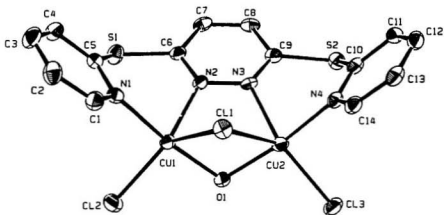


Fig. 1-8. Structural representation of $[Cu_2(PTP)(OH)Cl_3] \cdot 2CH_3CN$ (**11**), with hydrogen atoms omitted (40% probability ellipsoids).

Table 1-8. Selected bond distances (Å) and angles (deg) for $[\text{Cu}_2(\text{PTP})(\text{OH})\cdot\text{Cl}_3] \cdot 2\text{CH}_3\text{CN}$ (**9**)

Cu(1)-Cl(1)	2.560(1)	Cu(1)-Cl(2)	2.249(1)
Cu(1)-O(1)	1.910(3)	Cu(1)-N(1)	2.002(3)
Cu(1)-N(2)	2.089(3)	Cu(2)-Cl(3)	2.259(1)
Cu(2)-O(1)	1.905(3)	Cu(2)-N(3)	2.089(3)
Cu(2)-N(4)	1.994(4)	Cu(2)-Cl(1)	2.607(1)
Cu(1)-Cu(2)	3.0514(8)		
Cl(1)-Cu(1)-Cl(2)	127.39(5)	Cl(1)-Cu(1)-O(1)	81.21(9)
Cl(1)-Cu(1)-N(1)	92.5(1)	Cl(1)-Cu(1)-N(2)	91.2(1)
Cl(2)-Cu(1)-O(1)	94.61(9)	Cl(2)-Cu(1)-N(1)	92.9(1)
Cl(2)-Cu(1)-N(2)	141.2(1)	O(1)-Cu(1)-N(1)	172.2(1)
O(1)-Cu(1)-N(2)	87.2(1)	N(1)-Cu(1)-N(2)	88.3(1)
Cl(3)-Cu(2)-O(1)	95.68(9)	Cl(3)-Cu(2)-N(3)	141.5(1)
Cl(3)-Cu(2)-N(4)	92.0(1)	O(1)-Cu(2)-N(3)	87.1(1)
O(1)-Cu(2)-N(4)	171.8(1)	N(3)-Cu(2)-N(4)	88.6(1)
Cu(1)-Cl(1)-Cu(2)	72.38(4)	Cu(1)-O(1)-Cu(2)	106.2(1)

angle of 152.00° between the mean basal planes. The Cu-Cu separation and Cu-OH-Cu angle in **11** are slightly larger than those in **9** due in part to the larger

dihedral angle between the two basal N_2ClO mean planes in 11. The 'bite' of each ligand is comparable. The solid angle at hydroxide oxygen (O(1)) could not be determined due to the difficulty of locating the hydrogen atom.



The structure of 12 is shown in Fig. 1-9, and interatomic distances and angles relevant to the copper coordination spheres are given in Table 1-9. The complex consists of discrete $[Cu_2(PTPH)_2]^{2+}$ cations and uncoordinated perchlorate anions with two acetonitrile molecules of crystallization in the lattice. The dinuclear cation consists of two pseudo-tetrahedral copper(I) centres, separated by 3.313(2) Å and bridged by two phthalazine groups with terminal pyridine donors completing the four-coordination, and forming an almost planar Cu_2N_4 hexagonal, heterocyclic ring. Each ligand is bent in a 'lobster-like' *cis*-conformation with both pyridine rings oriented on the same side of the phthalazine group. Within each ligand the pyridine rings have dihedral angles of 124.4° relative to the mean phthalazine plane. The overall structure is very similar to that of $[Cu_2(PTP)_2](ClO_4)_2$ [53], which has a slightly longer Cu-Cu separation (3.422(1)Å). The copper-nitrogen separations (2.022 - 2.030 Å) are slightly longer than those in $[Cu_2(PTP)_2](ClO_4)_2$ (2.008 - 2.024 Å), but are quite normal. It is of

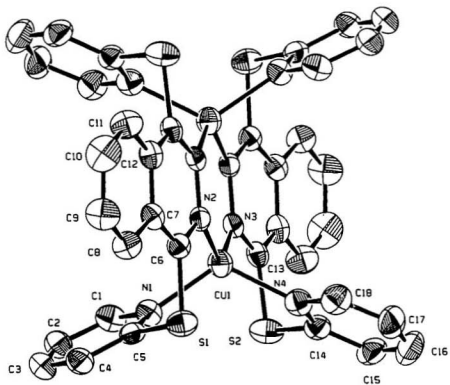


Fig. 1-9. Structural representation of $[\text{Cu}_2(\text{PTPH})_2](\text{ClO}_4)_2 \cdot 2\text{CH}_3\text{CN}$ (12), with hydrogen atoms omitted (40% probability ellipsoids).

Table 1-9. Selected bond distances (Å) and angles (deg) for $[\text{Cu}_2(\text{PTPH})_2] \cdot$

(ClO ₄) ₂ · 2CH ₃ CN (12)			
Cu(1)-N(1)	2.026(4)	Cu(1)-N(2)	2.030(4)
Cu(1)-N(3)	2.023(4)	Cu(1)-N(4)	2.022(5)
Cu(1)-Cu(1)a	3.313(2)		
N(1)-Cu(1)-N(2)	92.9(2)	N(1)-Cu(1)-N(3)	115.1(2)
N(1)-Cu(1)-N(4)	119.6(2)	N(2)-Cu(1)-N(3)	123.4(2)
N(2)-Cu(1)-N(4)	115.8(2)	N(3)-Cu(1)-N(4)	92.5(2)

interest to compare the structure of **12** with that of the complex $[\text{Cu}_4(\text{dppn})_4](\text{CF}_3\text{SO}_3)_4$ [92], which involves a similar N₄ diazine ligand, but has a rather different 'bite'. DPPN (Scheme 1-8) forms five membered chelate rings at each metal and two pairs of ligands bridge two pairs of metals, with a planar arrangement of four tetrahedral copper centres and two ligands lying above and below the Cu₄ plane. Inevitably the five-membered chelate rings in DPPN make it impossible to form dinuclear copper(I) complexes like those of P'P and PTPH and lead to larger copper-copper separations (3.566(1), 3.582(1) Å).



The preliminary ($R = 0.109$, $R_w = 0.092$) structure of 13 is shown in Fig. 1-10, and interatomic distances and angles relevant to the copper coordination spheres are given in Table 1-10. This complex is most unusual and contains three different mononuclear copper(II) centres. One is the familiar pseudo-tetrahedral CuCl_4^{2-} anion. The other two involve the new ligand 1-methoxy-4-(2'-pyridylthio)phthalazine (PTFO) (Scheme 1-11). Cu(2) is bound equatorially to two bidentate N_2 ligands, via one phthalazine and the pyridine nitrogen, with an axial contact to a water molecule in a distorted square-pyramidal geometry. Cu(1) is in a distorted square-planar geometry, coordinated by a similar bidentate PTFO ligand and two chlorines. Copper-ligand distances are typical for species of this sort. Although this crystal gave a good data set and solved easily, the final refinement was poor. This was attributed to the presence of non-stoichiometric water at several sites in the unit cell. The results nevertheless clearly account for the three unique copper fragments.

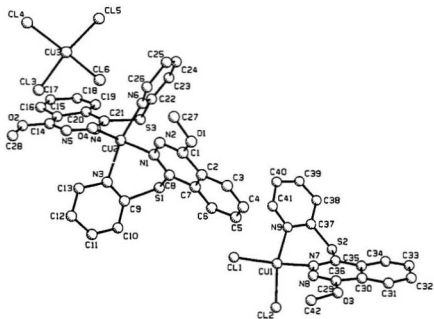


Fig. 1-10. Structural representation of $\{[\text{Cu}(\text{PTPO})_2(\text{H}_2\text{O})][\text{CuCl}_4][\text{Cu}(\text{PTPO})\text{-Cl}_2]\} \cdot 2.8\text{H}_2\text{O}$ (13), with hydrogen atoms omitted.

Table 1-10. Selected bond distances (Å) and angles (deg) for [Cu(PTPO)₂(H₂O)]·

[CuCl ₄][Cu(PTPO)Cl ₂] (13)			
Cu(1)-Cl(1)	2.209(8)	Cu(1)-Cl(2)	2.23(1)
Cu(1)-N(7)	2.03(2)	Cu(1)-N(9)	2.05(2)
Cu(2)-O(4)	2.27(2)	Cu(2)-N(1)	2.02(2)
Cu(2)-N(3)	2.10(2)	Cu(2)-N(4)	2.02(2)
Cu(2)-N(6)	2.09(3)	Cu(3)-Cl(3)	2.30(1)
Cu(3)-Cl(4)	2.18(1)	Cu(3)-Cl(5)	2.24(1)
Cu(3)-Cl(6)	2.31(1)		
Cl(1)-Cu(1)-Cl(2)	95.8(3)	Cl(1)-Cu(1)-N(7)	160.0(8)
Cl(1)-Cu(1)-N(9)	95.4(7)	Cl(2)-Cu(1)-N(7)	90.5(7)
Cl(2)-Cu(1)-N(9)	152.1(7)	N(7)-Cu(1)-N(9)	87.6(9)
O(4)-Cu(2)-N(1)	96.0(7)	O(4)-Cu(2)-N(3)	96.8(7)
O(4)-Cu(2)-N(4)	99.8(8)	O(4)-Cu(2)-N(6)	103.0(9)
N(1)-Cu(2)-N(3)	87.6(8)	N(1)-Cu(2)-N(4)	164.2(9)
N(1)-Cu(2)-N(6)	91.1(9)	N(3)-Cu(2)-N(4)	91.5(8)
N(3)-Cu(2)-N(6)	160(1)	N(4)-Cu(2)-N(6)	84.0(1)
Cl(3)-Cu(3)-Cl(4)	93.1(4)	Cl(3)-Cu(3)-Cl(5)	141.5(4)
Cl(3)-Cu(3)-Cl(6)	97.8(5)	Cl(4)-Cu(3)-Cl(5)	97.6(5)
Cl(4)-Cu(3)-Cl(6)	141.1(5)	Cl(5)-Cu(3)-Cl(6)	96.7(5)

1.4.3. Reactions

In a most unusual reaction involving copper(II) nitrate with PTPH, two very different complexes, one dinuclear and the other tetranuclear, are produced by employing small but subtle differences in reaction conditions. For PTP and DPTD only dinuclear complexes are produced. The copper centres in these copper nitrate complexes are generally bridged by the diazine and hydroxide groups.

The direct reactions of CuX_2 ($X = \text{Cl}, \text{Br}$) with MIP, PPD, and PAPR (Scheme 1-8) [35, 51, 52] in aqueous alcoholic media generally form hydroxide bridged dinuclear complexes, but under the same conditions PTP only forms dihalide bridged complexes [53, 57]. The difficulty of synthesizing hydroxide bridged dinuclear copper(II) halide complexes of PTP led to the use of a $\text{NEt}_3/\text{MeOH}/\text{H}_2\text{O}$ mixture, with the formation of $[\text{Cu}_2(\text{PTP})(\text{OH})\text{X}_3]$ ($X = \text{Cl}, \text{Br}$) [57] in which the two copper(II) ions are triply bridged by a pyridazine diazine group, a halide atom and a hydroxide group. Since similar problems were encountered in the synthesis of corresponding PTPH complexes in aqueous alcoholic media, with the formation of $[\text{Cu}_2(\text{PTPH})\text{X}_4]$ ($X = \text{Cl}, \text{Br}$) only, the same approach was tried with PTPH. However the expected products were not obtained and ligand decomposition occurred. The structure of 13 reveals that the new phthalazine derivative PTPO is produced and that hydrolysis of PTPH has

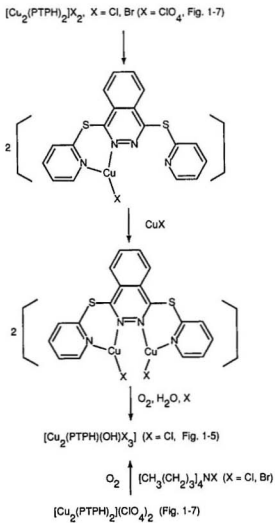
apparently occurred. Base induced attack by methanol at a phthalazine carbon adjacent to the coordinated nitrogen could reasonably be enhanced by the electron withdrawing inductive effect of four coordinated chlorines in a dinuclear species like $[\text{Cu}_2(\text{PTPH})\text{Cl}_4]$, which would clearly exist initially in the reaction mixture. No pyridine thiol was detected, but in the presence of excess copper(II) salt a spontaneous redox reaction would have occurred eliminating the thiol with the formation of a copper(I) species. This presumably corresponds to the unidentified, insoluble material formed in the reaction. The question of why the same reaction does not appear to occur with PTP is pertinent, but may be largely a function of the inherent properties of the phthalazine moiety compared with the pyridazine. It is well known that 1,4-dichlorophthalazine is much more hydrolytically unstable than 3,6-dichloropyridazine, forming the corresponding mono-hydroxy species with ease.

The synthesis of the desired hydroxo bridged complexes of PTPH was finally achieved by the oxidation of their copper(I) analogues in air. The red solutions produced by the reaction of $[\text{Cu}(\text{CH}_3\text{CN})_4]\text{X}$ ($\text{X}=\text{Cl}, \text{Br}$) in acetonitrile with PTPH can reasonably be associated with species like the air-stable red, dimeric complex $[\text{Cu}_2(\text{PTPH})_2](\text{ClO}_4)_2$ (12) and in fact they have identical electronic spectra. The irreversible oxidation of copper(I) complexes by oxygen to give hydroxo or alkoxo

complexes is common [2, 93, 94] but the mechanisms of such reactions are not well understood. It is presumed that they proceed through the initial formation of a dioxygen-copper complex, $\text{Cu}_2\text{-O}_2$, which then undergoes further reduction or reaction to give oxo and/or hydroxo products derived from fully four-electron-reduced O_2 [95 - 97]. We have carried out low-temperature oxygenations of the dicopper(I) complexes $[\text{Cu}_2(\text{L})_2](\text{ClO}_4)_2$ ($\text{L}=\text{PTPH}, \text{PTP}$) in the hope of trapping the intermediate $\text{Cu}_2\text{-O}_2$ species. The copper(I) complexes of these two ligands seem very stable and their red color does not change even after bubbling oxygen at -78 , -25 , or 0°C in methanol-dichloromethane (1:1) mixture for as long as 2 h, or even at room temperature overnight. The red copper(I) solutions prepared from Cu(I)X ($\text{X}=\text{Cl}, \text{Br}$) behaved similarly.

The high stability of **12** and its PTP analogue is surprising, but may reflect an inherent thermodynamic stability of the dinuclear cation or the inability of oxygen to attack the copper centres by virtue of some steric effect. The ‘*syn*’ ligand conformation and the resulting tetrahedral geometry at the Cu(I) centres leads to a situation where the sulfur lone pairs project over the ends of the cations (Fig. 1-9). This will make it difficult for O_2 to attack the copper centres. It would seem reasonable that significant reorganization of the dinuclear species would also be required before oxidation could proceed. Electrochemical studies for **12** in

Scheme 1-12.



DMF(GC/Pt/SCE) show an irreversible CV wave at $E_{1/2} = +0.30$ V ($\Delta E_p = 370$ mV) indicating a thermodynamic possibility of oxidation, but one which must involve considerable molecular reorganization. The role of the halide ion is, therefore, considered to be important and it is significant that for the oxidation reaction involving copper(I) chloride after extended exposure to air, the rate of oxidation, although still low, was higher than that for bromide. Perhaps the initial step in the process involves attack by halide (Scheme 1-12), splitting the dinuclear complex cation up into two mononuclear three-coordinate species, in which the copper is bound at one end of the ligand only. Reaction with excess copper(I) chloride could then produce a 1:2 dinuclear three-coordinate species involving copper chlorine bonds, which would render the copper centres more electrophilic (an effect which would diminish in the presence of bromide) and thus more susceptible to oxidation than the original 1:1 dinuclear species. Since the ultimate product is a hydroxy-bridged species the involvement of atmospheric water in the oxidation step seems inevitable, and a two electron oxidation of the 1:2 copper(I) species, combined with coordination of adventitious chloride would complete the process. The addition of small amounts of water does in fact speed up the oxidation process, confirming the involvement of water in the oxidation step.

Additional support for these suggestions comes from two key experiments

in which compound **12** was reacted with air in acetonitrile, in the presence of tetraethylammonium chloride and tetrabutylammonium bromide for an extended period. While the acetonitrile solution of **12** itself can not be oxidized (Scheme 1-12), green crystalline materials were produced after two weeks, which were shown to be identical to the hydroxy-bridged complexes **9** and **10** respectively by comparison of their IR spectra, which are characterized by the presence a very sharp and strong band at around 3600 cm^{-1} , associated with an OH stretch.

The analogous PTP compound, $[\text{Cu}_2(\text{PTP})(\text{OH})\text{Cl}_2]$ (**11**) can also be prepared from Cu(I) chloride reactions in the presence of air in a similar manner. This compound was reported before [57] and isolated in a $\text{NEt}_3/\text{MeOH}/\text{H}_2\text{O}$ mixture, but was not structurally characterized.

1.4.4. Spectroscopy

Infrared spectra of **1** and **3** are virtually identical above 500 cm^{-1} with similar shifts of major peaks compared with those in free ligand, indicating the likelihood of a similar dinuclear structural arrangement in **3**. In the far infrared two prominent bands at 300 and 275 cm^{-1} for **1** (associated with terminal and bridging copper-chlorine bonds respectively) (Table 1-11) are shifted to 285 and 245 cm^{-1} in **3**, confirming the mixed terminal and bridging arrangement of bromine

ligands. Infrared spectra of **2** and **4** are very similar in the range 4000 - 500 cm^{-1} , and they are also similar to that of **1** and **3**, especially in the far IR region (Table 1-11) which suggests the mixed terminal and bridging arrangement of halides. It is reasonable to assume that the structures of **2** and **3** are similar to that of **1** and **4** containing the same triply bridged dinuclear copper centres. In the conventional infrared region **5** and **6** have very similar spectra, but with a marked difference in the OH stretching frequency which occurs at 3523 cm^{-1} (Table 1-11) in **5** and 3428 cm^{-1} in **6**. However, since water is present in both complexes it is perhaps unwise to attach much significance to these differences in terms of hydroxide OH stretch alone. Difference in the nitrate combination band region can, however, be associated with observed structural features due to the nitrate groups. The tetranuclear complex **5**, which has just monodentate nitrates, has two prominent nitrate ($\nu_1 + \nu_4$) combination bands [98] at 1750 and 1721 cm^{-1} , which can be associated with monodentate nitrate. The dinuclear complex **6** has a more complicated spectrum with two prominent bands at 1747 and 1723 cm^{-1} , a broad 'shoulder' at 1760 cm^{-1} and a should at 1735 cm^{-1} . The band at 1747 cm^{-1} is assigned to ionic nitrate and the pair at 1760 and 1735 cm^{-1} to monodentate nitrate. This accounts for the two unambiguous nitrates in the structure. The N(7) nitrate, which is disordered can, therefore, be associated with the combination band at

Table 1-11. Spectral and electrochemical data of copper complexes of PTPH, PTP, DPTD

Compound	IR(cm ⁻¹)	UV/VIS ^a (cm ⁻¹)	E _{1/2} ^b V (vs.SCE)
[Cu ₂ (PTPH)Cl ₄] · 2H ₂ O (1)	3420(H ₂ O), 1022 ^c , 300, 275 (νCu-Cl)	[25000] ^d 14000	0.43
[Cu ₂ (DPTD)Cl ₄] (2)	1016 ^c , 295, 278(νCu-Cl)	24700 14080	0.435
[Cu ₂ (PTPH)Br ₄] · 1.5H ₂ O (3)	3440(H ₂ O), 1021 ^c , 285, 245(νCu-Br)	20000 14300	0.425
[Cu ₂ (DPTD)Br ₄] (4)	1016 ^c , 282, 250(νCu-Br)	23800 14300	0.48
[Cu ₂ (PTPH)(OH) (NO ₃) ₂ (H ₂ O) ₂ (5)	3523(OH), 1750, 1721 (ν ₁ + ν ₄ NO ₃), 1025 ^c	16370	-
[Cu ₂ (PTPH)(OH) (NO ₃) ₂ (H ₂ O) ₂] · (NO ₃) ₂ (6)	3428(OH), [1760], 1747, [1735], 1723 (ν ₁ + ν ₄ NO ₃), 1027 ^c)	16560	-
[Cu ₂ (PTP)(OH) (NO ₃) ₂ (7)	3481(OH), 1755, 1723 (ν ₁ + ν ₄ NO ₃), 1026 ^c	16400	-
[Cu ₂ (DPTD)(OH) (NO ₃) ₂ (8)	3512(OH), 1754, 1724 (ν ₁ + ν ₄ NO ₃), 1017 ^c	16400	-
[Cu ₂ (PTPH)(OH) Cl ₃] · 1.2CHCl ₃ (9)	3599(OH), 1025 ^c , 295, 275(νCu-Cl)	[24400] 15300	0.43
[Cu ₂ (PTPH)(OH) Br ₃] · CHCl ₃ (10)	3584(OH), 1024 ^c , 272, 240(νCu-Br)	[22000] 14700	0.41
[Cu ₂ (PTP)(OH) Cl ₃] (11)	3449(OH), 1025 ^c , 290, 273(νCu-Cl)	[24700] 15400	0.42

Table 1-11. Spectral and electrochemical data of copper complexes of PTPH, PTP, DPTD

Compound	IR(cm ⁻¹)	UV/VIS ^a (cm ⁻¹)	E _{1/2} ^b V (vs.SCE)
[Cu ₂ (PTPH) ₂] (ClO ₄)·2CH ₃ CN (12)	2288, 2251(ν-CH ₃ CN) 1093(ClO ₄ ⁻), 1024 ^c	36100 ^d 31000	0.30
{[Cu(PTPO) ₂ (H ₂ O)] [CuCl ₄][Cu(PTPO) Cl ₂]}·2.8H ₂ O (13)	3480(H ₂ O), 1020 ^e , 310, 297 (ν-Cu-Cl)	14700 10200	-

^aMull transmittance.

^bGC/DMF/TEAP/SCE, scan rate: 100 mVs⁻¹.

^cPyridine ring breathing mode indicative of pyridine coordination.

^d[] shoulder.

^eCH₃CN solution spectra.

1723 cm⁻¹, which is probably too low in energy for monodentate or ionic nitrate and may have a high energy, bidentate counterpart in the broad, pronounced shoulder at 1760 cm⁻¹. In the absence of a complete analysis from the X-ray structure on this disordered nitrate, the infrared data suggest that it may have some bidentate character. The dark blue complexes **7** and **8** are characterized in the infrared by absorptions at 3481, 3512 cm⁻¹ respectively associated with hydroxide stretch. Two prominent nitrate combination bands for **7** and **8** with a difference larger than 31 cm⁻¹ (Table 1-11) suggest that the nitrates are involved in coordination and in bidentate fashion [98]. The structure may be similar to that in

6 containing dinuclear copper(II) centres doubly bridged by diazine and hydroxide group. Infrared spectra of **9** and **10** also show the likelihood of a similar dinuclear structural arrangement in the two complexes. The sharp absorption at 3599 cm^{-1} for **9** and 3584 cm^{-1} for **10** confirms the presence of a hydroxide bridge in **10**. In the far infrared two prominent bands at $295, 275\text{ cm}^{-1}$ for **9** and $272, 240\text{ cm}^{-1}$ for **10** indicate copper(II) centres are coordinated by terminal and bridging bromines. We assume that **10** has a similar structure to **9** involving dinuclear copper centres triply bridged by phthalazine diazine, hydroxide and bromine groups. The infrared spectrum of **11** is consistent with its X-ray structure. The strong and sharp absorption at 3449 cm^{-1} is associated with OH stretch. Far infrared absorptions at $290, 273\text{ cm}^{-1}$ are associated with terminal and bridging chlorine groups respectively. The dinuclear copper(I) derivative **12** exhibits a strong perchlorate (ν_3) vibration at 1093 cm^{-1} , indicative of ionic perchlorate, and two prominent bands at $2288, 2251\text{ cm}^{-1}$ associated with lattice acetonitrile in the complex [99]. Terminal Cu-Cl stretching vibrations were observed at 310 and 297 cm^{-1} for **13**, indicating that the Cu-Cl bonds in the complex are nonequivalent. All the complexes show a single pyridine ring vibration in the range of $1016 - 1025\text{ cm}^{-1}$ (Table 1-11), associated with coordinated pyridine [28].

Electronic spectra (Table 1-11) for **1** and **3** have visible absorptions at similar

energies (14000, 14300 cm^{-1} respectively), which is somewhat surprising considering the likely structural similarities and the different ligands. However charge transfer bands at 25000 cm^{-1} (1) and 20000 cm^{-1} (3) clearly differentiate the two compounds and are associated with halogen to metal charge transfer. 2 and 4 have absorptions similar to those in 1 and 3 and are associated with d-d and charge transfer transitions. 5, 6, 7 and 8 have very similar visible absorptions (16370, 16560, 16400 and 16400 cm^{-1} respectively), which is not surprising considering the similarities in donor sets in these complexes. 9, 10 and 11 have major visible d-d absorptions at 15300, 14700 and 15400 cm^{-1} , consistent with square-pyramidal copper(II) centres. The charge transfer bands in these hydroxide bridged complexes are comparable with those found in their tetrahalide counterparts. The red copper(I) complex 12 has a solution (CH_3CN) spectrum dominated by two intense charge transfer bands at 36100 and 31000 cm^{-1} , associated with the dinuclear copper(I) cation. Mixtures of PTPH and excess Cu(I)X ($X = \text{Cl}, \text{Br}$), produce red solutions in CH_3CN with identical spectra, indicating the presence of the same dinuclear cation in these solutions. Complex 13 has a more complicated visible/near infrared spectrum with a major, broad asymmetric absorption at 14700 cm^{-1} and a prominent shoulder at 10200 cm^{-1} . The tetrahedrally distorted CuCl_4^{2-} anion would be expected to exhibit d-d absorption at relatively low energy and

would reasonably be associated with the band at 10200 cm^{-1} band. The broad band at 14700 cm^{-1} is associated both the square-pyramidal $[\text{Cu}(\text{PTPO})_2(\text{H}_2\text{O})]^{2+}$ and pseudo-square planar $[\text{Cu}(\text{PTPO})\text{Cl}_2]$ species.

All the dinuclear copper(II) complexes are esr silent in the solid state at room temperature, due to the presence of moderate to strong antiferromagnetic coupling between the copper(II) centres, except for **2** which shows a broad peak centred at $g_{av} = 2.11$, due to exceptionally high monomeric impurity (> 5%) in the complex.

1.4.5. Magnetism

Room temperature magnetic moments for complexes **1-11** are subnormal (Table 1-12), falling in the range 1.03 - 1.68 BM, indicating spin-coupling between the copper(II) centres and the presence of net antiferromagnetism. Variable temperature magnetic studies were carried out on **1 - 11** in the temperature range of 5 - 300 K. A plot of the experimental susceptibility data for **1** is given in Fig. 1-11. The data for **1 - 11** were fitted to the Bleaney-Bowers expression (eq. 2), using a non-linear regression procedure containing four parameters (g , $-2J$, θ and ρ) ($N\alpha = 60 \times 10^6$ cgsu per copper). The best fit data are presented in Table 1-12.

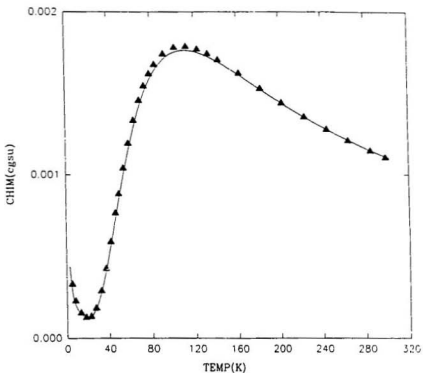


Fig. 1-11. Magnetic data for $[\text{Cu}_2(\text{PTPH})\text{Cl}_4] \cdot 2\text{H}_2\text{O}$ (1). The solid line was calculated from eq. 2 with $g = 2.10(3)$, $-2J = 124(2) \text{ cm}^{-1}$, $\rho = 0.003$, $N\alpha = 60 \times 10^{-6} \text{ cgsu}$ ($R = 0.59$).

Table 1-12. Magnetic and structural data of dinuclear copper(II) complexes of PTPH, PTP, DPTD

Compound	-2J(cm ⁻¹)	g	θ (K)	μ_{eff} BM(RT)	Cu-Cu	Cu-O-Cu	Ref.
[Cu ₂ (PTPH)Cl ₄] ·2H ₂ O (1)	124(2)	2.10(3)	-1.0	1.62	3.194(2)	-	this work
[Cu ₂ (DPTD)Cl ₄](2)	35.0(1)	2.079(1)	0.2	1.68	-	-	this work
[Cu ₂ (PTPH)Br ₄] ·1.5H ₂ O (3)	174(5)	2.03(6)	1.0	1.52	-	-	this work
[Cu ₂ (DPTD)Br ₄] (4)	69.4(9)	2.02 ^a (7)	0.7	1.59	-	-	this work
[Cu ₂ (PTPH)(OH) (NO ₃) ₂ (H ₂ O) ₂ (5)	313(2)	2.043(7)	0.2	1.28	3.215(1)	112.0(1)	this work
[Cu ₂ (PTPH)(OH) (NO ₃) ₂ (H ₂ O) ₂] ·(NO ₃) ₂ (6)	308(5)	2.03(4)	-0.2	1.34	3.101(2)	109.0(3)	this work
[Cu ₂ (PTP)(OH) (NO ₃) ₂] (7)	464(11)	2.05(4)	0.3	1.04	-	-	this work

Table 1-12. Magnetic and structural data of dinuclear copper(II) complexes of PTPH, PTP, DPTD (continued)

Compound	-2J(cm ⁻¹)	g	θ (K)	μ_{eff} BM(RT)	Cu-Cu	Cu-O-Cu	Ref.
[Cu ₂ (DPTD)(OH)(NO ₃) ₂] (8)	537(4)	2.24(2)	0.5	1.03	-	-	this work
[Cu ₂ (PTPH)(OH)Cl ₂]·1.5CHCl ₃ (9)	390(3)	2.15(1)	-1.0	1.23	3.019(1)	104.0(2)	this work
[Cu ₂ (PTPH)(OH)Br ₂]·CHCl ₃ (10)	369(4)	2.05(2)	0.8	1.22	-	-	this work
[Cu ₂ (PTP)(OH)Cl ₂]·2CH ₃ CN (11)	296(1)	2.09(5)	0.5	1.35	-	106.2(1)	this work
[Cu ₂ (PTP)(OH)Br ₂]	326(6)	2.16(1)		1.27	-		57
[Cu ₂ (PTP)Cl ₄]·CH ₂ CH ₂ OH	131(0.4)	2.03		1.61	3.198(1)	-	57
[Cu ₂ (PTP)Br ₄]	243.5(0.3)	2.07		1.43	3.318(3)	-	57

For compound **1** and **3**, we have assumed that they have the same structural arrangement. The asymmetric halogen bridging arrangement in these two molecules will create a situation where the antiferromagnetic exchange cannot occur via these bridge groups. This is based on the assumption that the copper ion ground state is $d_{x^2-y^2}$. The bridging halogen bridges the magnetic lobe of one copper centre and an axial orbital of the other. This effectively orthogonal situation would, therefore, dictate that any antiferromagnetic spin-coupling should occur through the phthalazine diazine bridge. A comparison of the magnetic data for **1** and **3** (Table 1-12) indicates greatly enhanced exchange in the case of bromo derivative. This can be attributed to the difference in electronegativity of the halide ligands which we have discussed in the Introduction of this chapter. A comparison of **1** and **3** with isostructural complexes of PTP [57] reveals that the exchange for the pyridazine bridged complexes is larger than that in corresponding phthalazine complexes, indicating again the capacitive nature of the fused benzene ring in the phthalazine entity [62]. These results also compliment an earlier study on diazine bridged linear chain complexes Cu_2LX_2 (L = pyridazine, phthalazine; X = Cl, Br), which were treated using both Heisenberg and Ising models. Net antiferromagnetic behaviour was observed in all cases and significantly larger exchange integrals were evident for the pyridazine bridged complexes [100]. Unfortunately no

structures were reported. A comparison of magnetic data for **2** and **4** again indicates that the bromo derivative **4** has a larger exchange integral ($-2J = 69.4(9) \text{ cm}^{-1}$) than the chloro derivative **2** ($-2J = 35.0(1) \text{ cm}^{-1}$) due to the polarizing effect of the coordinated halogens. The effective magnetic pathway in these two complexes involves just the thiadiazole diazine group, similar to the situations in the corresponding tetrahalide counterparts of PTPH and PTP. A comparison of these tetrahalide complexes of DPTD, PTPH, and PTP (Table 1-12) suggests that the thiadiazole bridge is a less effective pathway for antiferromagnetic coupling than phthalazine and pyridazine bridges. This can be associated with the five-membered thiadiazole ring in DPTD which will increase the copper-copper separation in its complexes and involve less extensive π delocalization within the thiadiazole ring.

Compound **6** resembles some copper nitrate complexes of the PAPR (1,4-di-(2'-pyridyl(R)amino)phthalazine) ligands, in which comparable dinuclear centre dimensions were observed, with Cu-OH-Cu angles in the range $112.6-115.5^\circ$, and yet larger exchange integrals were found ($-2J = 497-597 \text{ cm}^{-1}$) [35, 37, 56] (Table 1-2). In these complexes, the two copper centres are bridged by in-plane diazine and hydroxide groups. The magnetic exchange interaction is assumed to occur largely through overlap of the 'magnetic', $d_{x^2-y^2}$, orbitals with an oxygen orbital.

The diazine group is considered to provide a relatively small contribution to the total exchange. A linear relationship (eq. 3) between $-2J$ and Cu-OH-Cu angle (α) was obtained based on a series of hydroxide bridged PAPR complexes [56]. According to this equation, the angle of 109.0° found in **6** would correspond to a $-2J$ value of 370 cm^{-1} , which is somewhat larger than that found in **6**, but because of the ligand differences, and in particular the longer linkages between the exocyclic sulfur atoms and the phthalazine and pyridine rings, the agreement is reasonable.

The fitting of the variable temperature data for **5** to the Bleaney-Bowers equation gave a very good data analysis (Table 1-12) with a value of $-2J$ ($313(2) \text{ cm}^{-1}$) comparable with that found for **6**, but it is lower than expected, based on the Cu-OH-Cu bridge angle within each dinuclear half of the dimeric structure (112.0°) ($-2J_{\text{calc.}} = 440 \text{ cm}^{-1}$). The dimerization in **5** may produce some possible magnetic connections which would reduce the net antiferromagnetic coupling. Although the Cu(1)-O(1) dimer distance ($2.440(3) \text{ \AA}$), within the Cu_2O_2 ring, is a significant bonding contact, it links the dinuclear halves via an axial orbital interaction, which will not contribute in an antiferromagnetic sense, but perhaps may result in some ferromagnetism. If any significant interdimer interaction existed it would show up in the θ corrective term included in the Bleaney-Bowers

equation. In this case, even though the θ value (0.2 K) indicates possible ferromagnetic interdinuclear coupling consistent with the orbital argument, the very small value indicates an insignificant interaction. Also the result indicates that treating the data with a trinuclear or even a tetranuclear model would not improve the data fit. The distortion at the hydroxide oxygen atom after dimerization may result in less effective overlap between a d_{xy} orbital of oxygen and the magnetic orbitals of the copper centres. With a simple μ_2 -hydroxide bridge it is difficult to estimate the degree of trigonal distortion at the oxygen atom itself because of the difficulty in accurately locating the bonded hydrogen atom. In this case the solid angle at O(1) is 340.5° , indicating substantial pyramidal distortion. A strictly planar (sp^2) geometry at the bridging oxygen, coupled with coplanarity of the copper equatorial planes, can lead to efficient magnetic overlap via the bridging atom and strong antiferromagnetic exchange, if the angle Cu-O(H)-Cu is sufficiently large [56]. A pyramidal distortion at the oxygen bridge (approaching sp^3) leads to a situation where less efficient magnetic orbital overlap with the oxygen bridge occurs, thus reducing antiferromagnetic coupling and in some cases leading to ferromagnetic coupling [101 - 104]. Such a situation is often accompanied by a bending of the copper equatorial planes as well, which leads to reduced antiferromagnetic coupling, particularly in 'roof shaped' dihydroxo-

bridged dicopper complexes [105]. The additional bonds between O(1) and the neighbouring Cu(1) atoms in **5**, which would act as Lewis acids to O(1) and effectively polarize the electron density on the oxygen bridge to a larger extent than would be the case for **6**, will also reduce antiferromagnetic coupling in **5**.

The observation of much stronger antiferromagnetic coupling in **7** than that in **6** is not surprising considering their similar structures and pyridazine is a more effective exchange pathway than phthalazine. The large $-2J$ value in **8** ($537(4) \text{ cm}^{-1}$) is substantially higher than that in **6** and **7** and suggests a larger hydroxide bridge angle in this complex associated with the five-membered thiadiazole ring.

The hydroxo-bridged complexes **9** and **10** are more strongly coupled than their tetrahalide counterparts **1** and **3**, and this is a clear consequence of replacing an orthogonal arrangement of halogen bridges with an equatorial hydroxide. The two square-pyramidal copper(II) centres are bridged equatorially by phthalazine and hydroxide and axially by halide. The net antiferromagnetic coupling would be the sum of the effects of both the phthalazine and hydroxide, like the situations in **5** and **6**. Values of $-2J$ for **9** and **10** are significantly larger than those for the analogous complexes of PTP $[\text{Cu}_2(\text{PTP})(\text{OH})\text{X}_3]$ ($\text{X}=\text{Cl}, \text{Br}$) [57] (Table 1-12), which on face value contradicts an earlier observation concerning the capacitive action of a fused benzene ring in diazine complexes of this sort [57, 62]. This is

Table 1-13. Comparison of structural parameters of $[\text{Cu}_2(\text{PTPH})(\text{OH})\text{Cl}_3] \cdot 1.5\text{CHCl}_3$ (9) and $[\text{Cu}_2(\text{PTP})(\text{OH})\text{Cl}_3] \cdot 2\text{CH}_3\text{CN}$ (11)

Parameter	$[\text{Cu}_2(\text{PTPH})(\text{OH})\text{Cl}_3] \cdot 1.5\text{CHCl}_3$ (9)	$[\text{Cu}_2(\text{PTP})(\text{OH})\text{Cl}_3] \cdot 2\text{CH}_3\text{CN}$ (11)
Ligand conformation	<i>syn</i>	<i>syn</i>
Cu geometry	square pyramidal	square pyramidal
Cu-Cu distance (Å)	3.019(1)	3.0514(8)
Cu-O (hydroxide) (Å)	1.915(4) 1.916(4)	1.905(3)
Cu-N (diazine) (Å)	2.059(5) 2.057((5)	2.089(3)
Cu-O(H)-Cu (°)	104.0(2)	106.2(1)
Dihedral angle ^a (°)	134.40	152.00
Fold angle ^b (°) ^c	111.19	120.25
Solid angle at O (°)	312	-
Cu-N=N (diazine) (°)	113.6(4) 113.8(4)	113.8(2) 114.4(2)

^aAngle defined by two basal N_2ClO planes.

^bAngle defined by Cu_2N_2 (diazine) and Cu_2O (hydroxide) planes.

^cThe sum of three angles around O.

emphasized especially in the cases of **9** and **11**, since they clearly have comparable structures (Table 1-13), with a larger Cu-OH-Cu angle, fold angle defined by Cu₂N₂ and Cu₂O planes and dihedral angle defined by the two basal N₂ClO planes in **11**, all of which will favour antiferromagnetic coupling. However a detailed comparison of these systems must await a solid angle analysis of the hydroxide bridge in these complexes, since hydroxide is the dominant bridging pathway for magnetic exchange. The distortion at this oxygen would affect the superexchange a great deal. The solid angle at O(1) in **11** cannot be determined due to the difficulty in locating the hydrogen atom. We might expect it to have a much smaller angle than that in **9** (312°), which will result in large distortion. The exchange integral determined for **11** was obtained with the structurally characterized sample (296(1) cm⁻¹) and agrees very well with the data reported previously (294(3) cm⁻¹) [57]. This clearly indicates that the complexes isolated from NEt₃/MeOH/H₂O mixtures are the right ones with the proposed structures.

An internal comparison of **9** and **10** indicates that the chloro-complex is slightly more strongly coupled than the bromo-complex. Previous discussions have shown that in isostructural pairs of halide bridged complexes [Cu₂(L)X₄] (L=PTP, PTPH, DPTD; X=Cl,Br) and other related complexes (Table 1-2), the chloride complexes are less strongly antiferromagnetically coupled, due to a stronger

electronic inductive effect associated with the bonded chlorines. However, the observations for **9** and **10** are consistent with data for $[\text{Cu}_2(\text{PAP})(\text{OH})\text{X}_2] \cdot 1.5\text{H}_2\text{O}$ ($\text{X}=\text{Cl}, \text{Br}$) ($-2J(\text{Cl})=200 \text{ cm}^{-1}$; $-2J(\text{Br})=190 \text{ cm}^{-1}$) (Table 1-2) [35]. This may be a result of the domination of the exchange situation by the hydroxide bridge. A difference in the hydroxide bridge angle would make the exchange quite different. The hydroxide bridge angle in **10** is probably smaller than that in **9** and leads to less effective antiferromagnetic coupling. The exchange integrals for **9** and **10** are almost doubled when compared with the related PAP complexes ($[\text{Cu}_2(\text{PAP})(\text{OH})\text{X}_2] \cdot 1.5\text{H}_2\text{O}$ ($\text{X} = \text{Cl}, \text{Br}$)) (Table 1-2) [35]. Structurally these complexes are all similar, with equatorial interactions to diazine and hydroxide groups and axial, orthogonal halides. The hydroxide bridge angle in **9** ($104.0(2)^\circ$) is only slightly higher than those found in the PAP complexes ($101.8^\circ(\text{Cl})$; $102.9^\circ(\text{Br})$) [35], and would not be expected to change the exchange situation very much. Based on the eq. 3, the angle in **9** leads to a calculated $-2J$ value of 255 cm^{-1} which is much lower than observed ($390(3) \text{ cm}^{-1}$). This suggests a fundamental difference on the part of the ligand, and in particular the role of the diazine bridge. The two ligands PAP and PTPH differ only with respect to the exocyclic groups (S in PTPH and NH in PAP). Two factors can be considered that might account for the significantly different role of the phthalazine bridge in these

two systems. The exocyclic NH groups could polarize spin density in the fused diazine ring more than would be the case for the less electronegative S in PTPH. This would have the effect of localizing exchange coupled spin more within the diazine ring in PAP, leading to reduced net antiferromagnetism. Alternatively a small admixture of tautomeric forms, involving a proton shift to a diazine ring nitrogen, would reduce the aromatic nature of the diazine ring and thus limit the π ring current, and therefore exchange.

1.4.6. Electrochemistry

Electrochemical data for **1** - **4** and **9** - **11** are listed in Table 1-11. Cyclic voltammetry in dried DMF gave single redox waves for each compound with $E_{1/2}$ values in the range 0.41 - 0.48 V (vs. SCE) ($\Delta E_p = 120 - 180$ mV at 100 mVs^{-1}) (see Fig. 1-12 for **1**). These data are comparable with those reported for related dinuclear copper(II) complexes (Table 1-2). Cyclic voltammograms run at varying scan rates in the range $50 - 500 \text{ mVs}^{-1}$ show little change in peak to peak separation (Fig. 1-13 for **1**), but the large ΔE_p value (160 mV for **1**, and 160 - 180 mV for **3**, **9**, **10**, **11**) indicates non reversible behaviour in these complexes. ΔE_p values for **2** and **4** (120 mV) are comparable with the reversible ferrocene /ferrocenium couple ($\Delta E_p = 90$ mV at 100 mVs^{-1} under identical conditions), and

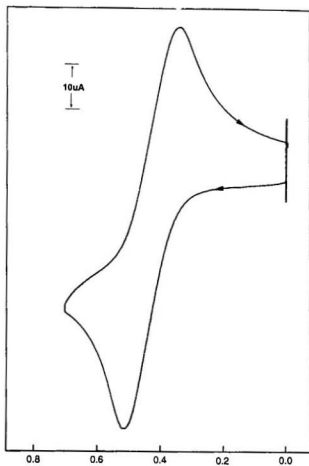


Fig. 1-12. Cyclic voltammogram for $[\text{Cu}_2(\text{PTPH})\text{Cl}_4] \cdot 2\text{H}_2\text{O}$ (1) in DMF
(3×10^{-3} M, 0.1 M TEAP, GC, SCE; 100 mVs^{-1})

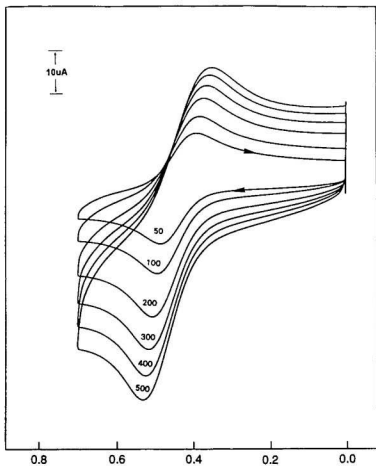


Fig. 1-13. Cyclic voltammograms for $[\text{Cu}_2(\text{PTPH})\text{Cl}_4] \cdot 2\text{H}_2\text{O}$ (1) in DMF (3×10^{-3} M, 0.1 M TEAP, GC, SCE; 50-500 mVs^{-1})

suggest quasi-reversible behaviour for these two complexes. Additional, irreversible oxidations observed above +0.60 V are associated with oxidation of chloride and bromide. Controlled potential electrolysis of DMF solutions of these complexes at a potential of 0.1 V gave electron counts that correspond to approximately two electron equivalents of charge, with the formation of red solutions (1, 3), pale red solutions (2, 4) and pale yellow solutions (9 - 11). The electrochemical non reversibility of the diazine bridged dinuclear copper (II) complexes indicates the likelihood of a molecular rearrangement on reduction to a dinuclear copper(I) species, and this is strongly supported by the synthesis of the complex $[\text{Cu}_2(\text{PTPH})_2](\text{ClO}_4)_2$ (12), which contains a dinuclear cation in which two tetrahedral metals are bonded in between two tetradentate ligands (Fig. 1-9). A similar complex was isolated from the corresponding pyridazine ligand PTP [53] in which the two copper(I) centres have the same geometry. Compounds 5 - 8 did not dissolve appreciably in suitable solvents and were not examined electrochemically.

1.5. Conclusion

PTPH, PTP and DPTD act as typical tetradentate N_4 diazine ligands producing dinuclear complexes with copper(II) salts, in which the two copper

centres are antiferromagnetically coupled. However, in a most unusual reaction involving copper(II) nitrate with PTPH, two very different complexes, one dinuclear and the other tetranuclear, are produced by employing slight and subtle differences in reaction conditions. The tetranuclear, dimerized dinuclear derivative involves μ_3 -hydroxide groups with substantial pyramidal distortion, which is seen as a contributing factor to lower than expected antiferromagnetic exchange. The hydroxo-bridged dinuclear copper(II) halide complexes are synthesized by using an unusual synthetic procedure in which copper(I) analogues are oxidized in situ by reaction with air. The magnetic studies of isostructural tetrahalide complexes $[\text{Cu}_2(\text{L})\text{X}_4]$ ($\text{L} = \text{PTPH}, \text{PTP}, \text{DPTD}$; $\text{X} = \text{Cl}, \text{Br}$) in which the diazine bridge is the only exchange pathway for antiferromagnetic coupling suggest that the capacity of diazine groups in mediating antiferromagnetic coupling is pyridazine > phthalazine > thiodiazole, and also indicate the dominant polarizing effect of electronegative halide ligands with chloride > bromide. In the isostructural hydroxo-bridged complexes $[\text{Cu}_2(\text{L})(\text{OH})(\text{NO}_3)_3]$ ($\text{L} = \text{PTPH}, \text{PTP}, \text{DPTD}$), in which the hydroxide is the dominant pathway for antiferromagnetic exchange, the complex with DPTD is more strongly coupled due to the five-membered thiadiazole ring, which would result in a larger hydroxide bridge angle. In the isostructural, triply bridged complexes $[\text{Cu}_2(\text{L})(\mu_2\text{-OH})(\mu_2\text{-X})\text{X}_2]$ ($\text{L} = \text{PTPH}, \text{PTP}$; $\text{X} = \text{Cl}, \text{Br}$), the results are in contrast to the observations for the complexes

$[\text{Cu}_2(\text{L})\text{X}_4]$ (L = PTPH, PTP; X = Cl, Br), in which phthalazine bridged complexes are more strongly coupled than pyridazine analogous and the chloro-complex is more strongly coupled than the bromo-derivative (for PTPH). These differences are attributed to differences in the Cu-O(H)-Cu bridge angles and the solid angles at the hydroxide bridges.

Chapter 2

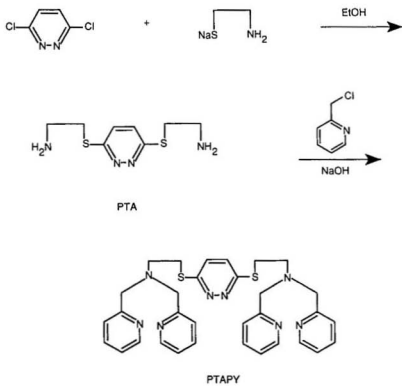
Dinuclear and Tetranuclear Copper(II) Complexes of 3,6-Bis-(N,N,N',N'-tetrakis-(pyridine-2-ylmethyl) - aminoethanethiolato)-pyridazine (PTAPY) - a Modified N₈ Diazine Ligand Exhibiting Hexadentate Coordination Behaviour

2.1. Introduction

The diazine (N₂) fragment forms a large number of polydentate ligands (Chapter 1) in which tetradentate (N₄) ligands are common, hexadentate (N₆) ligands are less common and octadentate (N₈) ligands are rare.

In continuing our interest in dinuclear and polynuclear complexes of polyfunctional ligands involving diazine moieties, we have examined one new ligand, PTAPY (3,6-bis-(N,N,N',N'-tetrakis-(pyridine-2-ylmethyl)-aminoethanethiolato)-pyridazine) (Scheme 2-1), which is a potentially octadentate (N₈) ligand and contains one pyridazine unit and two tripodal (N₃) groups. The effect of adding flexible pendant arms to the typical N₄ tetradentate diazine ligands (Chapter 1) on the copper coordination geometries and magnetic interaction will be illustrated.

Scheme 2-1.



2.2. Experimental*

2.2.1. Synthesis of the Ligands

3,6-Di-(aminoethanethiolato)-pyridazine (PTA)

Sodium metal (9.5 g, 0.4 mol) was dissolved in degassed absolute ethanol (200 mL) under N₂ and the solution refluxed for 30 min. A solution of 2-aminoethanethiol hydrochloride (22.5 g, 0.2 mol) in warm degassed absolute ethanol (150 mL) was then added, whereupon a white solid (NaCl) separated immediately. The reaction mixture was stirred at 60-70 °C for 30 min and a solution of 3,6-dichloropyridazine (15.0 g, 0.1 mol) in degassed absolute ethanol (100 mL) added dropwise, with stirring, over a period of 1 h. The reaction mixture was then refluxed for 6 h and left at room temperature overnight. The white solid was filtered off, the filtrate concentrated to a volume of about 40 mL, and diethyl ether (50 mL) added. After storage in a refrigerator, a pale yellow solid separated which was filtered, washed with ether and dried. A second crop of product was obtained from the filtrate by repeating the same procedure. Yield: 87%. Mp: 63-64 °C. Mass spectrum, major mass peaks (m/e(relative intensity)): 231(1) P, 201(5), 189(4), 187(27), 171(7), 158(32), 144(10), 139(7), 125(11), 79(11). ¹H NMR (DMSO-d₆) (δ(relative intensity)): 2.07(4) (broad singlet, NH₂),

*For general procedures, see 1.2.

2.82(4) (triplet, CH₂), 3.24(4) (triplet, CH₂), 7.44(2) (singlet, pyridazine).

3,6-bis-(N,N,N',N'-tetrakis-(pyridine-2-ylmethyl)-aminoethanethiolato)-pyridazine (PTAPY)

PTA (5.20 g, 22.6 mmol) and 2-(chloromethyl)-pyridine (14.83 g, 90.4 mmol) were dissolved in water (100 mL). A solution of sodium hydroxide (7.24 g, 181 mmol) in water (50 mL) was added dropwise with stirring to the mixture, over a period of ca. 1 h. The mixture was stirred for a further 12 h and the brown oil formed was extracted with dichloromethane. The extract was washed with water (3 x 50 mL) and dried over sodium sulphate. After removing the dichloromethane the remaining dark brown oil was chromatographed (silica gel: hexane/CHCl₃) to give a pale yellow crystalline compound. Yield: 6.44 g (48%). M.p. 88-90 °C. ¹H nmr (CDCl₃) (δ(relative intensity)): 2.97(4) (triplet, CH₂), 3.52(4) (triplet, CH₂), 3.90(8) (singlet, CH₂), 7.16(8) (multiplet, pyridine), 7.60(8) (multiplet, pyridine), 8.50(2) (doublet, pyridazine). Mass spectrum (m/e): 502 (the highest mass peak corresponds to the parent ion minus one methyl-pyridine residue).

2.2.2. Synthesis of the complexes

Safety note:

Copper(II) azide and perchlorate and their complexes are potentially very explosive and should be prepared in small amounts.

[Cu₂(PTAPY)(NO₃)₄]·H₂O (14)

Copper nitrate (0.36 g, 1.5 mmol) and PTAPY (0.25 g, 0.50 mmol) were dissolved in methanol (40 mL) and the reaction mixture was refluxed for 24 h. The resulting bluish green solution was concentrated to ca. 5 mL and 40 mL of ethanol added. A bluish green solid separated, which was filtered off, washed with ethanol (3 x 5 mL) and dried under vacuum at room temperature for 24 h. Recrystallization from methanol/ethanol (1:1) mixture produced bluish green crystals. Yield: 0.35 g (71%). Anal. calcd. for C₃₂H₃₆N₁₂O₁₃S₂Cu₂: C 38.90, H 3.67, N 17.01; Found: C 38.68, H 3.45, N 17.15.

[Cu₂(PTAPY)Br₄]·2H₂O (15)

A solution of PTAPY (0.25 g, 0.50 mmol) in methanol (10 mL) was added to a solution of copper bromide (0.34 g, 1.5 mmol) in 20 mL of methanol, and the reaction mixture was refluxed for 24 h. A dark grey solid separated, which was filtered off and washed with ethanol (3 x 5 mL). Recrystallization from methanol/water (1:1) mixture produced green crystals. Yield: 0.38 g (70%).

Anal. calcd. for $C_{32}H_{38}N_4O_2S_2Br_4Cu_2$: C 35.64, H 3.55, N 10.40; Found: C 35.92, H 3.43, N 10.02. Crystals used for the X-ray structure analysis were obtained as $[Cu_2(PTAPY)Br_4] \cdot 2DMF$ by the slow diffusion of ether into a DMF solution of the complex.

$[Cu_2(PTAPY)(CH_3CN)_2](ClO_4)_4 \cdot 0.5C_2H_5OH$ (16)

A solution of PTAPY (0.60 g, 1.0 mmol) in ethanol (20 mL) was added to a solution of copper perchlorate (1.1 g, 3.0 mmol) in ethanol (20 mL) and the mixture refluxed for 3 h. A blue crystalline compound formed, which was filtered off and washed with ethanol (3 x 5 mL). Recrystallization from acetonitrile/ethanol (1:1) mixture produced deep blue crystals. Yield: 0.44 g (40%). Anal. calcd. for $C_{37}H_{43}N_{10}O_{16.5}S_2Cl_4Cu_2$: C 36.28, H 3.04, N 11.43; Found: C 36.31, H 3.58, N 11.20.

$[Cu_2(PTAPY)(NO_3)_2(N_3)(H_2O)]_2(NO_3)_2 \cdot 1.2CH_3OH$ (17)

A solution of copper(II) nitrate (0.72 g, 3.0 mmol) in methanol (50 mL) was added to a solution of PTAPY (0.60 g, 1.0 mmol) in the same solvent (50 mL). A blue solution formed which was stirred at ambient temperature for about 5 minutes, followed by the addition of a solution of NaN_3 (0.20 g, 6.0 mmol) in 20 mL of hot methanol. A green coloured solution was produced along with a small amount of a dark brown solid (probably copper(II) azide). The brown solid

was filtered off and discarded and the green filtrate was concentrated to 10 mL. A greenish-blue solid separated, which was dissolved by adding 10 mL of DMF followed by 30 mL of methanol and the reaction mixture was refluxed for 5 minutes and filtered hot. The filtrate, which was allowed to stand at room temperature for several days, deposited a blue solid, which was filtered off, washed with methanol (3 x 3 mL) and ether (3 x 10 mL) and dried under vacuum at room temperature. Yield: 0.49 g (50%). The crystals used for X-ray structure determination were obtained by the slow diffusion of ether into a solution of the complex in a mixture of dimethylsulphoxide/methanol/acetonitrile (1:1:1).

2.3. Results and Discussion

2.3.1. Ligands

The synthesis of PTAPY is shown in Scheme 2-1. The design of PTAPY has several features. The central pyridazine group is well studied and should bind two copper atoms in close proximity [39, 40, 42, 44, 45, 47, 51, 56, 57, 66, 67]. There is a balance of symmetry and flexibility in the 'arms' of the ligand, that should lead to the compounds having a workable solubility. The ligand can be compared with a series of m-xylyl-bridged or hydrocarbon-linked bis(2-(2-pyridyl)ethyl)amine and bis(2-(2-pyridyl)methyl)amine N_6 dinucleating ligands [6, 97, 108 - 114]. These ligands contain two tripodal groups similar to that in

PTAPY which provide three nitrogen donors to each copper ion and have been used to prepare biomimics of the type III copper protein centres [6]. The synthetic starting material for the ligand is 3,6-di-(aminoethanethiolato)-pyridazine (PTA), which should be capable of binding two metals in the same manner as the tetradentate (N_4), pyridazine and phthalazine ligands [28 - 62]. However PTA is difficult to prepare and handle and is susceptible to decomposition. If PTA is exposed to air for a long period of time a polymeric material of unknown composition is formed, which is insoluble in most common solvents. PTA will form copper complexes readily, but they are unstable and undergo spontaneous reduction with the formation of what appear to be non-stoichiometric, mixed oxidation state species. As a consequence these complexes are difficult to characterize. However open chain and macrocyclic ligands [115 - 117], which are synthesized from PTA, and their complexes, have much greater stability. PTAPY does not give a molecular ion in its mass spectrum, giving only fragments resulting from sulphur-carbon bond cleavage, suggesting an inherent instability for the ligand. However supporting evidence for the ligand structure came from the 1H -NMR spectrum and C,H,N analyses and the X-ray crystal structures of its complexes.

2.3.2. Structures

[Cu₂(PTAPY)Br₂]·2H₂O (15)

The structure of **15** is shown in Fig. 2-1, and selected bond distances and angles relevant to the copper coordination spheres are given in Table 2-1. Each copper ion is bonded to two pyridine nitrogen atoms, a tertiary amine nitrogen atom and two bromine atoms in distorted five coordinate arrangements. However the two copper centres are quite different. Addison et al. [118] have proposed a structural index τ for the geometry of five coordinated copper centres, which has been defined as $\tau = (\beta - \alpha)/60$, with α and β being the two largest coordination angles. In a perfect square-pyramidal geometry, τ equals 0, while it equals 1 in a perfect trigonal-bipyramidal geometry. For Cu(1), τ equals 0.18 ($\alpha = 149.8^\circ$ (Br(1)-Cu(1)-N(2)), $\beta = 160.5^\circ$ (N(1)-Cu(1)-N(3))), hence the stereochemistry at Cu(1) can best be described as a distorted square pyramid with four short in-plane contacts involving pyridine nitrogens (N(1), N(3)), amine nitrogen (N(2)) and a bromine atom (Br(1)) and a weak axial interaction to Br(2) (2.608 Å), which is somewhat shorter than those reported for other, related five-coordinate square pyramidal copper(II) complexes of thio-diazine ligands PTP [57] and DPTD (Table 1-4) involving axially bound bromine. Cu(1) is displaced by 0.429(4) Å from the mean plane of the four in plane donors, N(1), N(2), N(3), Br(1) towards the apical

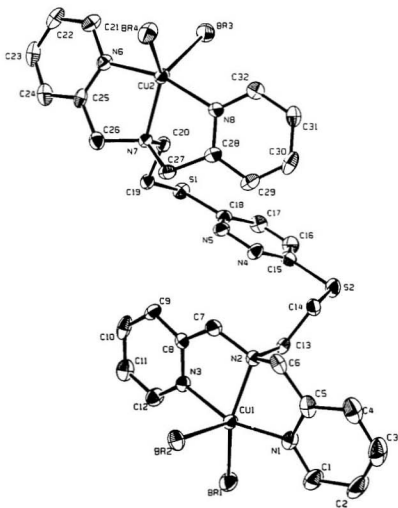


Fig. 2-1. Structural representation of $[\text{Cu}_2(\text{PTAPY})\text{Br}_4] \cdot 2\text{DMF}$ (**15**), with hydrogen atoms omitted (40% probability ellipsoids).

Table 2-1. Selected bond distances (Å) and angles (deg) for [Cu₂(PTAPY)·Br₄]·2DMF (15)

Br(1)-Cu(1)	2.384(1)	Br(2)-Cu(1)	2.608(1)
Br(3)-Cu(2)	2.549(2)	Br(4)-Cu(2)	2.447(1)
Cu(1)-N(1)	2.040(4)	Cu(1)-N(2)	2.060(4)
Cu(1)-N(3)	2.027(4)	Cu(2)-N(6)	1.991(4)
Cu(2)-N(7)	2.104(4)	Cu(2)-N(8)	1.993(4)
Cu(1)-Cu(2)	7.406(2)		
Br(1)-Cu(1)-Br(2)	109.82(4)	Br(1)-Cu(1)-N(1)	96.6(1)
Br(1)-Cu(1)-N(2)	149.8(1)	Br(1)-Cu(1)-N(3)	96.9(1)
Br(2)-Cu(1)-N(1)	95.8(1)	Br(2)-Cu(1)-N(2)	100.3(1)
Br(2)-Cu(1)-N(3)	92.8(1)	N(1)-Cu(1)-N(2)	80.6(2)
N(1)-Cu(1)-N(3)	160.5(2)	N(2)-Cu(1)-N(3)	80.6(2)
Br(3)-Cu(2)-Br(4)	112.44(4)	Br(3)-Cu(2)-N(6)	94.0(1)
Br(3)-Cu(2)-N(7)	115.1(1)	Br(3)-Cu(2)-N(8)	94.0(1)
Br(4)-Cu(2)-N(6)	97.2(1)	Br(4)-Cu(2)-N(7)	132.4(1)
Br(4)-Cu(2)-N(8)	94.4(1)	N(6)-Cu(2)-N(7)	81.2(2)
N(6)-Cu(2)-N(8)	162.2(2)	N(7)-Cu(2)-N(8)	81.0(2)

bromine atom Br(2). For Cu(2), τ equals 0.50 ($\alpha = 132.4^\circ$ (Br(4)-Cu(2)-N(7)), $\beta = 162.2^\circ$ (N(6)-Cu(2)-N(8))), therefore the stereochemistry at Cu(2) is midway between a square-pyramid and a trigonal-bipyramid, but can best be described as a distorted trigonal-bipyramid. The axial ligands (N(6), N(8)) form an almost linear arrangement about the copper centre (Cu(2)) with an angle N(6)-Cu(2)-N(8) of 162.2° . Equatorial angles of 115.1° , 112.44° and 132.4° are reasonable for a distorted trigonal bipyramid, and this is supported by the fact that the two equatorial copper bromine distances (2.549(2) Å, 2.447(1) Å) compare more closely than in the case of the square-pyramidal copper centre. The copper-copper separation is 7.406(2) Å, clearly indicating no possible intradimer association between the copper centres. The copper-nitrogen (pyridine) contacts (1.991 - 2.040 Å) are in the range reported for these coordination geometries in copper(II) complexes with thio-diazine ligands (Chapter 1) and other related ligands containing similar tripodal groups [97 - 110, 114]. The Cu-N_{min} bond lengths differ significantly with Cu(1)-N(2) (2.060(4) Å), and Cu(2)-N(7) (2.104(4) Å) lying in the range found in other structurally similar dinuclear copper(II) complexes [97 - 110] and in a series of copper(II) mononuclear complexes with tertiary amine ligands located in the basal plane of the tetragonal pyramid [119, 120]. The pyridazine nitrogen atoms remain uncoordinated and the two copper centres are held apart at two ends of the ligand by the two tripodal N₃

chromophores. Two DMF molecules are present in the asymmetric unit and are not bonded to the metal centres.

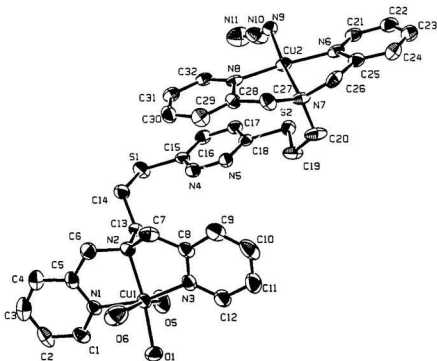


Fig. 2-2. Structural representation of the monomeric, dinuclear unit of $[\text{Cu}_2(\text{PTAPY})(\text{NO}_3)_2(\text{N}_3)(\text{H}_2\text{O})]$ (17), with hydrogen atoms and nitrates omitted (40% probability ellipsoids).

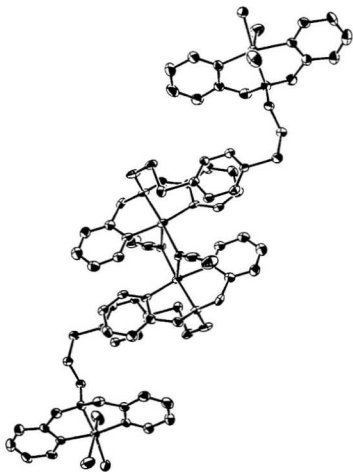


Fig. 2-3. Structural representation of the dimeric tetranuclear complex $[\text{Cu}_2(\text{PTAPY})(\text{NO}_3)_2(\text{N}_3)(\text{H}_2\text{O})]_2$ (17), with hydrogen atoms and nitrates omitted (40% probability ellipsoids).

Table 2-2. Selected bond distances (Å) and angles (deg) for $[\text{Cu}_2(\text{PTAPY}) \cdot (\text{NO}_3)_2(\text{N}_3)(\text{H}_2\text{O})]_2(\text{NO}_3)_2 \cdot 1.2\text{CH}_3\text{OH}$ (**17**)

Cu(1)-O(1)	1.980(6)	Cu(1)-N(1)	1.979(8)
Cu(1)-N(2)	2.036(7)	Cu(1)-N(3)	1.959(8)
Cu(2)-N(6)	1.978(8)	Cu(2)-N(7)	2.058(7)
Cu(2)-N(8)	1.966(8)	Cu(2)-N(9)	1.978(8)
Cu(1)-O(5)	2.363(8)	Cu(1)-O(6)	2.717(9)
Cu(2)-N(9)*	2.857(9)	Cu(1)-Cu(2)	10.228(5)
O(1)-Cu(1)-N(1)	93.3(3)	O(1)-Cu(1)-N(2)	167.6(3)
O(1)-Cu(1)-N(3)	99.9(3)	N(1)-Cu(1)-N(2)	82.9(3)
N(1)-Cu(1)-N(3)	164.7(4)	N(2)-Cu(1)-N(3)	82.6(3)
N(6)-Cu(2)-N(7)	83.0(3)	N(6)-Cu(2)-N(8)	166.3(3)
N(6)-Cu(2)-N(9)	93.4(3)	N(7)-Cu(2)-N(8)	84.5(3)
N(7)-Cu(2)-N(9)	173.7(3)	N(8)-Cu(2)-N(9)	98.5(3)



The structure of complex **17** is shown in Fig. 2-2 and Fig. 2-3, which illustrate the monomeric dinuclear and the dimeric tetranuclear units respectively. Bond lengths and angles relevant to the copper coordination spheres are listed in

Table 2-2. The two metallic centres are located at the two ends of the ligand which is very similar to the situation found in **15**. The copper-copper separation in **17** (10.228(4) Å) is much larger than that in **15** (7.406(2) Å). The two copper centres in **17** have quite different geometries. Cu(1) is six-coordinated in a distorted tetragonal structure with four short in plane contacts involving pyridine nitrogens (N(1), N(3)), amino nitrogen (N(2)) and an oxygen atom from a water molecule and two axial contacts to two nitrate oxygen atoms (O(5), O(6)) of two monodentate nitrate groups. The copper centre is displaced by 0.160(8) Å from the mean plane of the four in plane donors (N₃O) towards the axial nitrate O(5) which is more strongly coordinated than O(6) (Cu(1)-O(5) 2.363(8)Å, Cu(1)-O(6) 2.717(9) Å). Cu(2) is five-coordinate and the structural index τ equals 0.12 ($\alpha = 166.3^\circ$ (N(6)-Cu(2)-N(6)), $\beta = 173.7^\circ$ (N(7)-Cu(2)-N(9))). Hence Cu(2) is in a distorted square-pyramidal geometry involving two pyridine nitrogens (N(6), (N8)), amino nitrogen (N(7)) and azido nitrogen (N(9)) in the basal plane, all with contacts <2.06 Å and with a very weak axial interaction to an azido nitrogen atom (Cu(2)-N(9) 2.857(9) Å) from another dinuclear molecule. The weak axial interaction of Cu(2) with N(9) results in the formation of a weakly associated tetranuclear, dimeric structure. Cu(2) is slightly displaced by 0.101(7) Å from the mean plane of the four in plane donors (N(6), (N7), N(8), N(9)), towards apical

azido nitrogen atom (N(9)). Non-stoichiometric solvent (methanol) was found in the unit cell, but is not bonded to the metal centres.

2.3.3. Spectroscopic Properties

The IR spectra of compounds **14** - **17** are similar in the spectral region where ligand absorptions are observed. Compound **14** exhibits two prominent bands at 1742 cm^{-1} and 1727 cm^{-1} associated with the combination bands ($\nu_1 + \nu_4$) of the nitrate groups, and the difference of 15 cm^{-1} of the two bands suggests the presence of monodentate nitrates [98]. Compound **16** exhibits strong absorptions at 1091 cm^{-1} and 623 cm^{-1} due to ν_3 and ν_4 modes respectively of ionic perchlorate and two sharp νCN absorptions at 2315 cm^{-1} and 2286 cm^{-1} associated with coordinated acetonitrile. In copper and silver complexes involving pyridazinophane ligands, which have been shown to contain uncoordinated lattice acetonitrile, νCN bands occur at lower energies (2293, 2253 cm^{-1} (Ag); 2297, 2253 cm^{-1} (Cu)) [121, 122]. The uncoordinated acetonitrile in $[\text{Cu}_2(\text{PTPH})_2](\text{ClO}_4)_2 \cdot \text{CHCl}_3 \cdot \text{CH}_3\text{CN}$ (Table 1-11) shows two bands in the similar region (2288, 2251 cm^{-1}). However in the complex $([\text{Cu}(\text{DPP})(\text{H}_2\text{O})(\text{CH}_3\text{CN})](\text{ClO}_4)_2 \cdot 2\text{H}_2\text{O})_x$ (DPP=4,6-di-(2'-pyridylthio)-pyrimidine) [99] involving coordinated acetonitrile, νCN bands occur at higher energies (2301, 2273 cm^{-1}), comparable with those observed for **16**. In compound **17** a strong band at 2044 cm^{-1} is assigned to the coordinated azido

group in μ -1,1 bridging mode [6]. A major nitrate combination band for **17** observed at 1744 cm^{-1} is indicative of ionic nitrate, while the low energy shoulders at 1737 and 1725 cm^{-1} are associated with the monodentate nitrates [98].

The electrical conductivities of millimolar solutions of compounds **14** - **17** were measured in DMF (Table 2-3). The conductance values for compounds **14**, **15** and **17** (Table 3-3) lie in the range $128 - 168\text{ ohm}^{-1}\text{ cm}^2\text{ mol}^{-1}$, which is characteristic for 2:1 electrolytes [123], and suggests the partial displacement of coordinated anions by DMF molecules. The conductance value of $336\text{ ohm}^{-1}\text{ cm}^2\text{ mol}^{-1}$ for compound **16** is indicative of 4:1 electrolytic behaviour, as expected due to weak coordination of perchlorate anions.

The solid state electronic spectrum of compound **14** exhibits one broad visible d-d absorption, while **15**, **16** and **17** show two prominent bands. These are probably due to the presence of two different copper ion stereochemistries rather than lower symmetry ligand field components. The spectra of **15** and **17** are clearly consistent in this regard with structural features which show the presence of two different copper centres in each compound. Such a situation may also exist in compound **16**. More intense, high energy absorptions are clearly due to charge transfer in the compounds and may be associated with ligand to metal charge

Table 2-3. Magnetic, spectral, conductance and electrochemical data of dinuclear copper(II) complexes of PTAPY

Complex	μ_{eff} (μ_{B}) ^a	λ_{max} (nm) (ϵ) ^b	$E_{1/2}$ V (vs SCE) ^c (ΔE_p mV)	Conductance ^d ($\text{ohm}^{-1}\text{cm}^2\text{mol}^{-1}$)
$[\text{Cu}_2(\text{PTAPY})(\text{NO}_3)_4] \cdot \text{H}_2\text{O}$ (14)	1.84	670, 330 ^e 655(340) ^d	0.0 (160)	147
$[\text{Cu}_2(\text{PTAPY})\text{Br}_4] \cdot 2\text{H}_2\text{O}$ (15)	1.83	920, 725, 345 ^e [970](280), [850] (400), 785(440) ^d	0.06 (100)	168
$[\text{Cu}_2(\text{PTAPY})(\text{CH}_3\text{CN})_2]$ $(\text{ClO}_4)_4 \cdot 0.5\text{EtOH}$ (16)	1.88	680, [600], 330 ^e 830(130), 645(380) ^d	-0.015 (70) -0.115 (70)	336
$[\text{Cu}_2(\text{PTAPY})(\text{NO}_3)_2(\text{N}_3)(\text{H}_2\text{O})_2]$ $(\text{NO}_3)_2 \cdot 1.2\text{CH}_3\text{OH}$ (17)	1.73	660, [610], 385, 325 ^e 630(310), 395(2280) ^d	-0.02 (100) -0.145 (130)	155

^aAt room temperature; ^b $\epsilon(\text{dm}^3 \text{mol}^{-1} \text{cm}^{-1})$; [] shoulder; ^csolid (mull transmittance); ^dDMF solutions,

^eDMF/0.1 M TEAP/GC/SCE at scan rate of 100 mV/sec.

transfer. In DMF solutions shifts in the positions of the solid state bands are observed for all compounds (Table 2-3), suggesting changes in the metal ion coordination spheres, consistent with solvent (DMF) coordination, as indicated by the conductance measurements. The similarities of infrared and electronic spectra between compounds **14** - **17** suggests that **14** and **16** have similar dinuclear structures involving two metal centres bound at the two ends of the ligand, with no pyridazine coordination.

X-Band esr spectra of complexes **14** - **17** were recorded on powdered solids or solutions (DMF) at room temperature (295 K) and at liquid nitrogen temperature (77 K). **14** exhibits an axial signal in the solid state, both at room temperature (Fig. 2-4) and 77 K, which can be interpreted in terms of a distorted trigonal bipyramidal species with $g_{\parallel} = 2.04$ and $g_{\perp} = 2.14$ (295 K). In DMF solution, both at room temperature and in frozen glass at 77 K, two sets of hyperfine lines indicate the presence of two different axial species. At 77 K the hyperfine splittings of 200 G and 164 G are too large for a trigonal bipyramidal species and so it appears that in solution **14** probably forms a tetragonal or distorted square-pyramidal species, in which the two copper centres are still different, and involves solvent coordination (1:2 electrolyte in DMF). In the solid state at room temperature a powdered sample of **15** exhibits an orthorhombic esr

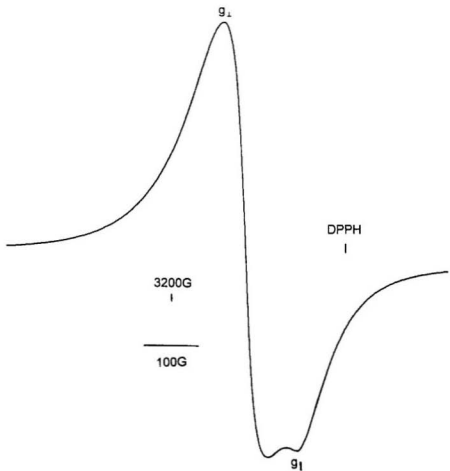


Fig. 2-4. Solid state esr spectrum for a powdered sample of $[\text{Cu}_2(\text{PTAPY})(\text{NO}_3)_4] \cdot \text{H}_2\text{O}$ (14) (9.76 GHz; 295 K).

spectrum (Fig. 2-5), with $g_1 = 2.208$, $g_2 = 2.114$, $g_3 = 2.032$, consistent with the five-coordinate Cu(II) geometries indicated from the structural determination. At 77 K a somewhat broadened signal is observed at $g = 2.18$. Solution esr spectra of **15**, both at room temperature and 77 K, exhibit only one broad band centred at $g = 2.10 - 2.12$.

16 exhibits only one isotropic signal in the solid state, both at room temperature and 77 K centred at $g_{av} = 2.06$. In DMF at 77 K **16** shows two overlapping sets of signals in the parallel region, with small and comparable hyperfine coupling constants (approx. 130 G). Although establishing g values was difficult, because of incomplete resolution of the lines, the small coupling constants suggest copper centres with appreciable tetrahedral distortion, which would be consistent with the N_4 coordination environment proposed for this complex.

The room temperature esr spectra of both solid bulk and recrystallized samples of **17** are identical and typical of axially elongated tetragonal species with $g_{\parallel} = 2.194$ and $g_{\perp} = 2.052$ (Fig. 2-6), consistent with the X-ray structure, which shows the presence of axially elongated tetragonal and square pyramidal stereochemistries at the Cu(1) and Cu(2) centres respectively. At 77 K an identical solid state spectrum is observed. In DMF solution a broad isotropic signal is observed at both 295 and 77 K.

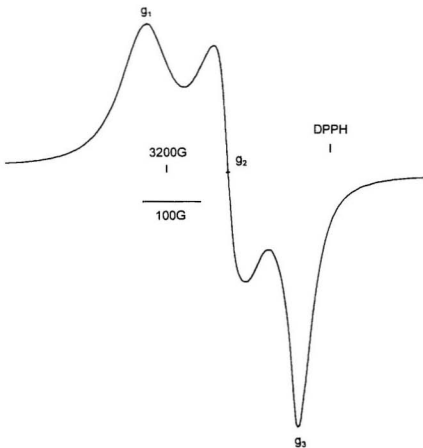


Fig. 2-5. Solid state esr spectrum for a powdered sample of $[\text{Cu}_2(\text{PTAPY})\text{Br}_4] \cdot 2\text{DMF} (15)$ (9.77 GHz; 295 K).

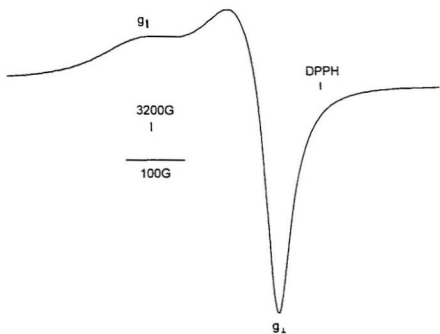


Fig. 2-6. Solid state esr spectrum for a powdered sample of $[\text{Cu}_2(\text{PTAPY})(\text{NO}_3)_2(\text{N}_3)(\text{H}_2\text{O})]_2(\text{NO}_3)_2 \cdot 1.2\text{CH}_3\text{OH}$ (17) (9.77 GHz; 295 K).

2.3.4. Magnetism

Room temperature magnetic moments for compounds **14** - **16** fall in the range μ_{eff} 1.83 - 1.88 BM /Cu (Table 2-3) which is typical for dilute copper (II) centres and suggests the absence of any type of magnetic interactions between the two copper (II) centres. This has been confirmed by the X-ray structure determination of compound **15**, in which the two copper centres are widely separated (7.406 Å), without any short bridge between them which could result in a spin interaction. It is reasonable to assume that in these dinuclear complexes each copper behaves independently, with structures similar to that in **15**. The room temperature magnetic moment for **17** (1.73 BM / Cu) is lower than that observed in **14** - **16**, and although it is nominally equal to the spin only value for a dilute copper(II) species some weak axial spin interaction may exist between the two dinuclear halves through azido bridges. The interaction is however likely to be weak and must await a variable temperature magnetic study to confirm this suggestion.

2.3.5. Electrochemistry

The electrochemical properties of compounds **14** - **17** have been studied by cyclic voltammetry in DMF solutions containing 0.1 M TEAP as supporting electrolyte at glassy carbon and/or platinum working electrodes. Data, including

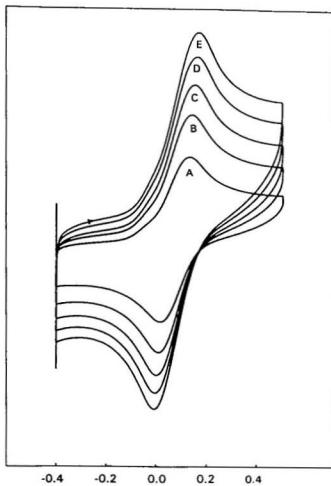


Fig. 2-7. Cyclic voltammograms for $[\text{Cu}_2(\text{PTAPY})\text{Br}_4] \cdot 2\text{H}_2\text{O}$ (15) in DMF (3×10^{-3} M, 0.1 M TEAP, GC, SCE, A-D: 100 - 500 mVs^{-1}).

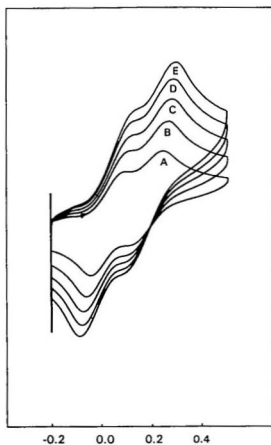


Fig. 2-8. Cyclic voltammograms for $[\text{Cu}_2(\text{PTAPY})(\text{NO}_3)_2(\text{N}_3)(\text{H}_2\text{O})]_2(\text{NO}_3)_2 \cdot 1.2\text{CH}_3\text{OH}$ in DMF (17) (3×10^{-3} M, 0.1 M TEAP, GC, SCE, A-D: 100 - 500 mVs^{-1}).

$E_{1/2}$ values and peak to peak separations, are given in Table 2-3 and cyclic voltammograms for **14** and **17** are shown in Fig. 2-7 and Fig. 2-8 respectively. Cyclic voltammograms for **14** and **15** are very similar and involve one quasi-reversible redox process at a potential around 0.0 V (vs SCE), associated with a one step reduction of the dinuclear copper(II) species to a dinuclear copper(I) species. The cyclic voltammograms of **16** and **17** (Fig. 2-8) are characterized by the presence of two quasi-reversible, overlapping redox processes at negative potentials ($E^1_{1/2} = -0.015$ V (**16**), -0.02 V (**17**); $E^2_{1/2} = -0.115$ V (**16**), -0.145 V (**17**) (vs SCE)), suggesting two stepwise, one electron reductions proceeding through a Cu(II)-Cu(I) intermediate to a dinuclear Cu(I) species. The observation of two closely separated redox processes would be consistent with the presence of two slightly different copper centres in solution which is clearly in agreement with the solid state structure of **17** in which two different Cu(II) centres are observed.

2.4. Conclusion

In this chapter, the synthesis, spectroscopic, magnetic and electrochemical properties of dinuclear copper(II) complexes with one new polydentate, dinucleating ligand have been discussed. Although PTAPY is a potentially octadentate (N_8) dinucleating ligand, it reacts with copper(II) salts to form

dinuclear complexes (**14** - **17**) of 2:1 (M:L) stoichiometry involving just six nitrogen donor centres. The copper centres in the dinuclear molecules (**15** and **17**) are widely separated without any magnetic interaction between them, as a result of the lack of coordination exhibited by the pyridazine group. The two tripodal N₃ donor groups are strong chelating groups and can coordinate strongly to the copper(II) centres and it is not obvious why all eight nitrogens are not involved in coordination simultaneously. Steric crowding and the formation of seven-membered chelate rings may make it difficult for pyridazine to coordinate, which is similar to the situations found in some macrocyclic ligands derived from PTA [116, 117]. In **17** dimerization leads to the formation of a tetranuclear complex involving azido bridges.

Chapter 3

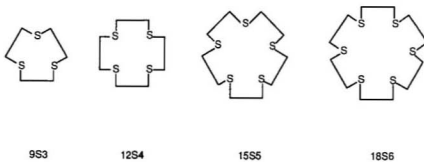
Mononuclear, Dinuclear, Trinuclear and Polymeric Polynuclear Copper(II) Complexes of Thioether-pyridazine Macrocycles

3.1. Introduction

The coordination chemistry of thioether ligands has been extensively studied and reviewed during the past decade [124 - 128]. This has been primarily due to the observation that crown thioethers can bind to a range of transition metal ions in different oxidation states to form stable metal complexes with different geometries [127 - 130]. Another impetus for the study of the coordination chemistry of thioethers stems from the discovery of the structure of the 'blue' copper proteins such as plastocyanin and azurin, which have demonstrated thioether sulfur coordination to the copper ions [131 - 136]. The intense visible absorption and the high reduction potentials of these proteins are associated with sulfur (cysteine) coordination to the copper centres. The binding of Cu(II) and Cu(I) centres to thioethers has led to a greater understanding of Cu-S (thioether)

interaction and the stereochemical preference of these metal centres [137 - 142]. Homoleptic thioether complexes represent the most promising synthetic systems to explain the electronic consequences of thioether coordination. So far a considerable number of four, five and six-coordinate copper complexes of homoleptic macrocyclic thioethers have been studied [127, 128, 137, 138, 143 - 148], and some typical ligands are illustrated in Scheme 3-1. These ligands also show extensive coordination chemistry with a large number of other metal ions [127, 128].

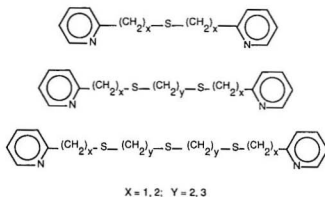
Scheme 3-1.



At the same time a variety of chelating ligands containing both sulfur and nitrogen donor atoms has been designed and synthesized. Typical ligands are shown in Scheme 3-2. These ligands usually have N_2S , N_2S_2 , and N_2S_3 donor sets.

The pyridine group can be substituted by other heterocycles such as 2-benzimidazole, 2-thiophene, 1-pyrazole and 2- or 4- imidazole [149 - 155].

Scheme 3-2.

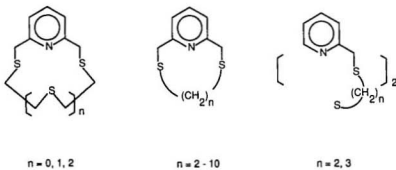


The complexes of these ligands supply a realistic model for 'blue' or 'type 1' copper centres since X-ray structural determinations of poplar plastocyanin (1.6 Å resolution) [134] and *alcaligenes denitrificans* azurin (1.8 Å resolution) [156] indicate that copper(II) is surrounded by two heterocyclic N-donors (histidine imidazole), a mercaptide-S and a thioether-S.

A series of macrocyclic ligands with thioether and amino, amido, pyridine, furan, thiophene, and benzene subunits has also been explored. Lehn, Cram,

Vögtle and their coworkers have synthesized a series of macrocyclic as well as macropolycyclic ligands containing pyridine and sulfur binding sites by condensation of a dithiol with 2,6-di(bromomethyl)pyridine or 2,6-pyridinedithiol with dihalide [157 - 163]. Some of these ligands are shown in Scheme 3-3. These ligands have been shown to complex various transition-metal cations involving the simultaneous coordination of pyridine nitrogen and thioether sulfur atoms. The coordination sites markedly influence the properties of the bound cations, for example stabilizing low oxidation states, which play an important role in reactions catalysed by many metal complexes.

Scheme 3-3.

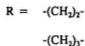
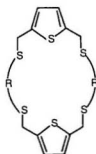
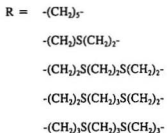
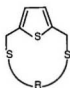


Some macrocycles containing furan and thioether were also synthesized from the reaction of 3,4-bis(chloromethyl)furan or 3,4-bis(mercaptomethyl)furan

with appropriate dithiols or dihalides [164], but little coordination chemistry was studied for these ligands.

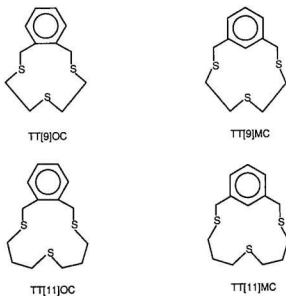
Recently, a series of thioether macrocycles containing one or two thiophene subunits were synthesized by Lucas and co-workers (Scheme 3-4) from the condensation of 2,5-bis(chloromethyl)thiophene and appropriate dimercaptans under high dilution condition in basic media. The coordination chemistry of these ligands with Cu(II), Cu(I), Ag(I), Pd(II), Pt(II) have been studied in detail [165 - 170].

Scheme 3-4.



Very recently, a series of thiacyclophanes was synthesized by Loeb and co-workers (Scheme 3-5) by condensation of α,α' -dibromo-*m*-xylene or α,α' -dibromo-*o*-xylene with appropriate dithiols [171 - 175]. The coordination chemistry of these ligands with Cu(I), Ag(I), Pd(II), and Mo(0) has been studied.

Scheme 3-5.



Though crown thioether chemistry can be dated from 1886, when Mansfeld reported the synthesis of 9S3 [176], the study of the coordination chemistry of

these macrocyclic thioethers has been hindered by the difficulties in the synthesis of the free ligands. The synthesis of 9S3 by Ochrymowycz and coworkers was in very low yield (only 0.04% !) [177]. However advances in synthetic methodology nowadays afford crown thioethers in high yield, which has encouraged the rapid development of the coordination chemistry of these ligands.

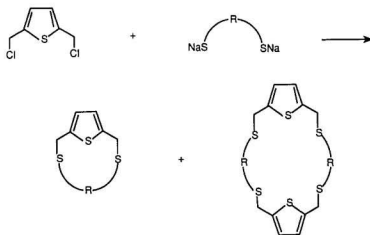
The weak coordination of sulfur for active metal ions makes template methods less effective than in the case for the synthesis of macrocyclic polyoxoethers. The competition between cyclization and linear polymerization in the synthesis of thioethers is more statistically defined, with cyclization kinetically favoured only at high dilution [178 - 180]. Therefore, most of the synthetic methods for polythioethers involve high-dilution techniques and with relatively long reaction time.

One of the most common synthetic methods for macrocyclic thioether is the reaction of α,ω -dihalides (chlorides, bromides) with α,ω -dimercaptans under high dilution conditions in basic alcoholic media (NaOEt, or KOEt). This method is based on the pioneering work of Ochrymowycz and coworkers in this area [181]. The ring closure is based on S_N2 α -mercaptide displacement of an ω -halide group.

Most of the crown thioethers and the macrocyclic thioethers containing pyridine, thiophene (Scheme 3-6) and xylyl subunits are generally synthesized by using this method. This method was also used for the synthesis for some open

chain polythioethers [149]. It was observed that for conformationally flexible macrocycles with longer hydrocarbon chains, the yield of product is generally low by this method, even when the reaction is carried out under high dilution conditions, since entropy constrains cyclization, but favours polymerization. When rigid subunits such as thiophene, xylyl or pyridine are introduced into the macrocycles, cyclization proceeds in relatively high yield [165 - 168, 173].

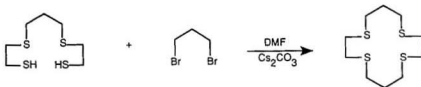
Scheme 3-6.



Buter and Kellogg improved this method by introducing the use of cesium carbonate to mediate formation of macrocycles [182 - 184]. The use of Cs_2CO_3

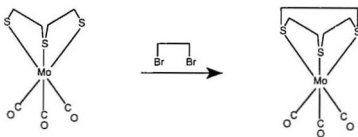
(not Na_2CO_3 and K_2CO_3) greatly diminishes the formation of polymer. The Cs^+ ion promotes cyclization by ion-pairing with RS^- [185]. This weak ion-pairing (due to the low charge-to-radius ratio of Cs^+) generates exceptionally nucleophilic thiolate anions. High reactivity ensures low concentration of unreacted starting materials and favours the desired cyclization. The 1,4,8,11-tetrathiacyclotetradecane (14S4) was synthesized by this method in 60% yield [184] (Scheme 3-7) while TT[11]OC and TT[11]MC are synthesized by using Cs_2CO_3 in DMF solution in 80% and 90% yield respectively [175].

Scheme 3-7.



Template methods are very important in the synthesis of macrocycles [186, 187]. Some organometallic centres such as $\text{Mo}(\text{CO})_3$ have been used as the template for the preparation of macrocyclic thioether ligands. High yield synthesis of 9S3 (60%) [188, 189] was achieved by Sellmann and Zapf based upon the mediation of a $\text{Mo}(\text{CO})_3$ template (Scheme 3-8).

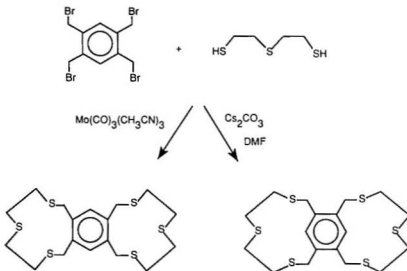
Scheme 3-8.



This methodology inhibits the formation of larger ring macrocycles and polymers to give the 1 + 1 condensation product 9S3, while the addition of more dithiol liberates 9S3 and regenerates the starting materials. Actually this reaction is catalytic.

By using the $\text{Mo}(\text{CO})_3$ template method and the high-dilution cyclization procedure in $\text{Cs}_2\text{CO}_3/\text{DMF}$ mixture, Loeb and coworkers [190] have prepared two kinds of ditopic, S_6 -type crown thioether ligands from the same starting materials with each ligand containing two potential S_3 binding sites separated by rigid xylyl fragments (Scheme 3-9).

Scheme 3-9.



Macrocyclic thioethers usually occur as colourless or white crystalline solids and are odour-free when pure. Their lack of odour results from their low vapour pressure. They have moderately low σ -donor and π -acceptor abilities, differing from polyoxo and polyaza ethers. The conformations of crown thioethers are quite different from those of polyoxo and polyaza macrocycles. In the free state, most crown thioethers adopt peculiar 'inside-out' or exodentate conformations with the sulfur donor atoms pointing out of the ring [124, 129], which is opposite to the endodentate orientation commonly found in oxo- and aza-crowns. This results from

the tendency of $-SCH_2CH_2SCH_2CH_2S-$ chains to adopt a 'bracket' structure that prefers *anti* placements for carbon-carbon bonds and *gauche* placements for carbon-sulfur bonds [191]. The difference in ring conformation will affect the coordination chemistry of these macrocycles. The polyaza and polyoxo macrocycles generally coordinate to the metal centre without involving conformational change, while thioether molecules must undergo substantial conformational change in order to attain the 'crown' conformation of the macrocycles, which is essential for metal ion coordination [124, 129, 130, 191 - 196]. The need for these large conformational changes often results in the formation of complexes with limited stability, as the energy for these conformational changes must be compensated from heats of chelate formation. This also leads the crown thioethers to bridge metal ions by employing exodentate sulfur atoms rather than coordination to a single metal center [124, 129, 165 - 170, 196, 197].

It was noted that the exodentate conformation of macrocyclic thioether ligands is largely dependent on the number of atoms in the ring, the flexibility of the hydrocarbon chain as well as ring strain. One such example is the small ring tridentate ligand 1,4,7-trithiacyclononane (9S3). This particular crown thioether is quite rigid and exhibits an all endodentate or crown conformation in the free ligand

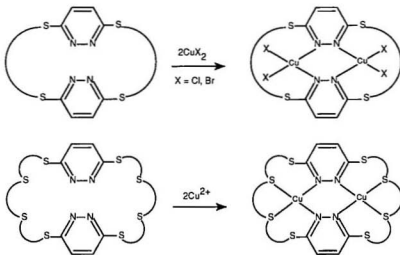
[198], which very closely resembles its triaza analogue. The introduction of rigid subunits may have some effect on the conformation of thioether ligands. For thiophenophane macrocycles the structural studies of the free ligands [165 - 167] show that in their solid state conformations all thioether sulfur atoms are still exodentate, but the thiophene-sulfur atoms point into the macrocycles, which is different from the aliphatic crown thioethers containing the same number of sulfur atoms. The structures of complexes with these ligands [165 - 170] show that the macrocycles cannot hold the metal ion inside the macrocyclic cavity, instead they hold the metal ion outside of the macrocycle with the thiophene-sulfur involved in coordination in some cases, while the crown thioethers of the same cavity size generally can hold the metal ions inside of the macrocycle.

The introduction of xylyl groups into the crown thioether framework also has some effects on their coordination behaviour. The inherent rigidity of these fragments may help in preorganization of the S donor atoms, or it may simply add to the stability of an exodentate conformation. Although macrocycles containing both ortho- and meta- substituted xylyl groups were shown to have exodentate conformations [173], the ortho and meta substituted groups were observed to have dramatically different effects on the coordination ability of each ligand due to the different rigidity of the substituents [175]. The o-xylyl fragment in TT[9]OC was found to introduce strain into the free ligand conformation, which favoured an exo-

to endodentate conformational change and facial S_3 -coordination to a single metal ion. In contrast, the effect of the *m*-xylyl group in TT[9]MC was to prevent this type of S_3 -coordination by reinforcing a rigid exodentate conformation.

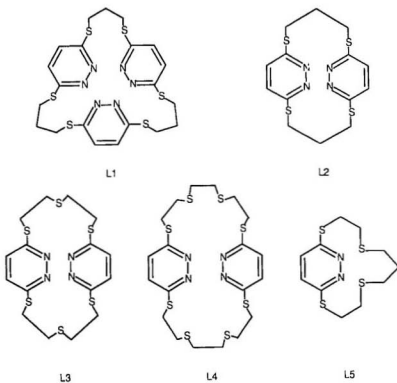
Our interest in mixed sulfur-nitrogen ligands involving thioether and diazine linkages stems from our earlier work on open-chain polydentate (N_4 , N_8) thioether-diazine ligands [33 - 38, 46 - 59, Chapter 1 & 2], which involve non-coordinating thioether groups and form predominantly dinuclear copper complexes with the two copper(II) centres antiferromagnetically coupled, and in some cases, with positive ($0 \rightarrow 0.5$ V vs SCE) reduction potentials.

Scheme 3-10.



The synthesis of thioether-diazine macrocycles with suitably disposed thioether and diazine groups for simultaneous NS coordination may produce dinuclear copper(II) complexes (e.g. Scheme 3-10), which are antiferromagnetically coupled, but with more positive reduction potentials.

Scheme 3-11.



It is also of interest to study the influence of the pyridazine and phthalazine subunits, which are rigid 1,4-aromatic fragments, on the conformations and coordination properties of these thioether macrocycles.

In this chapter we will discuss the synthesis of a series of new macrocyclic thioether-pyridazine ligands (Scheme 3-11) and their coordination chemistry with Cu(II) salts.

3.2. Experimental*

3.2.1. Synthesis of the Macrocycles**

L1 and L2

1,3-Propanedithiol (2.82 g, 25.0 mmol) was added to anhydrous ethanol (100 mL), in which sodium metal (1.15 g, 50.0 mmol) had been dissolved and the resulting solution was stirred for 1 h. 3,6-Dichloropyridazine (3.84 g, 25.0 mmol) was dissolved in anhydrous ethanol (100 mL) and both solutions were added dropwise, simultaneously, to refluxing anhydrous ethanol (500 mL) by using pressure equalizing funnels, under a dry nitrogen atmosphere. The addition took place over a period of 6 h, during which time a white precipitate formed. The mixture was stirred and refluxed for a further 2 h and then stirred at room

*For general procedures, see 1.2. **See List of Abbreviations for names.

temperature overnight. The white solid (L1) was filtered off, washed with anhydrous ethanol (3 x 80 mL) and deionized water (3 x 100 mL), dried in *vacuo* and recrystallized twice from CHCl_3 . Yield: 150 mg (3.2%). Mp: 190 - 210 °C. Further recrystallization from MeNO_2 produced white crystals, Mp: 188 - 190 °C. ^1H nmr (CDCl_3) (δ (relative intensity)): 2.25(6) (multiplet, CH_2), 3.36(12) (multiplet, CH_2), 7.00(6) (singlet, pyridazine). Mass spectrum, major mass peaks (m/e (relative intensity)): 552(5) P, 519(4), 367(7), 218(22), 184(43), 144(40), 106(39), 73(40), 41(100).

The initial filtrate obtained after isolation of L1 was removed on a rotatory evaporator and the residual solid extracted with CHCl_3 ; the extract was washed several times with deionized water and dried over Na_2SO_4 . The concentrated extract was chromatographed on silica gel, eluted with CHCl_3 , and the volume of the solution reduced to a few millilitres on a rotary evaporator and placed in a refrigerator. Colourless crystals of L2 were obtained. Yield: 0.52 g (11.3%). Mp: 215 - 217 °C. ^1H nmr (CDCl_3)(δ (relative intensity)): 2.43(4) (multiplet, CH_2), 3.34(8) (multiplet, CH_2), 7.00(4) (singlet, pyridazine). Mass spectrum, major mass peaks (m/e (relative intensity)): 368(88) P, 217(33), 191(31), 185(66), 151(100), 144(81), 114(62), 96(34), 79(49), 73(66).

L3, L4 and L5 were prepared in a similar manner by using 2-mercaptoethyl

sulfide, 1,4,7,10-tetrathiadecane [199] and 3,7-dithianonane-1,9-dithiol [184] respectively and isolated as single products. L3, white crystals, yield: 2.35 g (40.4%). Mp: 217 - 219 °C. ¹H nmr (CDCl₃) (δ(relative intensity)): 3.07(8) (triplet, CH₂), 3.62(8) (triplet, CH₂), 7.04(4) (singlet, pyridazine). Mass spectrum, major mass peaks (m/e(relative intensity)): 460(1) P, 401(22), 374(11), 231(47), 144(32), 87(100). L4, white crystals, yield: 1.74 g (24%). Mp: 206 - 208 °C. ¹H nmr (CDCl₃) (δ(relative intensity)): 3.02(16) (multiplet, CH₂), 3.55(8) (multiplet, CH₂), 7.24(4) (singlet, pyridazine). Mass spectrum, major mass peaks (m/e(relative intensity)): 580(1.4) P, 521(10), 461(9), 291(19), 170(49), 144(4), 87(92), 60(100). L5, white crystals, yield: 2.75 g (72%). Mp: 234 - 236 °C. ¹H nmr (CDCl₃) (δ(relative intensity)): 1.88(2) (multiplet, CH₂), 2.65(4) (multiplet, CH₂), 2.85(4) (multiplet, CH₂), 3.53(4) (multiplet, CH₂), 7.11(2) (singlet, pyridazine). Mass spectrum, major mass peaks (m/e(relative intensity)): 304(20) P, 271(5), 202(8), 170(40), 133(100), 105(28), 41(42).

3.2.2. Synthesis of the Complexes

Safety note

Perchlorate salts of copper complexes with organic ligands are potentially explosive. Only small amounts of material should be prepared and these should be handled with caution. The complexes described in this thesis have, so far, been

found to be safe when used in small quantities.

[Cu₃(L1)₂Cl₆]·2CH₃CN (18)

CuCl₂·2H₂O (170 mg, 1.0 mmol) was dissolved in CH₃CN (20 mL) and added to a solution of L1 (110 mg, 0.20 mmol) in CHCl₃ (20 mL). The resulting deep-green solution was filtered immediately and allowed to stand at room temperature overnight. A very small amount of an unidentified green solid formed, that was filtered off and the filtrate allowed to stand at room temperature for 1 week. Blue-green crystals formed, which were filtered off, washed with CH₃CN and CHCl₃, and air dried. Yield: 31 mg (18%). Anal. calcd. for C₄₄H₅₀N₁₂S₁₂Cl₁₂Cu₃: C 30.24, H 2.88, N 9.62; found: C 30.66, H 3.04, N 9.81.

[Cu(L2)Cl₂] (19), [Cu(L2)Br₂] (20) and [Cu(L2)(NO₃)₂] (21)

CuCl₂·2H₂O (140 mg, 0.80 mmol) was dissolved in CH₃CN (20 mL) and added to a solution of L2 (140 mg, 0.38 mmol) in CHCl₃ (20 mL). The resulting dark-green solution was filtered immediately and allowed to stand at room temperature overnight. Bright green crystals formed, which were filtered off, washed with CH₃CN and CHCl₃, and air dried. Yield: 160 mg (84%). C₁₄H₁₆N₄S₄·Cl₂Cu (19): C 33.43, H 3.21, N 11.14; found: C 33.38, H 3.19, N 11.19.

[Cu(L2)Br₂] (20) and [Cu(L2)(NO₃)₂] (21) were prepared in a similar manner and were obtained as yellowish brown crystals, yield: 45 mg (57%) for

20, and green crystals, yield: 55 mg (50%) for 21. Anal. calcd. for $C_{14}H_{16}N_4S_4Br_2Cu$ (20): C 28.41, H 2.72, N 9.47; found: C 28.31, H 2.67, N 9.49. Anal. calcd. for $C_{14}H_{16}N_4O_6S_4Cu$ (21): C 30.35, H 2.90, N 15.11; found: C 30.24, H 2.91, N 15.31.

$[Cu(L2)_2](ClO_4)_2 \cdot CH_3CN \cdot CHCl_3$ (22)

$Cu(ClO_4)_2 \cdot 6H_2O$ (150 mg, 0.40 mmol) was dissolved in CH_3CN (10 mL) and added to a solution of L2 (150 mg, 0.40 mmol) in $CHCl_3$ (10 mL). The resulting brown solution was filtered and allowed to stand at room temperature for several days. A small quantity (15 mg) of pale yellow crystals formed, which were filtered off and identified as the perchlorate salt of L2 [122]. The brown filtrate was evaporated slowly at room temperature. Red-brown crystals (22) formed, which were filtered off, washed with CH_3CN and $CHCl_3$, and air dried. Yield: 100 mg (43%). Anal. calcd. for $C_{31}H_{36}N_8S_8O_8Cl_3Cu$ (22): C 32.10, H 3.13, N 10.87; found: C 32.11, H 3.20, N 10.90.

$([Cu_2(L3)Cl_4] \cdot 0.5CHCl_3)_x$ (23)

Method A

To a solution of $CuCl_2 \cdot 2H_2O$ (85 mg, 0.50 mmol) in CH_3CN (20 mL) was added a solution of L3 (92 mg, 0.20 mmol) in $CHCl_3$ (20 mL). The resulting dark green solution was filtered and allowed to stand at room temperature overnight.

Dark brown crystals formed which were filtered off, washed with CH_3CN , and dried in air. Yield: 125 mg (78%). Anal. calcd. for $\text{C}_{16.5}\text{H}_{20.5}\text{N}_4\text{S}_6\text{Cl}_{3.5}\text{Cu}_2$ (23): C 25.11, H 2.62, N 7.10; found: C 24.75, H 2.70, N 7.27.

Method B

Cu powder (190 mg, 3.0 mmol) was added to a solution of $\text{CuCl}_2 \cdot 2\text{H}_2\text{O}$ (51 mg, 0.30 mmol) in CH_3CN (20 mL). The mixture was stirred for 6 h under N_2 and the resulting colourless solution filtered into a solution of L3 (92 mg, 0.20 mmol) in CHCl_3 (20 mL). The yellow solution was exposed to the air for a couple of weeks and brown crystals formed. Yield: 75 mg (52%). Suitable crystals were chosen for X-ray diffraction.

[Cu(L3)Cl₂] (24)

$\text{CuCl}_2 \cdot 2\text{H}_2\text{O}$ (34 mg, 0.20 mmol) was dissolved in CH_3CN (20 mL) and added to a solution of L3 (92 mg, 0.20 mmol) in CHCl_3 (20 mL). The resulting green solution was filtered and allowed to stand at room temperature overnight. Bright green crystals formed, which were filtered off, washed with CH_3CN and CHCl_3 , and air dried. Yield: 85 mg (71%). Anal. calcd. for $\text{C}_{16}\text{H}_{20}\text{N}_4\text{S}_6\text{Cl}_2\text{Cu}$: C 32.29, H 3.39, N 9.41; found: C 32.08, H 3.44, N 9.38.

[Cu(L3)(NO₃)₂] (25)

A solution of L3 (55 mg, 0.12 mmol) in CHCl_3 (20 mL) was added to a

solution of $\text{Cu}(\text{NO}_3)_2 \cdot 3\text{H}_2\text{O}$ (97 mg, 0.40 mmol) in CH_3CN (20 mL). The resulting solution was filtered and then refluxed for 2 h to form a dark green solution. The solution was allowed to stand at room temperature overnight. Bluish green crystals formed which were filtered, washed with CH_3CN , and dried in air. Yield: 46 mg (59%). Anal. calcd. for $\text{C}_{16}\text{H}_{20}\text{N}_8\text{O}_8\text{S}_8\text{Cu}$: C 29.64, H 3.11, N 12.96; found: C 29.75, H 3.13, N 13.13.

[Cu(L4)Cl] \cdot THF (26)

L2 (92 mg, 0.16 mmol) was dissolved in THF (40 mL) and added to a solution of $\text{CuCl}_2 \cdot 2\text{H}_2\text{O}$ (85 mg, 0.50 mmol) in THF (20 mL). The resulting dark green solution was filtered and allowed to stand at room temperature overnight. Brown crystals formed, which were filtered off, washed with CHCl_3 and CH_3CN , and dried in air. Yield: 72 mg (57%). Anal. calcd. for $\text{C}_{21}\text{H}_{36}\text{N}_4\text{S}_2\text{OCl}_2\text{Cu}$: C 36.60, H 4.61, N 7.11; found: C 36.90, H 4.88, N 7.00.

[Cu(L5)Cl] $_2$ (27) and [Cu(L5)Br] $_2$ (28)

A solution of L5 (182 mg, 0.6 mmol) in CHCl_3 (20 mL) was added to a solution of $\text{CuCl}_2 \cdot 2\text{H}_2\text{O}$ (256 mg, 1.5 mmol) in MeOH (20 mL). The resulting solution was filtered and then refluxed for 20 min whereupon dark brown crystals formed. Yield: 200 mg (76%). Anal. calcd. for $\text{C}_{11}\text{H}_{16}\text{N}_2\text{S}_4\text{Cl}_2\text{Cu}$: C 30.10, H 3.67, N 6.38; found: C 29.80, H 3.48, N 6.28. $[\text{Cu}(\text{L5})\text{Br}]_2$ (28) was prepared

similarly by reaction of L5 with CuBr_2 and was obtained as dark brown crystals. Yield: 210 mg (66%). Anal. calcd. for $\text{C}_{11}\text{H}_{16}\text{N}_2\text{S}_4\text{Br}_2\text{Cu}$: C 25.02, H 3.05, N 5.31; found: C 24.98, H 3.00, N 5.29.

3.3. Results and Discussion

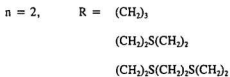
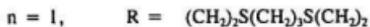
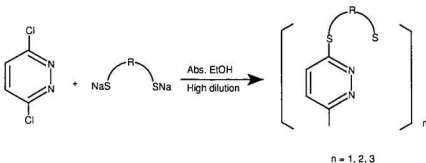
3.3.1. Synthesis

Thiopyridazinophane ligands were prepared from the condensation of 3,6-dichloropyridazine with appropriate dithiols under high dilution conditions in basic media. The general preparation for these macrocycles is shown in Scheme 3-12.

It is interesting to note that the chain length of the dithiols plays a very important role in the formation of the macrocycle. When R is propylene, 3:3 (L1) and 2:2 (L2) oligomeric thiopyridazinophanes were isolated. The yields are very low. When R becomes longer dimeric L3 and L4 were isolated as the only products in moderately high yield, and no trace of any monomer containing one pyridazine subunit and trimer containing three pyridazine subunits was detected. When R contains seven carbon atoms, monomeric L5 was isolated as the only product and the yield is high. It seems that the flexibility of the hydrocarbon chain is an important factor in the ring closure. For the more flexible 3,7-dithianonane-1,9-dithiol, it favours the formation of monomer only. For the relatively rigid 1,3-propanedithiol, both trimer and dimer can be formed. For 2-mercaptoethyl sulfide

and 1,4,7,10-tetrathiadecane, which have reasonable flexibility, the dimer is the only product.

Scheme 3-12



All these thiopyridazinophanes are soluble in CHCl_3 , CH_2Cl_2 , THF, MeNO_2 and benzene, but not in ethanol, methanol and DMF. Their proposed structures are

consistent with ir, nmr and mass spectroscopic data and have been confirmed (except L4) by the X-ray structures of their complexes.

All complexes were prepared from the reaction of ligands with copper(II) salts in an acetonitrile/chloroform mixture while $[\text{Cu}(\text{L4})\text{Cl}_2] \cdot \text{THF}$ (**26**) was isolated from THF. The 1:2 and 1:1 complexes of L3 with CuCl_2 were prepared by controlling the molar ratio of ligand and copper salt, otherwise excess copper salts are used. It is of interest to note that the 1:2 complex **23** can be synthesized from either copper(I) or copper(II) starting materials. All the complexes, except $[\text{Cu}(\text{L2})_2](\text{ClO}_4)_2 \cdot \text{CH}_3\text{CN} \cdot \text{CHCl}_3$ (**22**), did not dissolve appreciably in any solvent and so were studied exclusively in the solid state.

3.3.2. Structures

$[\text{Cu}_3(\text{L1})\text{Cl}_6] \cdot 2\text{CHCl}_3$ (**18**)

The structure of $[\text{Cu}_3(\text{L1})_2\text{Cl}_6] \cdot 2\text{CHCl}_3$ (**18**) is shown in Fig. 3-1, and interatomic distances and angles relevant to the copper coordination spheres are given in Table 3-1. The molecule contains a trinuclear arrangement of Cu(II) centres and has a centre of symmetry at Cu(1), which results in the collinear arrangement of three copper atoms. The central copper (Cu(1)) bridges two macrocycles through coordination to two pyridazine nitrogens one on each

macrocycle with each macrocycle coordinated to another copper centre (Cu(2)) via two more separate pyridazine atoms. The Cu(1)-Cu(2) separation is 7.360(2)Å. All copper atoms are coordinated by two pyridazine nitrogens and two chlorides in almost square-planar geometries. The two pyridazine nitrogen atoms which coordinate to the central copper come from two different macrocycles, with the copper atom having an almost planar *trans* CuN₂Cl₂ arrangement. The two Cu-N (1.99(1) Å) and two Cu-Cl (2.246(4) Å) distances are the same and the N(1)-Cu(1)-N(1)a and Cl(1)-Cu(1)-Cl(1)a angles are exactly 180°. The two pyridazine nitrogens which coordinate to the terminal copper come from two different pyridazine units of the same macrocycle. The copper centre has a *cis* arrangement of two nitrogens and two chlorides. The two Cu-N and Cu-Cl distances are slightly different with N(4)-Cu(2)-Cl(3) and N(6)-Cu(2)-Cl(2) angles smaller than 180°. The Cu-N and Cu-Cl distances around Cu(1) and Cu(2) are comparable and in the normal range for ligands of this sort. L1 is a 27-membered macrocycle and a potentially hexadentate (N₆) ligand. It only coordinates to Cu(II) centres in a tridentate (N₃) fashion, with each pyridazine unit utilizing only one nitrogen. The sulfur atoms in the macrocycle are not considered as potential donors to the Cu(II) centres since simultaneous coordination of adjacent sulfur and nitrogen atoms will result in the formation of a rigid four-membered chelate ring. The stronger

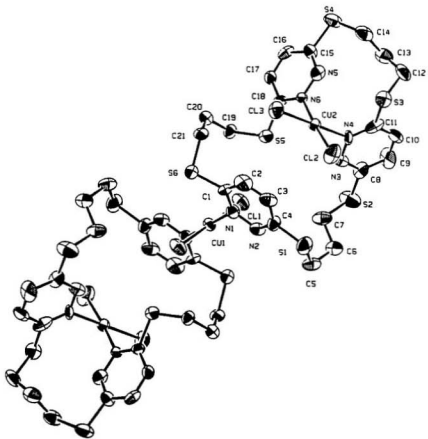


Fig. 3-1. Structural representation of $[\text{Cu}_2(\text{L}1)_2\text{Cl}_4] \cdot 2\text{CHCl}_3$ (**18**), with hydrogen atoms omitted (40% probability ellipsoids).

Table 3-1. Selected bond distances (Å) and angles (deg) for $[\text{Cu}_2(\text{L}1)_2\text{Cl}_4] \cdot 2\text{CHCl}_3$ (**18**)

Cu(1)-N(1)	1.99(1)	Cu(1)-Cl(1)	2.246(4)
Cu(1)-N(1)a	1.99(1)	Cu(1)-Cl(1)a	2.246(4)
Cu(1)-N(4)	2.02(1)	Cu(2)-N(6)	2.00(1)
Cu(2)-Cl(2)	2.206(4)	Cu(2)-Cl(3)	2.229(4)
Cl(1)-Cu(1)-N(1)	91.5(3)	Cl(1)-Cu(1)-Cl(1)a	180.00
N(1)-Cu(1)-N(1)a	180.00	Cl(1)a-Cu(1)-N(1)a	88.5(3)
N(4)-Cu(2)-N(6)	87.7(4)	N(6)-Cu(2)-Cl(3)	89.2(3)
Cl(3)-Cu(2)-Cl(2)	94.3(2)	Cl(2)-Cu(2)-N(6)	87.7(4)
N(4)-Cu(2)-Cl(3)	176.3(4)	N(6)-Cu(2)-Cl(2)	175.9(3)

chloride ligands also prevent sulfur coordination. Cu(2) is held inside the macrocyclic cavity by N(4) and N(6) and this results in the formation of two very large chelate rings, one is 11-membered, the other 20-membered.

[Cu(L2)Cl₂] (19)

The structure of $[\text{Cu}(\text{L}2)\text{Cl}_2]$ (**19**) is shown in Fig. 3-2, and interatomic distances and angles relevant to the copper coordination sphere are given in Table 3-2. The structure of **19** consists of an almost square-planar *cis* copper(II) centre

bound by two pyridazine nitrogens, one from each pyridazine ring and two chlorides in a similar way for Cu(2) in **18**. Copper-chlorine (2.246(2) Å) and copper-nitrogen (2.028(4) Å) distances are normal and are comparable with those in **18**. The square plane is slightly compressed (Cl1-Cu1-Cl1a 94.39(8)°, Cl1-Cu1-N1 88.8(1)°) with the copper centre displaced by 0.082 Å from the mean N₂Cl₂ plane. The tetrathiapyridazinophane ligand L2 utilizes two nitrogen donor atoms on the same relative side of the macrocyclic ring as opposed to opposite sides for each *endo*-macrocyclic copper centre in **18** and holds the copper centre outside the macrocyclic cavity. This results in the formation of two chelate rings of different size, one is 10-membered and the other 12-membered. The two pyridazine ring least-squares planes are inclined by a dihedral angle of 83.5°.

Table 3-2. Selected bond distances (Å) and angles (deg) for [Cu(L2)Cl₂] (**19**)

Cu(1)-Cl(1)	2.246(2)	Cu(1)-N(1)	2.028(4)
Cl(1)-Cu(1)-Cl(1)a	94.39(8)	Cl(1)-Cu(1)-N(1)	174.5(1)
Cl(1)-Cu(1)-N(1)a	88.8(1)	Cl(1)a-Cu(1)-N(1)a	174.5(1)
N(1)-Cu(1)-N(1)a	87.7(2)		

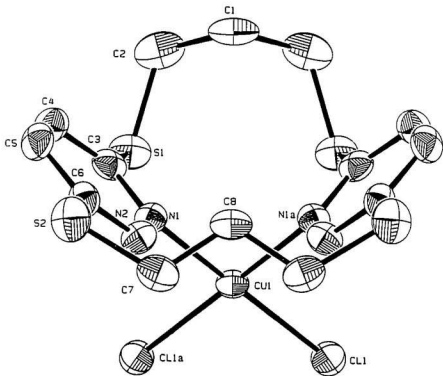
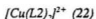


Fig. 3-2. Structural representation of [Cu(L2)Cl₂] (19), with hydrogen atoms omitted (40% probability ellipsoids).



The structure of $[\text{Cu}(\text{L}2)_2]^{2+}$ (22) is shown in Fig. 3-3, and interatomic distances and angles relevant to the copper coordination sphere are given in Table 3-3. Two L2 macrocycles, acting as bidentate N_2 ligands, coordinate to a slightly distorted square-planar copper(II) centre in a *cis* fashion. Unlike the situation in 19, the macrocycle utilizes two opposite pyridazine nitrogens with each pyridazine unit supplying one nitrogen and the copper atom is still held outside the macrocyclic cavity. This produces a situation where the two chelate rings have the same size with each one being 11-membered. The Cu-N distances are in the range of 1.973(9) - 2.010(9) Å and are comparable with the Cu-N distances in 18 and 19. The copper square plane is compressed slightly within each chelating half (N1-Cu1-N2 86.6(4)°, N5-Cu1-N7 86.3(4)°). The copper centre is displaced slightly from the mean N_4 plane by 0.011 Å. The complex contains one acetonitrile molecule and one chloroform molecule of crystallization. A packing diagram (Fig.3-4) shows that there are no significant associations between cations and that perchlorate oxygens and acetonitrile nitrogen are not involved in coordination. The dihedral angle between the pyridazine rings defined by N1 and N3 is 76.1°, while that between the pyridazine rings defined by N5 and N7 is 81.8°.

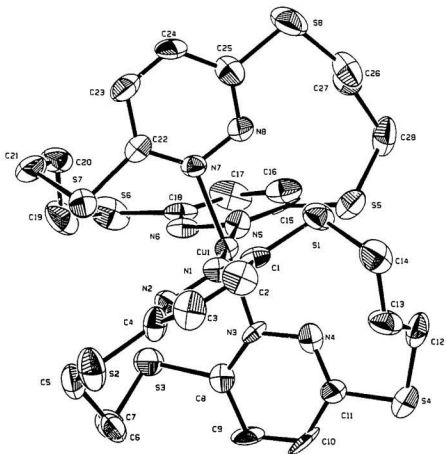


Fig. 3-3. Structural representation of $[\text{Cu}(\text{L}2)_2]^{2+}$ (22), with hydrogen atoms omitted (40% probability ellipsoids).

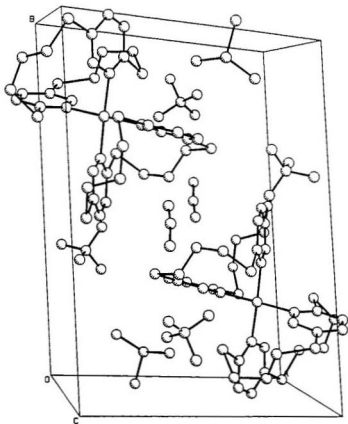


Fig. 3-4. Packing diagram for $[\text{Cu}(\text{L}2)_2](\text{ClO}_4)_2 \cdot \text{CH}_3\text{CN} \cdot \text{CHCl}_3$ (22).

Table 3-3. Selected bond distances (Å) and angles (deg) for $[\text{Cu}(\text{L}2)]_2(\text{ClO}_4)_2 \cdot \text{CH}_3\text{CN} \cdot \text{CHCl}_3$ (22)

Cu(1)-N(1)	1.986(8)	Cu(1)-N(3)	1.997(9)
Cu(1)-N(5)	1.973(9)	Cu(1)-N(7)	2.010(9)
N(1)-Cu(1)-N(3)	86.6(4)	N(3)-Cu(1)-N(5)	94.6(4)
N(5)-Cu(1)-N(7)	86.3(4)	N(7)-Cu(1)-N(1)	92.6(4)
N(1)-Cu(1)-N(5)	177.6(4)	N(3)-Cu(1)-N(7)	176.6(4)

$[\text{Cu}_2(\text{L}3)\text{Cl}_4]_x$ (23)

The structure of $[\text{Cu}_2(\text{L}3)\text{Cl}_4]_x$ (23) is shown in Fig. 3-5 and Fig. 3-6, and interatomic distances and angles relevant to the copper coordination spheres are given in Table 3-4. The macrocycle L3 is a more flexible (22-membered) ring than L2 and contains aliphatic sulfur donors and can coordinate in a tetradentate fashion. It first binds a copper centre (Cu(1)) by using two pyridazine nitrogens. Unlike the situation in **19**, it holds the *trans* square-planar CuN_2Cl_2 centre effectively inside the macrocyclic cavity by using two opposite pyridazine nitrogens. It then coordinates to external *trans* square-planar copper(II) centres by using two exocyclic sulfur atoms. The overall structure is an infinite, single stranded polymer (Fig. 3-6). Both Cu(1) and Cu(2) are very close to being in

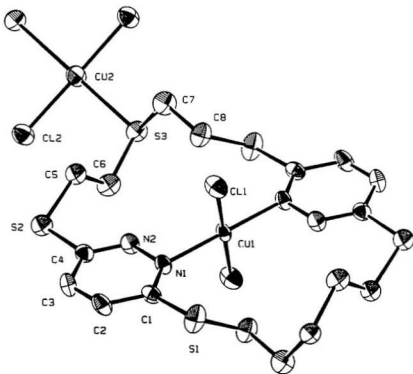


Fig. 3-5. Structural representation of $[\text{Cu}_2(\text{L3})\text{Cl}_4]_2$ (**23**) showing a single dinuclear fragment, with hydrogen atoms omitted (40% probability ellipsoids).

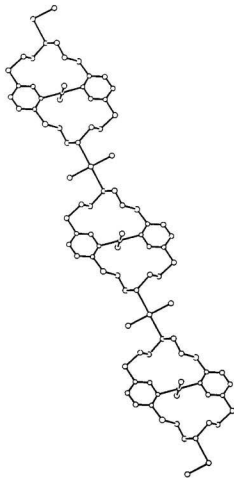


Fig. 3-6. Structural representation of $[Cu_2(L_3)Cl_4]_x$ (23) illustrating the single stranded polymer.

Table 3-4. Selected bond distances (Å) and angles (deg) for [Cu₂(L3)Cl₄], (**23**)

Cu(1)-Cl(1)	2.260(2)	Cu(1)-N(1)	1.962(6)
Cu(2)-Cl(2)	2.212(2)	Cu(2)-S(3)	2.458(2)
Cl(1)-Cu(1)-Cl(1)a	180.00	Cl(1)-Cu(1)-N(1)	88.1(2)
Cl(1)-Cu(1)-N(1)a	91.9(2)	N(1)-Cu(1)-N(1)a	180.00
Cl(2)-Cu(2)-Cl(2)a	180.00	Cl(2)-Cu(2)-S(3)	88.49(7)
Cl(2)-Cu(2)-S(3)a	91.51(7)	S(3)-Cu(2)-S(3)a	180.00

exactly square-planar geometries as Cl(1)-Cu(1)-Cl(1)a, N(1)-Cu(1)-N(1)a, Cl(2)-Cu(2)-Cl(2)a, and S(3)-Cu(2)-S(3)a are exactly 180°. The other angles around Cu(1) and Cu(2) lie in the range 88.1 - 91.9°. The Cu-N and Cu-Cl distances are in the normal range and are comparable with those in **18**, **19** and **22**. The Cu-S distance (2.458(2) Å) is comparable with similar bonds in Cu(II) complexes with other thioether macrocycles [137, 143, 146, 148, 200, 201], but is slightly longer than that in CuCl₂ complexes with thiophenophane ligands (2.349(3) - 2.358(3) Å) [165]. The endo/exo coordination of L3 in **23** is similar to the bonding of L1 in **18**, in which one square-planar copper(II) centre is bound inside the macrocycle

by two pyridazine nitrogens, with the third pyridazine nitrogen binding externally to another copper centre. For the first time, the ligand L3 exhibits the desired mixed N/S coordination mode for thioether-pyridazine macrocycles, but the N and S donors of the ligand do not coordinate to the same metal centre simultaneously.

[Cu(L3)Cl₂] (24)

The structure of [Cu(L3)Cl₂] (**24**) is shown in Fig. 3-7, and interatomic distances and angles relevant to the copper coordination spheres are given in Table 3-5. The structure consists of an almost square-planar *trans* copper(II) centre bound by two opposite pyridazine nitrogens, one from each pyridazine ring and two chlorines. The coordination sphere is similar to that of Cu(1) in **23**. The copper-nitrogen and copper-chlorine distances are slightly different from those in **23** but still in the normal range for ligands of this sort. The Cl(1)-Cu(1)-Cl(2) and N(1)-Cu(1)-N(3) angles are not exactly 180°, but the angles around the copper centre fall in the range 88.1 - 91.9°, comparing very closely with those in **23**.

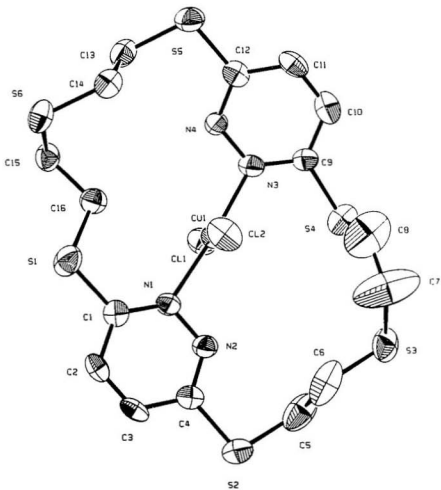


Fig. 3-7. Structural representation of [Cu(L3)Cl₂] (24), with hydrogen atoms omitted (40% probability ellipsoids).

Table 3-5. Selected bond distances (Å) and angles (deg) for [Cu(L3)Cl₂] (24)

Cu(1)-Cl(1)	2.264(3)	Cu(1)-Cl(2)	2.274(3)
Cu(1)-N(1)	1.974(7)	Cu(1)-N(3)	1.987(7)
Cl(1)-Cu(1)-Cl(2)	178.8(1)	Cl(1)-Cu(1)-N(1)	91.7(2)
Cl(1)-Cu(1)-N(3)	91.8(2)	Cl(2)-Cu(1)-N(1)	88.0(2)
Cl(2)-Cu(1)-N(3)	88.5(2)	N(1)-Cu(1)-N(3)	173.8(3)

[Cu(L3)(NO₃)₂] (25)

The structure of [Cu(L3)(NO₃)₂] (25) is shown in Fig. 3-8, and interatomic distances and angles relevant to the copper coordination sphere are given in Table 3-6. The structure consists of a highly distorted *cis*-octahedral copper(II) centre bound by two opposite *cis*-pyridazine nitrogens, one from each pyridazine ring and two bidentate nitrates. Two copper-oxygen distances (1.980(12), 1.933(12) Å) and copper-nitrogen distances (1.992(6), 1.982(6) Å) are normal, but two copper-oxygen distances (Cu(1)-O(5) 2.461(6) Å, Cu(1)-O(2) 2.547(6) Å) are quite long, but still within a reasonable bonding distance. The O(2)-Cu(1)-O(1) and O(4)-Cu(1)-O(5) angles are significantly different from 90° (O(2)-Cu(1)-O(1) 55.3(2)°,

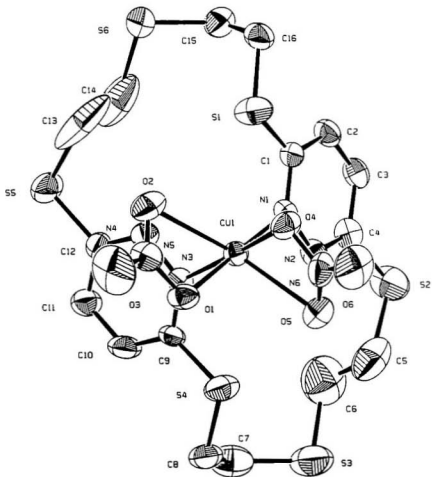


Fig. 3-8. Structural representation of $[\text{Cu}(\text{L3})(\text{NO}_3)_2]$ (**25**), with hydrogen atoms omitted (40% probability ellipsoids).

Table 3-6. Selected bond distances (Å) and angles (deg) for [Cu(L3)(NO₃)₂] (25)

Cu(1)-O(1)	2.003(5)	Cu(1)-O(2)	2.547(6)
Cu(1)-O(4)	1.987(5)	Cu(1)-O(5)	2.461(6)
Cu(1)-N(1)	1.992(6)	Cu(1)-N(3)	1.982(6)
O(1)-Cu(1)-O(4)	89.0(2)	O(1)-Cu(1)-N(1)	177.8(3)
O(1)-Cu(1)-N(3)	87.7(2)	O(4)-Cu(1)-N(1)	93.2(2)
O(4)-Cu(1)-N(3)	175.5(2)	N(1)-Cu(1)-N(3)	90.1(2)
N(3)-Cu(1)-O(5)	126.1(2)	N(3)-Cu(1)-O(2)	90.4(2)
N(3)-Cu(1)-N(2)	80.9(2)	O(4)-Cu(1)-O(5)	56.6(2)
O(4)-Cu(1)-O(2)	85.2(2)	O(4)-Cu(1)-N(2)	103.4(2)
N(1)-Cu(1)-O(5)	96.2(2)	N(1)-Cu(1)-O(2)	124.7(2)
N(1)-Cu(1)-N(2)	27.8(2)	O(1)-Cu(1)-O(5)	85.1(2)
O(1)-Cu(1)-O(2)	55.3(2)	O(1)-Cu(1)-N(2)	151.4(2)
O(5)-Cu(1)-O(2)	126.3(2)	O(5)-Cu(1)-N(2)	80.8(2)
O(2)-Cu(1)-N(2)	149.9(2)		

O(4)-Cu(1)-O(5) 56.6(2)°) and clearly imply a distorted structure. When bonding to a single metal atom a nitrate group may behave as a monodentate ligand or a symmetrical or unsymmetrical bidentate ligand. It is suggested [202] that a nitrate is to be considered as a bidentate ligand if the difference in the two closest metal-oxygen distances is less than 0.7 Å. In **25** the difference between the distances of Cu-O(5) and Cu-O(1) is 0.567 Å and the difference between Cu-O(5) and Cu-O(4) is 0.474 Å. It is clear that from the structural information the nitrates are bidentate, and the copper centre is best regarded as a highly distorted *cis*-octahedral species.

3.3.3. Spectroscopy

Both ligands L1 and L2 have simple infrared spectra with weak ν CN bands at 1573 and 1570 cm^{-1} respectively, strong bands at 1146 and 1146 and 1150 cm^{-1} respectively, and weaker absorptions in the range 720-820 cm^{-1} . Coordination of the pyridazine rings, all of which are ligands in the compounds that have been structurally characterized, does not cause a major shift in the CN stretch frequency [121, 122, 203]. Shifts of -10 (**18**), -11 (**19**), and -5(**22**) cm^{-1} (Table 3-7) are observed for those cases where the pyridazine rings have been shown to coordinate via one nitrogen atom. In each case the absorption appears as a single, sharp band,

Table 3-7. Infrared and electronic spectral data of Cu(II) complexes with thioether-pyridazine macrocycles.

Compound	Colour	Infrared bands (cm ⁻¹) ^a	UV/VIS (cm ⁻¹) ^a
[Cu ₂ (L1)Cl ₄] · 2CHCl ₃ (18)	Blue-green	1563 (νCN), 320, 308 (νCu-Cl), 288 (νCu-N)	16000
[Cu(L2)Cl ₂] (19)	Green	1559 (νCN), 320, 304 (νCu-Cl), 287, 273 (νCu-N)	15900 [14500] ^b
[Cu(L2)Br ₂] (20)	Yellow-brown	1558 (νCN), 264, 257 (νCu-N), 248, 235 (νCu-Br)	15600 [14300]
[Cu(L2)(NO ₂) ₂] (21)	Green	1564 (νCN), 1747, 1708 (ν ₁ + ν ₄ NO ₂), 334, 320, 298 (νCu-O), 284, 270 (νCu-N)	15600 [14300]
[Cu(L2) ₂](ClO ₄) ₂ · CH ₃ CN · CHCl ₃ (22)	Brown	1565(νCN), 1090(νClO ₄), 2297, 2253(νCH ₃ CN), 270, 264 (νCu-N)	20000 18200
[Cu ₂ (L3)Cl ₄] _x (23)	Brown	1572(νCN), 306, 295 (νCu-Cl), 272(νCu-N)	19600 14300
[Cu(L3)Cl ₂] (24)	Green	1559 (νCN), 308, 298 (νCu-Cl), 268 (νCu-N)	13300
[Cu(L3)(NO ₂) ₂] (25)	Deep green	1568(νCN), 1758, 1753, 1721 1709(ν ₁ + ν ₄ NO ₂), 323, 304 (νCu-O), 275 (νCu-N)	17400 14300
[Cu(L4)Cl ₂] · THF (26)	Brown	1571(νCN), 307(νCu-Cl)	21300 15500
[Cu(L5)Cl ₂] ₂ (27)	Brown	1562(νCN), 355, [350] 280, 260 (νCu-Cl)	[29400] 20400 [17900]

Table 3-7. Infrared and electronic spectral data of Cu(II) complexes with thioether-pyridazine macrocycles (continued).

Compound	Colour	Infrared bands (cm ⁻¹)*	UV/VIS (cm ⁻¹)*
[Cu(L5)Br ₂] ₂ (28)	Brown	1563(ν CN), 268, 252(ν Cu-Br)	28600 19000 [15900]

*Mull transmittance; * [] Shoulder.

even though two different CN groups would be expected in the coordinated ligand.

The infrared spectra of [Cu(L2)Cl₂] (**19**) and [Cu(L2)Br₂] (**20**) are identical in the range 4000-500 cm⁻¹, indicating an identical *cis* structure. The nitrate complex [Cu(L2)(NO₃)₂] (**21**) exhibits a ν CN band at 1564 cm⁻¹, shifted by 6 cm⁻¹ to lower energy than the free ligand, indicating coordinated pyridazine. Prominent nitrate combination ($\nu_1 + \nu_2$) bands are observed at 1708 and 1747 cm⁻¹ (Table 3-7) [98], and the difference between these bands (39 cm⁻¹) strongly suggests a bidentate role for coordinated nitrate. In view of the *cis* coordination of L2 in compounds **19** and **22** a similar bonding situation would be expected for **21** with a six-coordinate *cis* structural arrangement like that found for **25**.

The ligand L3 has a simple infrared spectrum with a sharp ν CN band at 1580

cm^{-1} . This band shifts 8-21 cm^{-1} to lower energy in its complexes (Table 3-7), suggesting the coordination of pyridazine rings [121, 122, 203]. The shifts to lower energy for **23**, **24** and **25** are clear cut because X-ray data confirm pyridazine nitrogen coordination. The ($\nu_1 + \nu_2$) nitrate combination bands of **25** are observed at 1758, 1753, 1721, 1709 cm^{-1} [98], and are associated with two different coordinated nitrates. The separation of each pair of bands is usually a reasonable indication of the bonding mode of such a group [98] and differences of 37 and 44 cm^{-1} are large enough to suggest a bidentate role for two different coordinated nitrates. In this case, X-ray data formally define the coordinated nitrates in a bidentate mode. For each nitrate, therefore, one oxygen is strongly coordinated, and one weakly coordinated.

The ligand **L4** has single, sharp infrared absorption at 1572 cm^{-1} . A very small shift to lower energy (1 cm^{-1}) (Table 3-7) is observed for this band in its complex **26**. It is reasonable to suggest that **26**, which involves a 2:2 pyridazinophane macrocycle and involves a shift of νCN of only 1 cm^{-1} to lower energy, might be expected to involve just sulfur coordination of the ligand.

The ligand **L5** has an infrared absorption at 1568 cm^{-1} , associated with CN stretch in the pyridazine ring. A very small shift in this band (less than 6 cm^{-1}) in **27** and **28** is observed (Table 3-7). The absence of pyridazine coordination in its

Cu(I) and Ag(I) complexes and the similarity in the position of this absorption in these complexes [122] (-6 cm^{-1} (Cu(I)), -4 cm^{-1} (Ag(I))) (*vide infra*) suggests that pyridazine nitrogen atoms are not involved in coordination in **27** and **28**.

A comparison of the far infrared spectrum of **18** (Table 3-7) with that of the free ligand L1 reveals three strong bands associated with copper-ligand stretching. The bands at 320 and 308 cm^{-1} are assigned to Cu-Cl stretch, while the single band at 288 cm^{-1} is assigned to Cu-N stretch. A *cis*-CuN₂Cl₂ system, with local C_{2v} symmetry, would require the presence of two Cu-Cl stretching bands, while the *trans* square-planar CuN₂Cl₂ system, with local D_{2h} symmetry would require just one Cu-Cl stretch. Although **18** contains two pseudo *cis* square-planar centres and one pseudo *trans* square-planar centre, it does not appear to be reflected in the far-infrared spectrum and the third absorption is probably hidden in the general Cu-Cl stretching envelope. However the *cis* square-planar structure of [Cu(L2)Cl₂] (**19**) is clearly reflected in its far infrared spectrum with two strong bands at 320 , 304 cm^{-1} assigned to Cu-Cl stretch and two bands at 287 , 273 cm^{-1} assigned to Cu-N stretch. The analogous bromo-complex **20** shows two pairs of bands at 264 , 257 cm^{-1} (ν Cu-N) and 248 , 235 cm^{-1} (ν Cu-Br) consistent with a *cis*-CuN₂Br₂ structural assignment.

The nitrate complex **21** exhibits three very strong far infrared bands (Table

3-7) associated with Cu-O stretch and two bands associated with Cu-N stretch, consistent with the proposed structure. The perchlorate complex **22** involves a slightly compressed square-planar arrangement of four monodentate pyridazine rings from two ligands. The presence of two far infrared bands at 270, 264 cm^{-1} , assigned to Cu-N stretch, is consistent with such a structure, and assumes an idealized C_{2v} local site symmetry. The uncoordinated acetonitrile exhibits two prominent peaks at 2297, 2253 cm^{-1} which are comparable with those observed for acetonitrile in **12** (Table 1-11). The very strong, broad band at 1090 cm^{-1} (ν_3) and a sharp band at 629 cm^{-1} (ν_4) are associated with non-coordinated perchlorate stretch.

Absorptions in **23** at 306 and 295 cm^{-1} assigned to Cu-Cl stretch, can be associated with two different *trans* dichloro-copper(II) species, and one Cu-N stretch at 272 cm^{-1} is consistent with its *trans* structure. Complex **24** exhibits one strong band at 308 cm^{-1} ($\nu_{\text{Cu-Cl}}$) and one strong band at 268 cm^{-1} ($\nu_{\text{Cu-N}}$), consistent with a similar *trans* chromophore. In **25** there are two strong bands at 304 and 323 cm^{-1} , which are associated with Cu-O (NO_3) stretch. Only one band at 275 cm^{-1} was observed which is associated with Cu-N stretching.

For complex **26**, the pyridazine nitrogens are not involved in coordination, only the sulfur atoms of the ligand are involved in coordination. The appearance

of one strong band at 307 cm^{-1} , assigned to Cu-Cl stretch, suggests a *trans* CuS_2Cl_2 or CuS_4Cl_2 structure in this compound. The appearance of a very strong band at 21300 cm^{-1} , which can be assigned to S→Cu charge transfer, also supports sulfur coordination.

In the range $4000 - 500\text{ cm}^{-1}$ the spectra of **27** and **28** are virtually identical, indicating structurally similar complexes. Far infrared absorptions for **27** at 355 and 350 (sh) cm^{-1} are assigned to terminal copper-chlorine stretch, while bands at 280 and 260 cm^{-1} are assigned to bridging copper-chlorine bonds. Similar absorptions for **28** at 268 and 252 cm^{-1} are assigned to terminal copper-bromine stretch. In the absence of structural information, the infrared spectra suggest that these two complexes have dimeric structures.

Solid state, mull transmittance electronic spectra (Table 3-7) are characterized by the presence of one major visible absorption for compounds **18** - **21**, **23** and **24**, while **22** exhibits two high-energy bands. No distinction can be made between the *cis* and *trans* CuN_2Cl_2 sites in **18**, while the slightly lower energy bands associated with $[\text{Cu}(\text{L}2)\text{Br}_2]$, compared with $[\text{Cu}(\text{L}2)\text{Cl}_2]$, are consistent with a structurally analogous bromo complex. The lower energy absorptions associated with **21** and **25** are consistent with six-coordinate copper (II) centres with mixed CuN_2O_4 chromophores, especially when compared with the

square-planar complex **22**. Intense high energy absorptions were observed in **26** - **28** (Table 3-7), which are clearly associated with charge transfer, rather than d-d transitions.

The room temperature, solid state esr spectrum of **18** (Fig. 3-9) (Table 3-8) is rather complicated, but can be considered as the superposition of two axial species. A consideration of the solid spectrum of **19** is useful in assigning the g values in **18**. **19** exhibits an axial spectrum associated with a *cis*- CuN_2Cl_2 , square-planar species, with $g_{\parallel} = 2.16$ and $g_{\perp} = 2.08$ (Table 3-8). Assuming that the *cis*- CuN_2Cl_2 centre in **18** is comparable with that in **19**, then the resonance with $g_{\parallel} = 2.17$ and $g_{\perp} = 2.08$ is assigned to the *cis*- CuN_2Cl_2 centre while the resonance with $g_{\parallel} = 2.13$ and $g_{\perp} = 2.04$ is assigned to the *trans*- CuN_2Cl_2 centre in **18**. **24** exhibits an axial spectrum associated with a *trans*- CuN_2Cl_2 , square-planar species, with $g_{\parallel} = 2.27$ and $g_{\perp} = 2.06$ (Table 3-8) which is not comparable with the *trans*- CuN_2Cl_2 centre in **18**. Compounds **20**, **21**, **23**, **25**, **28** have uninformative isotropic spectra at both room temperature (Table 3-8) and at 77 K. Compound **26** and **27** exhibit three peaks both at room temperature and 77 K indicating a rhombic distorted coordination sphere.

The square-planar perchlorate complex **22** exhibits a most unusual solid state spectrum (Fig. 3-10) at room temperature, which is not an averaged

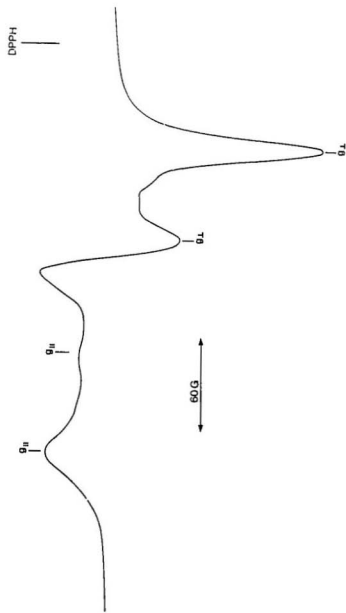


Fig. 3-9. Solid state esr spectrum for a powdered sample of $[\text{Cu}_x(\text{L})_2\text{Cl}_x] \cdot 2\text{CHCl}_3$ (18) (9.77 GHz, 295 K).

Table 3-8. Magnetic and esr data of Cu(II) complexes with thioether-pyridazine macrocycles.

Compound	μ_{eff} (BM)(RT)	ESR
[Cu ₂ (L1)Cl ₆] · 2CHCl ₃ (18)	1.87	$g_1 = 2.17, 2.13$ $g_i = 2.08, 2.04^*$
[Cu(L2)Cl ₂] (19)	1.77	$g_1 = 2.16, g_i = 2.08^*$
[Cu(L2)Br ₂] (20)	1.88	$g_{av} = 2.08^*$
[Cu(L2)(NO ₂) ₂] (21)	1.78	$g_{av} = 2.07^*$
[Cu(L2) ₂](ClO ₄) ₂ · CH ₃ CN · CHCl ₃ (22)	1.77	$g_1 = 2.22, g_i = 2.07^b$ $A_1 = 210 \times 10^{-4} \text{ cm}^{-1}$, $A_i = 35.7 \times 10^{-4} \text{ cm}^{-1}$
[Cu ₂ (L3)Cl ₄] (23)	1.84	$g_{av} = 2.09^*$
[Cu(L3)Cl ₂] (24)	1.80	$g_1 = 2.27, g_i = 2.06^*$
[Cu(L3)(NO ₂) ₂] (25)	1.76	$g_{av} = 2.11^*$
[Cu(L4)Cl ₂] · THF (26)	1.81	$g_1 = 2.04, g_2 = 2.06,$ $g_3 = 2.19^*$
[Cu(L5)Cl ₂] (27)	1.74	$g_1 = 2.03, g_2 = 2.06,$ $g_3 = 2.15^*$
[Cu(L5)Br ₂] (28)	1.83	$g_{av} = 2.10^*$

*Solid(RT).

^bMeNO₂ solution.

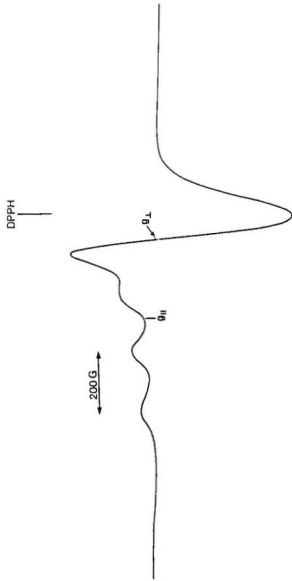


Fig. 3-10. Solid state esr spectrum for a powdered sample of $[\text{Cu}(\text{L}2)_2](\text{ClO}_4)_2 \cdot \text{CH}_3\text{CN} \cdot \text{CHCl}_3$, (22) (9.76 GHz, 295 K).

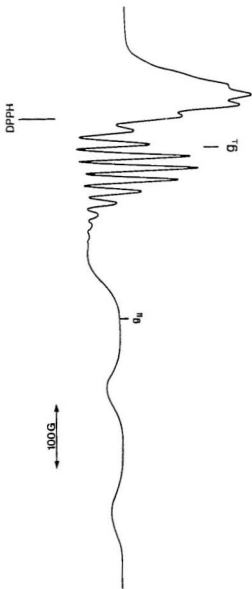


Fig. 3-11. Frozen glass (nitromethane) esr spectrum of $[\text{Cu}(\text{L-2})_2](\text{ClO}_4)_2 \cdot \text{CH}_3\text{CN} \cdot \text{CHCl}_3$, (22) (9.52 GHz, 77 K).

spectrum, but appears to be due to a unique axial species. The hyperfine structure in the g_{\parallel} region is due to the nuclear-electron interaction in the compound. A similar spectrum is also observed at 77 K. It closely resembles the frozen nitromethane glass (77 K) spectrum (Fig. 3-11) of the same compound. In fact values of g_{\parallel} , g_{\perp} , and A_{\parallel} observed in the solid state are very close to those observed in the frozen glass (Table 3-8). The superhyperfine structure in g_{\perp} is due to the coordination of four nitrogen atoms. The high values of g_{\parallel} and A_{\parallel} are typical of square-planar CuN_4 chromophores and the values of g and the superhyperfine coupling constants are comparable with those observed for the square-planar complex $[\text{Cu}(\text{LP})_2](\text{ClO}_4)_2$ ($\text{LP} = 1,2\text{-bis-}(4,5\text{-dihydroimidazol-2-yl})\text{-benzene}$), which has comparable dimensions ($g_{\parallel} = 2.232$, $g_{\perp} = 2.044$, $A_{\parallel} = 198 \times 10^{-4} \text{ cm}^{-1}$, $A_{\perp} = 46.7 \times 10^{-4} \text{ cm}^{-1}$) [16]. The frozen nitromethane spectrum also can be compared with frozen DMSO or DMF spectra of a series of tetrahedrally distorted tetragonal copper(II) complexes with a tridentate chelating ligand containing a bis(benzimidazole) donor set [204].

3.3.4. Magnetism

Room temperature magnetic moments for compounds 18 - 26 (Table 3-8) all exceed the spin-only value for a one-unpaired electron system and suggest the presence of dilute copper(II) centres in all cases, with no spin exchange. The large

distances separating the copper(II) centres in **18** and **23**, and the lack of appropriate magnetically active bridging groups would suggest the absence of any spin-spin interactions in these systems. The room temperature magnetic moments for **27** and **28** (Table 3-8) exceed the spin only value for copper(II) and do not give any clear indication of spin coupling and support for the proposed dimeric structures. Variable temperature magnetic measurements were therefore carried out on both **27** and **28** in the temperature range 4.5-300 K. The plots of χ_m versus T are both similar (Fig. 3-12 for **27**) with susceptibility maxima at low temperatures ($T_N \sim 18$ K for **27**; $T_N \sim 8$ K for **28**) and clearly indicate the presence of antiferromagnetic interactions. This kind of profile is typical of weakly antiferromagnetically coupled copper(II) dimers and supports the dimeric structures proposed for **27** and **28**.

The data for **27** and **28** were first fitted to the Bleaney-Bowers expression (eq.2, Chapter 1) with $-2J \approx 16 \text{ cm}^{-1}$ for **27** and $-2J \approx 5 \text{ cm}^{-1}$ for **28** indicating the presence of weak intradimer antiferromagnetic interactions in these two compounds. The Weiss corrective term, which is around 5 K for both compounds, suggests the presence of significant interdimer exchange in these complexes. The data were then fitted to the magnetization expression (eqs. 4 - 7) developed by Friedberg [205] and containing a molecular field correction. This express is

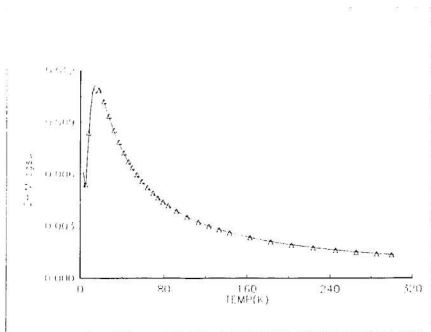


Fig. 3-12. Magnetic data for $[\text{Cu}(\text{L}5)\text{Cl}_2]_2$ (27). The solid line was calculated from eqs. [4], [5], [6] and [7] with $g = 2.061(3)$, $-2J = 17.77(7)$ cm^{-1} , $zJ' = -0.51(5)$ cm^{-1} , $\rho = 0.045$, $N\alpha = 60 \times 10^{-6}$ cgsu ($R = 0.22$).

$$M = \frac{Ng\beta \sinh(g\beta H/kT)}{\exp(-2J/kT) + 2 \cosh(g\beta H/kT) + 1} \dots \dots \dots [4]$$

$$\chi_m = M/H + N\alpha \dots \dots \dots [5]$$

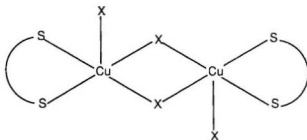
$$\chi'_{Cu} = \frac{\chi_{Cu}}{1 - (2zJ'\chi_{Cu}/Ng^2\beta^2)} \dots \dots \dots [6]$$

$$\chi''_{Cu} = \chi'_{Cu}(1 - \rho) + \frac{Ng^2\beta^2\rho}{4kT} + N\alpha \dots \dots \dots [7]$$

considered to be more appropriate for weakly coupled dinuclear complexes. The presence of an interdimer interaction was considered by using equation 6, where z is the number of nearest neighbour dimers and J' the interdimer exchange parameter. The data for **27** and **28** were fitted to an equation produced by

combination of eq. [4], [5], [6] and [7], allowing also for a paramagnetic impurity correction (ρ). The results show that both compounds have weak intradimer antiferromagnetic interaction ($-2J = 17.77(7) \text{ cm}^{-1}$ (**27**); $-2J = 8.56(6) \text{ cm}^{-1}$ (**28**)) with even weaker interdimer antiferromagnetic interaction ($zJ' = -0.51(1) \text{ cm}^{-1}$ (**27**); $zJ' = -0.29(1) \text{ cm}^{-1}$ (**28**)). The experimental data and the theoretical line fit very well (Fig. 3-12 for **27**) with $g = 2.061(3)$, $-2J = 17.77(7) \text{ cm}^{-1}$, $zJ' = -0.51(5) \text{ cm}^{-1}$, $\rho = 0.045$ for **27** and $g = 2.010(2)$, $-2J = 8.56(6) \text{ cm}^{-1}$, $zJ' = -0.28(5) \text{ cm}^{-1}$, $\rho = 0.025$ for **28**. Since we do not have structural information for these two compounds the mechanism of the magnetic interaction and the number of dimers involved is not clear. Structurally, complexes **27** and **28** could be similar to the dimeric CuCl_2 complexes of some thiophenophane ligands [165, 169] in which copper centres in square-pyramidal or octahedral geometries are bridged by two chlorides, with the macrocycles acting as bidentate S_2 chelate ligands (Scheme 3-13). The exchange integral for the bromo-complex **28** is smaller than that for the chloro-complex **27** which is not anticipated, due to the polarizing effect of coordinated halogens (discussed in Chapter 1) assuming both complexes had similar structures with comparable bridge angles. Perhaps the bridge angles in **28** are smaller than that in **27** and lead to a smaller exchange integral.

Scheme 3-13.



X = Cl, Br

3.4. Conclusion

Thioether-pyridazine macrocycles (L1 - L5) containing one, two and three pyridazine subunits were prepared from the condensation of 3,6-dichloropyridazine with appropriate dimercaptans under high dilution conditions in basic media. The length of the dithiol plays a very important role in the formation of the macrocycle. The desired dinuclear copper(II) complexes involving double pyridazine bridges with simultaneous coordination of peripheral sulfur atoms are not formed so far, due to the rigidity of the ligands. Instead these macrocycles act predominantly as nitrogen donors and form a series of mononuclear, dinuclear, trinuclear and polymeric polynuclear copper(II) complexes with isolated Cu(II)

centres. In one case sulfur coordination was observed. The IR and ESR spectra of the complexes were studied in detail and interpreted according to their structures. The presence of very weak intradimer antiferromagnetic exchange ($-2J < 18 \text{ cm}^{-1}$) and in some cases even weaker interdimer exchange ($-zJ' < 0.51 \text{ cm}^{-1}$) was observed.

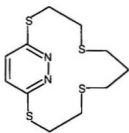
Chapter 4

Polymeric, Polynuclear Cu(I) and Ag(I) Complexes of Pyridazinophane and Phthalazinophane Macrocycles. Unusual Extended Metallo-cyclic Structures.

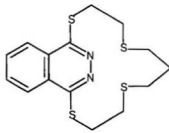
4.1. Introduction

In Chapter 3, we studied copper(II) coordination chemistry of five macrocyclic thioether-pyridazine ligands. A variety of mononuclear, dinuclear, trinuclear and polynuclear Cu(II) complexes were produced in which, in most instances, the macrocycles only act as nitrogen donors. Only one structurally

Scheme 4-1.



L5



L6

characterized polymeric derivative involved N_2S_2 coordination to Cu(II). To understand the coordination modes of these novel macrocycles further, we explore in this chapter the copper(I) and silver(I) coordination chemistry of two 1:1 macrocycles (Scheme 4-1) involving pyridazine and phthalazine subunits and a S_4 linkage between the diazine groups.

4.2. Experimental*

4.2.1. Synthesis of the Macrocycles**

L5

The synthesis of *L5* has been described in Chapter 3.

L6

3,7-Dithianonane-1,9-dithiol [184] (2.28 g, 10.0 mmol) was added to anhydrous ethanol (100 mL) in which sodium metal (0.46 g, 20.0 mmol) had been dissolved and the resulting solution was stirred for 30 min. 1,4-Dichlorophthalazine [207] (1.99 g, 10.0 mmol) was then dissolved in anhydrous THF (100 mL) and both solutions were simultaneously added dropwise to refluxing anhydrous THF (500 mL), by using pressure equalizing funnels under an atmosphere of dry nitrogen, over a period of 6 h. The mixture was then stirred

*For general procedure, see 1.2. **See List of Abbreviations for names.

under reflux overnight. The solvent was removed on a rotary evaporator and the residue dissolved in CHCl_3 . The extract was washed with water, dried over anhydrous Na_2SO_4 , filtered and the filtrate concentrated to about 50 mL, whereupon white crystals formed. Yield: 1.56 g (44%). Mp: 228-230 °C. ^1H nmr (CDCl_3)(δ (relative intensity)). 2.00(2) (multiplet, CH_2), 2.81(4) (triplet, CH_2), 2.91(4) (multiplet, CH_2), 3.60(4) (multiplet, CH_2), 7.85(2) (multiplet, phthalazine), 8.00(2) (multiplet, phthalazine). Mass spectrum, major mass peaks (m/e)(relative intensity): 354(17) P, 321(6), 252(10), 194(69), 133(100), 120(34), 105(24), 87(15).

4.2.2. Synthesis of the Complexes

[Cu(L5)Cl]_x (**29**), *[Cu(L5)Br]_x* (**30**) and *[Cu_{1.5}(L6)Cl_{1.5}]_x* (**31**)

Cu powder (190 mg, 3.0 mmol) was added to a solution of $\text{CuCl}_2 \cdot 2\text{H}_2\text{O}$ (51.2 mg, 0.30 mmol) in CH_3CN (20 mL). The mixture was stirred for 6 h under a nitrogen atmosphere and the resulting colourless solution filtered into a solution of L5 (91.2 mg, 0.30 mmol) in CHCl_3 (20 mL) under a nitrogen atmosphere. The resulting pale yellow solution was left at room temperature for several days and colourless crystals formed. Yield: 105 mg (87%). Anal. calcd. for $\text{C}_{11}\text{H}_{16}\text{N}_2\text{S}_4\text{ClCu}$ (**29**): C 32.74, H 3.99, N 6.94; found: C 32.87, H 3.97, N 6.98. **30** and **31** were

prepared in a similar manner as colourless and yellow crystals respectively. Yield: 106 mg (79%) for **30** and 104 mg (69%) for **31**. The compositions of **30** and **31** were obtained from X-ray structural analysis.

$[Ag(L5)(ClO_4)]_x$ (**32**), $([Ag(L5)(ClO_4)] \cdot CH_3CN)_x$ (**33**), $[Ag(L5)(NO_3)]_x$ (**34**) and $[Ag(L6)(ClO_4)]_x$ (**35**)

A solution of L5 (152 mg, 0.50 mmol) in $CHCl_3$ (20 mL) was added to a solution of $AgClO_4$ (250 mg, 1.2 mmol) in CH_3CN (20 mL). The combined solution was filtered and then allowed to stand at room temperature overnight. Colourless crystals formed which were filtered off, washed with CH_3CN and $CHCl_3$, and dried in air. Yield: 150 mg (63%). Anal. Calcd for $C_{11}H_{16}N_2S_4O_4ClAg$ (**32**): C 25.81, H 3.15, N 5.47; found: C 25.92, H 3.09, N 5.52. When the colourless crystals were kept in contact with the solution for several days they gradually became yellow crystals (**33**), which were found to contain one molecule of acetonitrile. Anal. calcd. for $C_{13}H_{19}N_3S_4O_4ClAg$ (**33**): C 28.24, H 3.46, N 7.60; found: C 28.06, H 3.35, N 7.53. $[Ag(L5)(NO_3)]_x$ (**34**) and $[Ag(L6)(ClO_4)]_x$ (**35**) were prepared similarly and obtained only as colourless crystals. Yield: 127 mg (54%) for **34** and 207 mg (74%) for **35**. Anal. calcd for $C_{11}H_{16}N_3S_4O_3Ag$ (**34**): C 27.85, H 3.40, N 8.86; found: C 27.76, H 3.26, N 8.87. Anal. Calcd for $C_{15}H_{18}N_3S_4O_4ClAg$ (**35**): C 32.06, H 3.23, N 4.99; found: C 32.04, H 3.24, N 5.00.

4.3. Results and Discussion

4.3.1. Synthesis.

The synthesis of L6 was achieved in moderately high yield by a traditional high dilution cyclization reaction and no trace of any 30-membered macrocycle containing two phthalazine subunits was detected.

The complexes did not dissolve appreciably in any solvent and were studied exclusively in the solid state.

4.3.2. Structures.

L6

The crown thioethers generally adopt 'inside-out' conformations in which all the sulfur atoms point out of the macrocyclic ring (the 'exodentate' conformation) due to the preference of -SCH₂CH₂SCH₂CH₂SCH₂CH₂- linkages [127, 128]. This conformational feature considerably influences their coordination chemistry. Many thiacycrowns, such as 12S4, show a diminished propensity for chelation because of the exodentate orientation of the S atoms in the free ligands [191, 208]. Instead they bind in a mono-, bi- or tridentate fashion, to form dimeric or oligomeric complexes. Endodentate coordination of crown thioethers has been reported for the Hg(II), Cu(I), Cu(II), Ni(II), Pd(II) complexes of 14S4 and 16S6 [127, 128]. The placement of rigid aromatic spacers in macrocyclic thioethers can

lead to some dramatic changes in the conformational characteristics of these ligands and also leads to different coordination modes. In the macrocyclic thiacyclophanes (Scheme 3-5), the rigid xylyl units seem to limit the conformational flexibility of the macrocyclic ring. In the potentially tridentate ligand 2,5,8-trithia[9] ortho-benzophane [TTOB], an *o*-xylyl group favours an *endo*-conformation in its complex with three sulfur atoms coordinating facially to the metal centre, even though the free ligand has an *exo* conformation [173]. The introduction of a more rigid *meta*-xylyl group stiffens the ligand 2,5,8-trithia[9]-*m*-benzophane [TTMB] even more, and its coordination capacity is diminished. So in its PdCl₂ complex, the macrocycle coordinates as an S₂ bidentate ligand with the third, uncoordinated sulfur remaining exodentate to the ring [172].

The aromatic units in L5 and L6 are 1,4-diazine groups which are different from 1,2 and 1,3 spacers in TTOB and TTMB. Also these diazine groups have been shown to be coordinating groups in their open chain or macrocyclic derivatives (Chapter 1 & 3). The two sulfur atoms connected to the diazine rings are not considered as possible donors in an intramolecular sense. According to molecular models, L5 and L6 can allow simultaneous N₂S₂ coordination to two metal centres by using two diazine nitrogens and two aliphatic sulfur atoms. Such a bonding mode has not been observed. Instead the rigid 1,4-diazine groups

encourage an exodentate binding mode of S(2) and S(3) in L5 and L6 (Fig. 4-1 for L6), to form a series of polymeric polynuclear Cu(I) and Ag(I) complexes and retain this conformation in their complexes.

The structure of L6 is shown in Fig. 4-1, and listings of atomic distances and angles are given in Table 4-1. Sulfur-carbon distances to the phthalazine ring (1.768(3) Å) are shorter than other aliphatic carbon-sulfur distances (1.809(3) - 1.826(3) Å) probably due to a conjugation effect of the sulfur lone pairs on S(1) and S(4) with the phthalazine ring, but compare closely with those of open chain, tetradentate thio-pyridazine ligands [51, 52] and thio-phthalazine ligands [63, 64]. The aliphatic sulfur-carbon distances compare closely with those found in other macrocyclic thioethers [165 - 175]. The aliphatic carbon-carbon distances are considered normal for thioethers of this sort.

The presence of the large phthalazine subunit in the macrocycle results in a higher degree of planarity of the molecule than that in thiophenophanes and thiacyclophanes [165, 167, 171, 172]. Dihedral angles between the least squares plane of the phthalazine itself and the planes defined by C(1)-S(4)-C(15) and C(8)-S(1)-C(9) (5.47(3)°, 4.62(3)° respectively away from the phthalazine plane), indicate an almost planar arrangement of the heterocyclic ring and the connected carbon-sulfur bonds. This serves to preorient and effectively fix the *exo*-ligand

conformation.

Even though the 15-membered macrocycles L6 and L5 do have a large enough cavity to accommodate some reasonably-sized transition metal ions such as copper, this did not happen due to the constraints imposed by the rigidity of the phthalazine subunit and the fact that the orientation of the electron pairs on the thioether sulfurs (S(2) and S(3)) is exocyclic. As a result, the macrocycle acts as a bidentate S_2 ligand to metal centres to accommodate this constraint and forms polymeric complexes.

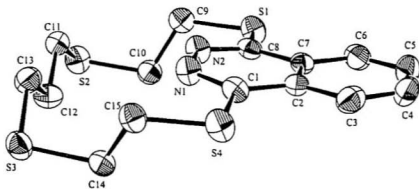


Fig. 4-1. Structural representation of L6, with hydrogen atoms omitted (40% probability ellipsoids).

Table 4-1. Selected bond distances (Å) and angles (deg) for L6

S(1)-C(8)	1.768(3)	C(9)-C(10)	1.524(4)
S(1)-C(9)	1.822(3)	C(11)-C(10)	1.522(4)
S(2)-C(10)	1.809(3)	C(12)-C(13)	1.518(4)
S(2)-C(11)	1.826(3)	C(14)-C(15)	1.519(4)
S(3)-C(13)	1.822(3)	S(3)-C(14)	1.817(3)
S(4)-C(1)	1.768(3)	S(4)-C(15)	1.823(3)
N(1)-N(2)	1.383(3)	N(1)-C(1)	1.312(3)
N(2)-C(8)	1.306(3)		
C(8)-S(1)-C(9)	100.4(1)	S(2)-C(10)-C(9)	112.0(2)
C(10)-S(2)-C(11)	101.6(1)	S(2)-C(11)-C(12)	114.0(2)
C(13)-S(3)-C(14)	100.5(1)	C(11)-C(12)-C(13)	111.4(3)
C(1)-S(4)-C(15)	100.5(1)	S(3)-C(13)-C(12)	115.0(2)
S(1)-C(8)-N(2)	116.9(2)	S(3)-C(14)-C(15)	112.2(2)
S(4)-C(1)-N(1)	116.9(2)	S(4)-C(15)-C(14)	113.4(2)
S(1)-C(9)-C(10)	114.0(2)		

[Cu(L5)Cl]_n (29)

The structure of $[\text{Cu}(\text{L5})\text{Cl}]_n$ (**29**) is shown in Fig. 4-2 and Fig. 4-3 and interatomic distances and angles relevant to the copper coordination spheres are given in Table 4-2. The ligand coordinates only as a sulfur donor by using S(1), a sulfur connected to the pyridazine ring, and S(3). The copper atom is four coordinate bound by two sulfur atoms and two chlorines in a slightly distorted tetrahedral geometry. The angles around the copper atom are in the range of 102.90(5) to 120.54(5)°. The Cu(1)-S(1) distance (2.367(2) Å) is longer than that of Cu(1)-S(3) (2.280(4) Å), associated with an inductive effect resulting from the proximity of S(1) to the pyridazine ring, but is within the normal range of other Cu(I) complexes with macrocyclic thioether ligands [167, 171]. The two Cu-Cl distances are very similar (Cu(1)-Cl(1) 2.340(2) Å, Cu(1)-Cl(1)a 2.350(1) Å), and can be compared with those in the polymeric complex $(\text{C}_3\text{H}_8\text{S}_2)_2(\text{CuCl})_3$ (2.30 to 2.413 Å) [209], which involves a canted $\text{Cu}_2\text{S}_4\text{Cl}_2$ dinuclear centre. It is worth noting that the S(1)-C(1) distance (1.772(4) Å) is significantly shorter than other S-C bonds (average 1.816 Å) [122], which is similar to the situation found in L6. The overall structure of the complex is an infinite double stranded polymer with two macrocycles acting as S_2 bidentate ligands linking chloro-bridged dinuclear copper(I) groups (Fig. 4-2). The repeating unit of the polymer is a tetranuclear

copper(I) entity with the two macrocyclic ligands and two dinuclear copper(I) groups forming a metallocycle with a very large cavity and two pyridazine rings parallel each other.

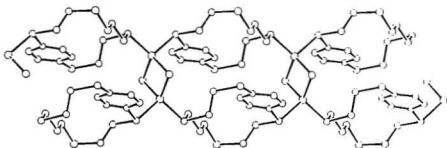


Fig. 4-2. Structural representation of $[\text{Cu}(\text{L}5)\text{Cl}]_n$ (**29**) illustrating the double stranded polymer, with hydrogen atoms omitted.

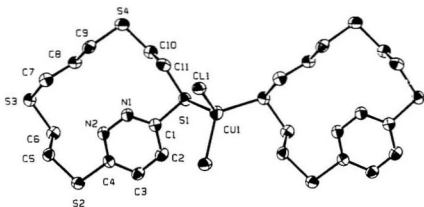


Fig. 4-3. Structural representation of fragment of $[\text{Cu}(\text{L}5)\text{Cl}]_x$ (**29**), with hydrogen atoms omitted (40% probability ellipsoids).

Table 4-2. Selected bond distances (Å) and angles (deg) for $[\text{Cu}(\text{L}5)\text{Cl}]_x$ (**29**)

Cu(1)-Cl(1)	2.340(2)	Cu(1)-Cl(1)a	2.350(1)
Cu(1)-S(1)	2.367(2)	Cu(1)-S(3)	2.280(1)
Cl(1)-Cu(1)-Cl(1)	106.19(5)	Cl(1)-Cu(1)-S(1)	108.41(5)
Cl(1)-Cu(1)-S(3)	111.21(5)	Cl(1)-Cu(1)-S(1)	102.90(5)
Cl(1)-Cu(1)-S(3)	120.54(5)	S(1)-Cu(1)-S(3)	106.84(5)

[Cu(L5)Br]_x (30)

The structure of $[Cu(L5)Br]_x$ (30) is shown in Fig. 4-4 and Fig. 4-5, and interatomic distances and angles relevant to copper coordination spheres are given in Table 4-3. The copper centre is coordinated by two sulfur and two bromine atoms, with two bromines bridging the two Cu(I) centres to form the dinuclear Cu_2Br_2 unit, which is similar to the Cu_2Cl_2 unit in 29. The copper atom has a similar distorted tetrahedral geometry with angles at copper in the range 101.11(6) to 121.44(5)°, which are comparable to the angles in 29. The Cu-S distances (2.321(1) and 2.315(2) Å) are slightly longer than those in 29. The Cu-Br distances (2.458(1) and 2.507(1) Å) are comparable with those in $[Cu_4(ddpt)_2Br_4]$ [210], which contains two similar Cu_2Br_2 fragments (ddpt = 1,5-bis(3',5'-dimethylpyrazolyl)-3-thiapentane). The macrocycle still coordinates in an *exo*-bidentate fashion, but in a different manner. Each ligand uses two adjacent, aliphatic thioether sulfurs, S(1) and S(2), to link the Cu_2Br_2 units in an interlocked, two-dimensional 'zig-zag' latticework (Fig. 4-5). Within each strand, the ligands alternate in a pseudo *trans* arrangement with the Cu_2Br_2 units cross-linking the strands. Since the pyridazine nitrogens are not involved in coordination, the pyridazine rings are forced to occupy an extra-strand position. The repeating unit is a much larger metallocycle than that in 29. It contains four macrocycles, two

Cu_2Br_2 fragments and half of two Cu_2Br_2 fragments.

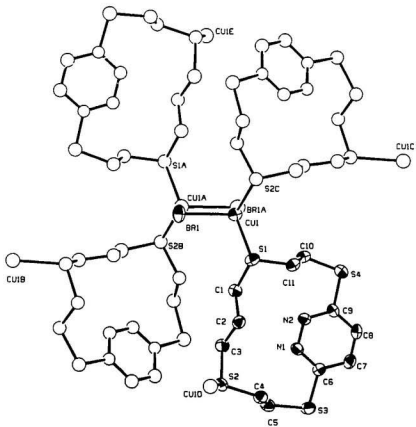


Fig. 4-4. Structural representation of fragment of $[\text{Cu}(\text{L}5)\text{Br}]_x$ (**30**), with hydrogen atoms omitted (40% probability ellipsoids).

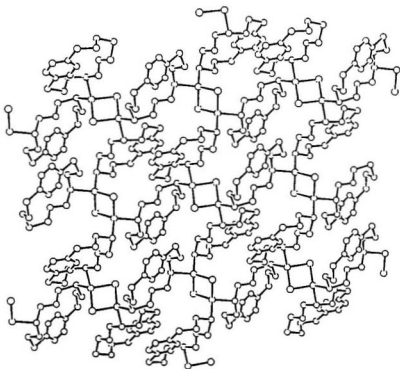


Fig. 4-5. Structural representation of $[\text{Cu}(\text{L}5)\text{Br}]_n$ (30) showing cross-linking, with hydrogen atoms omitted.

Table 4-3. Selected bond distances (Å) and angles (deg) for [Cu(L5)Br]_x (**30**)

Br(1)-Cu(1)	2.507(1)	Br(1)-Cu(1)	2.458(1)
Cu(1)-S(1)	2.321(2)	Cu(1)-S(2)	2.315(2)
Cu(1)-Br(1)-Cu(1)	76.09(4)	Br(1)-Cu(1)-Br(1)	103.91(4)
Br(1)-Cu(1)-S(1)	104.15(5)	Br(1)-Cu(1)-S(2)	104.88(5)
Br(1)-Cu(1)-S(1)	119.40(5)	Br(1)-Cu(1)-S(2)	121.44(5)
S(1)-Cu(1)-S(2)	101.11(6)		

*[Cu_{1,3}(L6)Cl_{1,3}]_x (**31**)*

The structure of **31** is shown in Fig. 4-6, and interatomic distances and angles are given in Table 4-4. The ligand coordinates by using two adjacent aliphatic thioether sulfurs, S(1) and S(4), which is similar to L5 in **30**. Three copper(I) ions are linked together by three chlorides forming a six-membered alternating Cu-Cl ring. The two macrocycles, with each one acting as a S₂ bidentate ligand, bridge the trinuclear Cu₃Cl₃ centres to form an infinite double-stranded polymer. So far few examples of trimeric Cu(I) aggregates are known [211 - 215], and to our knowledge this is the first example of polynuclear

Table 4-4. Selected bond distances (Å) and angles (deg) for [Cu_{1.5}(L6)Cl_{1.5}]_n (31)

Cu(1)-Cl(1)	2.353(2)	Cu(1)-Cl(2)	2.539(2)
Cu(1)-S(1)	2.262(1)	Cu(1)-S(8)	2.239(1)
Cu(2)-Cu(3)	2.783(1)	Cu(2)-Cl(2)	2.208(2)
Cu(2)-Cl(3)	2.293(2)	Cu(2)-S(4)	2.280(2)
Cu(3)-Cl(1)	2.237(2)	Cu(3)-Cl(3)	2.313(2)
Cu(3)-S(5)	2.234(2)		
Cl(1)-Cu(1)-Cl(2)	108.53(6)	Cl(1)-Cu(1)-S(8)	111.58(6)
Cl(2)-Cu(1)-S(1)	90.43(5)	Cl(2)-Cu(1)-S(8)	96.88(6)
S(1)-Cu(1)-S(8)	129.77(6)	Cu(3)-Cu(2)-Cl(2)	136.64(5)
Cu(3)-Cu(2)-Cl(3)	53.15(4)	Cu(3)-Cu(2)-S(4)	86.04(5)
Cl(2)-Cu(2)-Cl(3)	122.17(7)	Cl(2)-Cu(2)-S(4)	124.10(6)
Cl(3)-Cu(2)-S(4)	112.23(6)	Cu(2)-Cu(3)-Cl(1)	72.42(5)
Cu(2)-Cu(3)-Cl(3)	52.51(4)	Cu(2)-Cu(3)-S(5)	154.16(5)
Cl(1)-Cu(3)-Cl(3)	114.12(6)	Cl(1)-Cu(3)-S(5)	128.09(6)
Cl(3)-Cu(3)-S(5)	116.26(6)	Cu(1)-Cl(1)-Cu(3)	113.64(6)
Cu(1)-Cl(2)-Cu(2)	79.49(6)	Cu(2)-Cl(3)-Cu(3)	74.34(5)

copper(I) halide complex with trinuclear repeating units. The three copper centres have different geometries with very different copper-copper separations (Cu(1)-Cu(2) 3.046(2) Å, Cu(2)-Cu(3) 2.783(2) Å, Cu(1)-Cu(3) 3.843(2) Å), which results in a highly distorted six-membered metallocyclic ring. Cu(1) is four coordinated by two sulfur and two chlorine atoms in a tetrahedral geometry, which is more distorted than that in **29** with angles around Cu(1) in the range 90.43(5) to 129.77(6)°. Cu(2) and Cu(3) are three coordinate, with one sulfur and two chlorine atoms each. The Cu-S distances are in the normal range. The Cu(1)-Cl(2) distance (2.539(2) Å) is much longer than remaining Cu-Cl distances and that in comparable derivatives [209].

Since L6 only coordinates through two adjacent aliphatic thioether sulfur atoms, the noncoordinated phthalazine subunit is forced to orient itself on the periphery of the polymeric strand. This contrasts sharply with the structural features of $[\text{Cu}(\text{L}5)\text{Cl}]_x$ (**29**), where, in the double stranded polymer, the non-coordinating diazine rings are found within the polymeric strand. This may be associated with steric factors associated with the bulk of the fused benzene ring present in L6.

[Ag(LS)(ClO₄)₂]_n (32)

Homoleptic crown thioether complexes of silver(I) usually involve high coordination numbers. Examples include six-coordinate $[Ag([18]aneS_6)]^+$ [216] and $[Ag([9]aneS_3)]^+$ [196, 217], five-coordinate $[Ag_2L_2]^{2+}$ ($L = 2,5,7,10$ -tetrathia[12](2,5)-thiophene) [168] and four-coordinate $[Ag_3([9]aneS_3)]^{3+}$ [218], $[Ag_2([15]aneS_5)]^{2+}$ [219], and $[Ag(16S6)]^+$ (16S6 = 1,3,6,9,11,14-hexathiacyclohexadecane) [220] species. Part of the structure of 32 is shown in Fig. 4-7 and interatomic distances and angles are given in Table 4-5. The structure involves a polymeric chain structure in which distorted tetrahedral silver(I) ions are bridged by *exo*-bidentate macrocyclic ligands that involve sulfur atoms S1 and S2 only as donors, similar to the situations in 30 and 31. The silver-sulfur distances (Ag1-S1 2.452(2) Å, Ag1-S2 2.463(2) Å) are about 0.1 Å shorter than those found in other Ag(I) thioether complexes with high coordination number [168, 196, 215 -220], and about 0.1 Å longer than those in two-coordinate Ag(I) complexes [221, 222]. The other two donor sites are provided by perchlorate oxygens (O1, O2), with relatively long silver oxygen bonds (Ag1-O1 2.659(5) Å, Ag1-O2 2.655(6) Å). The coordination of perchlorate to Ag(I) in its complexes with thioether ligands is very rare. The silver-perchlorate contacts in the cyclo(L-methionyl-L-methionyl) complex are 3.00 and 3.03 Å, which are questionable in

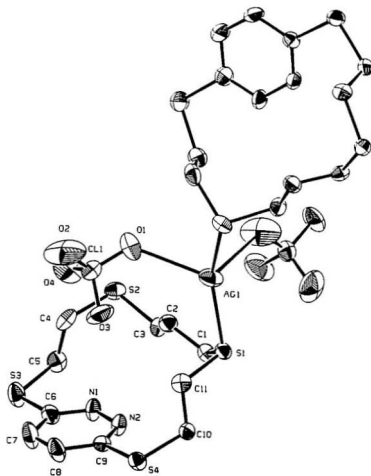


Fig. 4-7. Structural representation of fragment of $[\text{Ag}(\text{L5})(\text{ClO}_4)]_n$ (32), with hydrogen atoms omitted (40% probability ellipsoids).

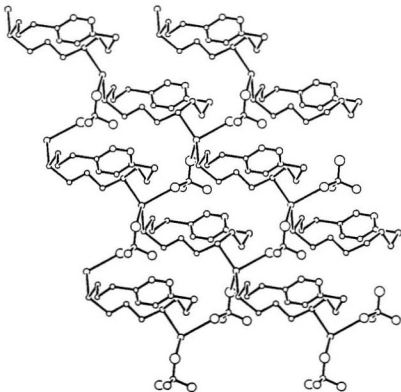


Fig. 4-8. Structural representation of $[\text{Ag}(\text{L5})(\text{ClO}_4)]_x$ (32) illustrating the 2-dimensional polymeric arrangement, with hydrogen atoms omitted.

terms bonding interactions [221]. The other silver-perchlorate bonds in for example, isothiocyanate [223] and dimethyl sulfoxide [224] complexes of silver fall in the range 2.40 - 2.75 Å and are considered to be real. As perchlorates only coordinate to Ag(I) weakly, the tetrahedral geometry at Ag(I) centre is highly distorted with angles around Ag(I) in the range 90.2(1) to 148.82(6)°. The overall structure of **32** is most unusual and involves bidentate perchlorates, which cross link the polymeric S₂ chains with the formation of a 2-dimensional, polymeric sheet (Fig. 4-8).

Table 4-5. Selected bond distances (Å) and angles (deg) for [Ag(L5)(ClO₄)]_n (**32**)

Ag(1)-S(1)	2.452(2)	Ag(1)-S(2)	2.463(2)
Ag(1)-O(1)	2.659(5)	Ag(1)-O(2)	2.655(6)
S(1)-Ag(1)-S(2)	148.82(6)	S(1)-Ag(1)-O(2)	101.0(1)
S(1)-Ag(1)-O(1)	114.2(2)	S(2)-Ag(1)-O(2)	90.2(1)
S(2)-Ag(1)-O(1)	90.5(1)	O(2)-Ag(1)-O(1)	104.2(2)

Table 4-6. Infrared spectral data of Cu(I) and Ag(I) complexes with L5 and L6

Compound	Colour	IR(cm^{-1})
$[\text{Cu}(\text{L5})\text{Cl}]_x$ (29)	Colourless	1562 (νCN)
$[\text{Cu}(\text{L5})\text{Br}]_x$ (30)	Colourless	1561 (νCN)
$[\text{Cu}_{1.5}(\text{L6})\text{Cl}_{1.5}]_x$ (31)	Yellow	1569 (νCN)
$[\text{Ag}(\text{L5})(\text{ClO}_4)]_x$ (32)	Colourless	1564 (νCN), 1078 (νClO_4)
$([\text{Ag}(\text{L5})(\text{ClO}_4)] \cdot \text{CH}_3\text{CN})_x$ (33)	Yellow	2293, 2253 ($\nu\text{CH}_3\text{CN}$), 1562 (νCN), 1072 (νClO_4)
$[\text{Ag}(\text{L5})(\text{NO}_3)]_x$ (34)	Colourless	1748, 1742, 1738, 1731 (νNO_3), 1562 (νCN)
$[\text{Ag}(\text{L6})(\text{ClO}_4)]_x$ (35)	pale yellow	1569 (νCN), 1096, 1050 (νClO_4)

4.3.2. Spectroscopy

The ligand L5 has an infrared absorption at 1568 cm^{-1} , associated with CN stretch in the pyridazine ring. A very small shift is observed in this band by 6 cm^{-1} or less in all the complexes (Table 4-6). The absence of pyridazine coordination in 29, 30 and 32 and the similarity in the position of this absorption in all the complexes suggests that the pyridazine nitrogen atoms are not involved in

coordination in the other complexes. The ν_3 perchlorate vibration for **32** appeared as a strong, broad absorption centred at 1078 cm^{-1} , with little peak resolution. This might not have been anticipated based on the bidentate bridging nature of the perchlorate groups. A similar broad, strong absorption is observed for **33**. Overall, the infrared spectra of **32** and **33** are very similar, suggesting a similar structural arrangement. The presence of two CN stretching bands at 2293 and 2255 cm^{-1} suggests that the CH_3CN occupies a lattice position only in **33** and is not coordinated to silver [99]. The nitrate complex **34** has an overall infrared spectrum similar to the perchlorate complex **32**, and in the nitrate combination band region an expanded spectrum reveals four bands at 1748 , 1742 , 1738 , and 1731 cm^{-1} . The fairly narrow range of this group of bands (17 cm^{-1}) is probably indicative of two slightly different monodentate nitrate groups [98]. So structurally **34** maybe similar to **32** with a polymeric exobidentate ligand bridging the Ag(I) ions, which are three coordinate with two thioether sulfur atoms and a monodentate nitrate.

The ligand **L6** has an infrared absorption at 1580 cm^{-1} , associated with CN stretch in the phthalazine ring. A shift of 11 cm^{-1} to lower energy (Table 4-6) for **31**, which has only sulfur coordination, suggests that much larger shifts to lower energy might be expected for nitrogen coordination with the phthalazine macrocycles. A similar shift for **35** suggests sulfur coordination. The structure is

probably similar to the structure of $[\text{Ag}(\text{L5})(\text{ClO}_4)]_x$ (32), which involved bidentate perchlorate bridges in a 2D lattice-work structure. Two prominent perchlorate bands for 35 at 1096 and 1050 cm^{-1} suggest a low symmetry ClO_4^- group, which is possibly involved in coordination.

4.4. Conclusion

Thioether-diazine macrocycles L5 and L6 form Cu(I) and Ag(I) complexes with the ligands acting predominantly as sulfur donors, not like the situations found in copper(II) complexes of the ligands of this sort discussed in Chapter 3. This is clearly a reflection that soft sulfur donors prefer to coordinate soft metal ions. Unlike the situation where ortho-, and to a lesser extent, meta-aromatic spacers in a cyclothiaphane ring encourage *endo*-dentate coordination, the inclusion of a 1,4-aromatic fragment in L5 and L6 seems to confer extra rigidity on the ring causing a preference for *exo*-dentate coordination and the formation of unusual, extended, polymeric derivatives. The exobidentate nature of these pyridazinophane and phthalazinophane macrocycles is consistent with the general trend for *exo*-dentate coordination observed for homoleptic, macrocyclic thioethers.

References

1. K.D. Karlin and J. Zubieta, *Copper Coordination Chemistry and Biochemistry: Biochemical and Inorganic Perspectives*, Adenine press, 1983.
2. K.D. Karlin and J. Zubieta, *Biological and Inorganic Copper Chemistry*, Vols. 1 & 2, Adenine press, 1986.
3. E.I. Solomon, Dinuclear Copper Active Site, in T.G. Spiro (Ed.), *Copper Proteins*, Wiley-Interscience, New York, 1981, Chapter 2.
4. D.M. Dooley, R.A. Scott, E. Ellinghaus, E.I. Solomon and H.B. Gray, *Proc. Natl. Acad. Sci., U.S.A.*, 75 (1978) 3019.
5. P.A. Vigato and S. Tamburini, *Coord. Chem. Rev.*, 106 (1990) 25.
6. T.N. Sorrell, *Tetrahedron*, 45 (1989) 3.
7. (a) M. Melnik, *Coord. Chem. Rev.*, 42 (1982) 259. (b) M. Kato and Y. Muto, *Coord. Chem. Rev.*, 92 (1988) 45.
8. C.J. O'Connor, *Prog. Inorg. Chem.*, 29 (1983) 203.
9. O. Kahn, *Angew Chem. Int. Ed. Engl.*, 24 (1985) 834.
10. P.J. Hay, J.C. Thibeault and R. Hoffmann, *J. Am. Chem. Soc.*, 97 (1975) 4884.

11. O. Kahn and M.F. Charlot, *Nouv. J. Chim.*, **4** (1980) 567.
12. M.F. Charlot, Y. Journaux, O. Kahn, A. Bencini, D. Gatteschi and C. Zanchini, *Inorg. Chem.*, **25** (1986) 1060.
13. R.L. Carlin, *Magnetochemistry*, Springer-Verlag, Berlin, 1986.
14. D.J. Hodgson, *Prog. Inorg. Chem.*, **19** (1975) 173 and references cited therein.
15. V.H. Crawford, H.W. Richardson, J.R. Wasson, D.J. Hodgson and W.E. Hatfield, *Inorg. Chem.*, **15** (1976) 2107.
16. S.K. Mandal, L.K. Thompson, M.J. Newlands, E.J. Gabe and F.L. Lee, *Inorg. Chem.*, **29** (1990) 3556.
17. O. Kahn, *Comments Inorg. Chem.*, **3** (1984) 105.
18. B. Bleaney and K.D. Bowers, *Proc. R. Soc. London, A*, **214** (1952) 451.
19. K. McGregor, J.A. Barnes and W.E. Hatfield, *J. Am. Chem. Soc.*, **95** (1973) 7993.
20. S. Sikorav, I. Bkouche-Waksman and O. Kahn, *Inorg. Chem.*, **23** (1984) 490.
21. P.J. Steel, *Coord. Chem. Rev.*, **106** (1990) 228.
22. H. Oshio, *J. Chem. Soc., Dalton Trans.*, (1990) 2985.
23. H. Oshio, K. Toriumi and Y. Hayashi, *J. Chem. Soc., Dalton Trans.*,

- (1990) 293.
24. A. Real, J. Zarembowitch, O. Kahn and X. Solans, *Inorg. Chem.*, **26** (1987) 2939.
 25. G. Brewer and E. Sinn, *Inorg. Chem.*, **24** (1985) 4580.
 26. G. De Munno and G. Bruno, *Acta. Cryst.*, **C40**, (1984) 2030.
 27. M. Julve, G. De Munno, G. Bruno and M. Verdaguer, *Inorg. Chem.*, **27** (1988) 3160.
 28. L.K. Thompson, V.T. Chacko, J.A. Elvidge, A.B.P. Lever and R.V. Parish, *Can. J. Chem.*, **47** (1969) 4141.
 29. J.C. Dewan and L.K. Thompson, *Can. J. Chem.*, **60** (1982) 121.
 30. D.V. Bautista, J.C. Dewan and L.K. Thompson, *Can. J. Chem.*, **60** (1982) 2583.
 31. G. Marongiu and E.C. Lingafelter, *Acta Crystallogr. Sect., B.*, **38** (1982) 620.
 32. G. Bullock, F.W. Hartstock and L.K. Thompson, *Can. J. Chem.*, **61** (1983) 57.
 33. L.K. Thompson, *Can. J. Chem.*, **61** (1983) 579.
 34. F.W. Hartstock and L.K. Thompson, *Inorg. Chim. Acta*, **72** (1983) 227.
 35. L.K. Thompson, F.W. Hartstock, P. Robichaud and A.W. Hanson, *Can.*

- J. Chem.*, 62 (1984) 2755.
36. P. Robichaud and L.K. Thompson, *Inorg. Chim. Acta*, 85 (1984) 137.
 37. L.K. Thompson, A.W. Hanson and B.S. Ramaswamy, *Inorg. Chem.*, 23 (1984) 2459.
 38. L.K. Thompson, F.W. Hartsock, L. Rosenberg and T.C. Woon, *Inorg. Chim. Acta*, 97 (1985) 1.
 39. M. Ghedini, G. De Munno, G. Denti, A.M. Manotti Lanfredi and A. Tiripicchio, *Inorg. Chim. Acta*, 57 (1982) 87.
 40. P. Dapporto, G. De Munno, G. Bruno and M. Romeo, *Acta Crystallogr., Sect C*, 39 (1983) 718.
 41. A. Tiripicchio, A.M. Manotti Lanfredi, M. Ghedini and F. Neve, *J. Chem. Soc., Chem. Commun.*, (1983) 97.
 42. G. De Munno, G. Denti and P. Dapporto, *Inorg. Chim. Acta*, 74 (1983) 199.
 43. G. De Munno and G. Denti, *Acta Crystallogr., Sect. C*, 40 (1984) 616.
 44. G. De Munno and G. Bruno, *Acta Crystallogr., Sect C*, 40 (1984) 2022.
 45. P. Dapporto, G. De Munno, A. Segà and C. Meali, *Inorg. Chim. Acta*, 83 (1984) 171.
 46. S.K. Mandal, L.K. Thompson and A.W. Hanson, *J. Chem. Soc., Chem.*

- Commun.*, (1985) 1709.
47. L.K. Thompson, T.C. Woon, D.B. Murphy, E.J. Gabe, F.L. Lee and Y. Le Page, *Inorg. Chem.*, 24 (1985) 4719.
 48. T.C. Woon, R. McDonald, S.K. Mandal, L.K. Thompson, S.P. Connors and A.W. Addison, *J. Chem. Soc., Dalton Trans.*, (1986) 2381.
 49. S.K. Mandal, L.K. Thompson, M.J. Newlands, F.L. Lee, Y. Le Page, J-P. Charland and E.J. Gabe, *Inorg. Chim. Acta*, 122 (1986) 199.
 50. L.K. Thompson and T.C. Woon, *Inorg. Chim. Acta*, 111 (1986) 45.
 51. L.K. Thompson, S.K. Mandal, E.J. Gabe, F.L. Lee and A.W. Addison, *Inorg. Chem.*, 26 (1987) 657.
 52. L.K. Thompson, S.K. Mandal, L. Rosenberg, F.L. Lee and E.J. Gabe, *Inorg. Chim. Acta*, 133 (1987) 81.
 53. S.K. Mandal, L.K. Thompson, E.J. Gabe, F.L. Lee and J.P. Charland, *Inorg. Chem.*, 26 (1987) 2384.
 54. S.K. Mandal, T.C. Woon, L.K. Thompson, M.J. Newlands and E.J. Gabe, *Aust. J. Chem.*, 39 (1986) 1007.
 55. L.K. Thompson, S.K. Mandal, E.J. Gabe and J-P. Charland, *J. Chem. Soc., Chem. Commun.*, (1986) 1537.
 56. L.K. Thompson, F.L. Lee and E.J. Gabe, *Inorg. Chem.*, 27 (1988) 39.

57. L.K. Thompson, S.K. Mandal, J-P. Charland and E.J. Gabe, *Can. J. Chem.*, *66* (1988) 348.
58. S.K. Mandal, L.K. Thompson, E.J. Gabe, J-P. Charland and F.L. Lee, *Inorg. Chem.*, *27* (1988) 855.
59. S.K. Mandal, L.K. Thompson, M.J. Newlands, J-P. Charland and E.J. Gabe, *Inorg. Chim. Acta*, *178* (1990) 169.
60. P. Lacroix, O. Kahn, L. Valade, P. Cassoux and L.K. Thompson, *Synthetic Metals*, *39* (1990) 81.
61. W. Vreugdenhil, J.G. Haasnoot and J. Reedijk, *Inorg. Chim. Acta*, *167* (1990) 109.
62. S.S. Tandon, L.K. Thompson and R.C. Hynes, *Inorg. Chem.*, *31* (1992) 2210.
63. L. Chen, L.K. Thompson and J.N. Bridson, *Inorg. Chem.*, *32* (1993) 2938.
64. L. Chen, L.K. Thompson and J.N. Bridson, *Inorg. Chim. Acta*, in press.
65. S.S. Tandon, L. Chen, L.K. Thompson and J.N. Bridson, *Inorg. Chem.*, submitted.
66. J. Manzur, A.M. Garcia, R. Letelier, E. Spodine, O. Pena, D. Grandjean, M.M. Olmstead and B.C. Noll, *J. Chem. Soc., Dalton Trans.*, (1993) 905.
67. F. Abraham, M. Lagrenee, S. Sueur, B. Mernari and C. Bremard, *J.*

- Chem. Soc., Dalton Trans.*, (1991) 1443.
68. W.M.E.K. Oudenniel, R.A.G. Graaff, J.G. Haasnoot, R. Prins and J. Reedijk, *Inorg. Chem.*, 28 (1989) 1128.
69. R. Prins, P.J.M.W.L. Birker, J.G. Haasnoot, G.C. Verschoor and J. Reedijk, *Inorg. Chem.*, 24 (1985) 4128.
70. A. Bencini, D. Gatteschi, C. Zanchini, J.G. Haasnoot, R. Prins and J. Reedijk, *Inorg. Chem.*, 24 (1985) 2812.
71. R. Prins, R.A.G. graaff, J.G. Haasnoot, C. Vader and J. Reedijk, *J. Chem. Soc., Chem. Commun.*, (1986) 1430.
72. J. Pons, X. López, J. Casabó, F. Teixidor, A. Caubet, J. Rius and C. Mirayvilles, *Inorg. Chim. Acta*, 195 (1992) 61.
73. D. Ajò, A. Bencini and F. Mani, *Inorg. Chem.*, 27 (1988) 2437.
74. A. Bencini, D. Gatteschi, C. Zanchini, J.G. Haasnoot, R. Prins and J. Reedijk, *J. Am. Chem. Soc.*, 109 (1987) 2926.
75. T. Kamiyuki, H. Ōkawa, E. Kitaura, M. Koikawa, N. Matsumoto, S. Kida and H. Oshio, *J. Chem. Soc., Dalton Trans.*, (1989) 2077.
76. T. Kamiyuki, H. Ōkawa, N. Matsumoto and S. Kida, *J. Chem. Soc., Dalton Trans.*, (1990) 195.
77. T. Kamiyuki, H. Ōkawa, E. Kitaura, K. Inoue and S. Kida, *Inorg. Chim.*

- Acta*, 179 (1991) 139.
78. T. Kamiyuki, H. Ōkawa, K. Inoue, N. Matsumoto, M. Kodera and S. Kida, *J. Coord. Chem.*, 23 (1991) 201.
79. J.J. Maloney, Ph.D. thesis, Case Western Reserve Univ. U.S.A., 1986.
80. S.S. Tandon, L.K. Thompson, J.N. Bridson, *J. Chem. Soc., Chem. Commun.*, in press.
81. S.S. Tandon, S.K. Mandal, L.K. Thompson and R.C. Hynes, *Inorg. Chem.*, 31 (1992) 2215.
82. S.S. Tandon, S.K. Mandal and L.K. Thompson, *J. Chem. Soc., Chem. Commun.*, (1991) 1572.
83. R.L. Lintvedt and K.L. Steder, *Inorg. Chem.*, 22 (1983) 796.
84. S.K. Mandal and K. Nag, *Inorg. Chem.*, 22 (1983) 2567.
85. S.K. Mandal and K. Nag, *J. Chem. Soc., Dalton Trans.*, (1983) 2429.
86. J.D.O. Cabral, M.F. Cabral, M. McCann and S.M. Nelson, *Inorg. Chim. Acta*, 86 (1984) L15.
87. W. Mazurek, A.M. Bond, K.S. Murray, M.J. O'Connor and A.G. Wedd, *Inorg. Chem.*, 24 (1985) 2484.
88. S.S. Tandon, L.K. Thompson and J.N. Bridson, *J. Chem. Soc., Chem. Commun.*, (1992) 991.

89. S.S. Tandon, L.K. Thompson, J.N. Bridson, V. Mckee and A.J. Downard, *Inorg. Chem.*, *31* (1992) 4635.
90. B.R.M. Reinhammar, *Biochim. Biophys. Acta*, *275* (1972) 245.
91. N. Makino, P. McMahon and H.S. Mason, *J. Biol. Chem.*, *249* (1974) 6062.
92. M-T. Youinou, N. Rahmouni, J. Fischer and J.A. Osborn, *Angew Chem. Int. Ed., Engl.*, *31* (1992) 733.
93. J.C. Thompson, *J. Am. Chem. Soc.*, *106* (1984) 4057.
94. J.C. Thompson, R.L. Harlow and J.F. Whitney, *J. Am. Chem. Soc.*, *105* (1983) 3552.
95. K.D. Karlin and Y. Gultneh, *Prog. Inorg. Chem.*, *35* (1987) 219.
96. K.D. Karlin, R.W. Cruse, Y. Gultneh, A. Farooq, J.C. Hayes and J. Zubieta, *J. Am. Chem. Soc.*, *109* (1987) 2668.
97. K.D. Karlin, M.S. Haka, R.W. Cruse, G.J. Meyer, A. Farooq, Y. Gultneh, J.C. Hayes and J. Zubieta, *J. Am. Chem. Soc.*, *110* (1988) 1196.
98. A.B.P. Lever, E. Mantovani and B.S. Ramaswamy, *Can. J. Chem.*, *49* (1971) 1957.
99. L. Chen, L.K. Thompson and J.N. Bridson, *Inorg. Chim. Acta*, *210*, (1993) 215.

100. S. Emori, I. Inoue and M. Kubo, *Bull. Chem. Soc. Jpn.*, **45** (1972) 2259.
101. P. Iliopoulos, K.S. Murray, R. Robson, J. Wilson and G.A. Williams, *J. Chem. Soc., Dalton Trans.*, (1987) 1585.
102. K.S. Murray in "*Biological & Inorganic Copper Chemistry*", K.D. Karlin and J. Zubieta, Eds.; Adenine press; New York, 1986; Vol 2, P161.
103. W. Mazurek, B.J. Kennedy, K.S. Murray, M.J. O'Connor, M.R. Snow, J.R. Rodgers, A.G. Wedd and P.R. Zwack, *Inorg. Chem.*, **24** (1985) 3258.
104. W. Mazurek, K.J. Berry, K.S. Murray, M.J. O'Connor, M.R. Snow and A.G. Wedd, *Inorg. Chem.*, **21** (1982) 3071.
105. M.F. Charlot, O. Kahn, S. Jeannin and Y. Jeannin, *Inorg. Chem.*, **19** (1980) 1410.
106. A.C. Fabretti, W. Malavasi, D. Gatteschi and R. Sessoli, *Inorg. Chim. Acta.*, **195** (1992) 157.
107. S. Ferrer, J. Borrás, C. Miratvilles and A. Fuertes, *Inorg. Chem.*, **29** (1990) 206.
108. P.P. Paul, Z. Tyeklár, R.R. Jacobson and K.D. Karlin, *J. Am. Chem. Soc.*, **113** (1991) 5322.
109. K.D. Karlin, J.C. Hayes, Y. Gultneh, R.W. Cruse, J.W. McKown, J.P. Hutchinson and J. Zubieta, *J. Am. Chem. Soc.*, **106** (1984) 2121.

110. V. Mckee, M. Zvagulis, J.V. Dagdigian, M.G. Patch and C.A. Reed, *J. Am. Chem. Soc.*, 106 (1984) 4765.
111. T.N. Sorrell, V.A. Vankai and M.L. Garrity, *Inorg. Chem.*, 30 (1991) 207.
112. T.N. Sorrell and M.L. Garrity, *Inorg. Chem.*, 30 (1991) 210.
113. M.S. Brett, B.I. Cohen and K.D. Karlin, *Inorg. Chim. Acta.*, 176 (1990) 185.
114. M.S. Nasir, K.D. Karlin, D. McGowty and J. Zubieta, *J. Am. Chem. Soc.*, 113 (1991) 698.
115. S.S. Tandon, L. Chen, L.K. Thompson, S.P. Connors and J.N. Bridson, *Inorg. Chim. Acta*, 213 (1993) 289.
116. S.S. Tandon, L.K. Thompson and J.N. Bridson, *Inorg. Chem.*, 32 (1993) 32.
117. S.S. Tandon, L.K. Thompson and J.N. Bridson, *Inorg. Chem.*, in press.
118. A. W. Addison, T.N. Rao, J. Reedijk, J.V. Rijn and G.C. Verschoor, *J. Chem. Soc., Dalton Trans.*, (1984) 1349.
119. J. Zubieta, K.D. Karlin and J.C. Hayes in "*Copper Coordination Chemistry: Biochemical & inorganic perspectives*"; K.D. Karlin and J. Zubieta, Eds, Adenine press: Guilderland, NY, 1983, p97.
120. K.D. Karlin, J.C. Hayes, S. Juen, J.P. Hutchinson and J. Zubieta,

- Inorg. Chem.*, 21 (1982) 4106.
121. L. Chen, L.K. Thompson and J.N. Bridson, *J. Can. Chem.*, 70 (1992) 1886.
 122. L. Chen, L.K. Thompson and J.N. Bridson, *J. Can. Chem.*, 70 (1992) 2709.
 123. W.J. Geary, *Coord. Chem. Rev.*, 7 (1971) 81.
 124. S.G. Murray and F.R. Hartley, *Chem. Rev.*, 81 (1981) 365.
 125. R. Bhula, P. Osvath and D.C. Weatherburn, *Coord. Chem. Rev.*, 91 (1988) 89.
 126. G.R. Newkome, J.D. Sauer, J.M. Roper and D.C. Hager, *Chem. Rev.*, 77 (1977) 513.
 127. A.J. Blake and M. Schröder, *Adv. Inorg. Chem.*, 35 (1990) 1.
 128. S.R. Cooper and S.C. Rawle, *Struct. and Bond.*, 72 (1990) 1.
 129. S.R. Cooper, *Acc. Chem. Rec.*, 21 (1988) 141.
 130. M. Schröder, *Pure Appl. Chem.*, 60 (1988) 517.
 131. E.T. Adman, R.E. Stenkamp, L.C. Sieker and L.H. Jesen, *J. Mol. Biol.*, 123 (1978) 35.
 132. H. Beinert, *Coord. Chem. Rev.*, 33 (1980) 55.
 133. P.M. Collman, H.C. Freeman, J.M. Guss, V.A. Murata, V.A. Norris,

- J.A.M. Ramshaw and M.P. Venkatappa, *Nature (London)*, 272 (1978) 319.
134. J.M. Guss and H.C. Freeman, *J. Mol. Biol.*, 169 (1983) 521.
135. K.D. Karlin and J. Zubieta, *Inorg. Perspect. Biol. Med.*, 2 (1979) 127.
136. L. Rydel and J.O. Lundgren, *Nature (London)*, 261 (1976) 344.
137. L.L. Diaddario, E.R. Dockal, M.D. Glick, L.A. Ochrymowycz and D.B. Rorabacher, *Inorg. Chem.*, 24 (1985) 356.
138. E.R. Dockal, T.E. Jones, W.F. Sokol, R.J. Engerer and D.B. Rorabacher, *J. Am. Chem. Soc.*, 98 (1976) 4322.
139. N.S. Ferris, W.H. Woodruff, D.B. Rorabacher, T.E. Jones and L.A. Ochrymowycz, *J. Am. Chem. Soc.*, 100 (1978) 5939.
140. T.E. Jones, D.B. Rorabacher and L.A. Ochrymowycz, *J. Am. Chem. Soc.*, 97 (1975) 7485.
141. D.B. Rorabacher, M.M. Bernado, A.M.Q. Vande Linde, G.H. Leggett, B.C. Westerby, M.J. Martin and L.A. Ochrymowycz, *Pure Appl. Chem.*, 60 (1988) 501.
142. D.B. Rorabacher, M.J. Martin, M.J. Koenigbauer, M. Malik, R.R. Schroeder, J.F. Endicott and L.A. Ochrymowycz in " *Copper Coordination Chemistry: Biochemical and Inorganic Perspectives*", K.D. Karlin and J. Zubieta Eds.; Adenine press, New York, 1983, p167.

143. M.D. Glick, D.P. Gravel, L.L. Diaddario and D.B. Rorabacher, *Inorg. Chem.*, *15* (1976) 1190.
144. E.R. Dockal, L.L. Diaddario, M.D. Glick and D.B. Rorabacher, *J. Am. Chem. Soc.*, *99* (1977) 4530.
145. P.W.R. Corfield, C. Ceccarelli, M.D. Glick, I. W-Y. Moy, L.A. Ochrymowycz and D.B. Rorabacher, *J. Am. Chem. Soc.*, *107* (1985) 2399.
146. V.B. Pett, L.L. Diaddario, P.W. Corfield, C. Ceccarelli, M.D. Glick, L.A. Ochrymowycz and D.B. Rorabacher, *Inorg. Chem.* *22* (1983) 3661.
147. J.R. Hartman and S.R. Cooper, *J. Am. Chem. Soc.*, *108* (1986) 1202.
148. S.C. Rawle, G.A. Admans and S.R. Cooper, *J. Chem. Soc., Dalton Trans.*, (1988) 93.
149. E. Bouwman, W.L. Driessen and J. Reedijk, *Coord. Chem. Rev.*, *104* (1990) 143.
150. D.E. Nikles, M.J. Powers and F.L. Urbach, *Inorg. Chim. Acta*, *37* (1979) L499.
151. H. Wu and C.R. Lucas, *Inorg. Chem.*, *31* (1992) 2354.
152. S. Liu, C.R. Lucas, R.C. Hynes and J-P. Charland, *Can. J. Chem.*, *70* (1992) 1773.
153. M. Zoeteman, E. Bouwman, R.A.G. de Graaff, W.L. Driessen, J. Reedijk

- and P. Zanello, *Inorg. Chem.*, 29 (1990) 3487.
154. D.E. Nikles, M.J. Powers and F.L. Urbach, *Inorg. Chem.*, 22 (1983) 3210.
155. W.G. Haanstra, W.A.J.W. Van der Donk, W.L. Driessen, J. Reedijk, J.S. Wood and M.G.B. Drew, *J. Chem. Soc., Dalton Trans.*, (1990) 3123.
156. G.E. Norris, B.F. Anderson and E.N. Baker, *J. Am. Chem. Soc.*, 108 (1986) 2784.
157. F. Vögtle and H. Risler, *Angew Chem. Int. Ed. Engl.*, 11 (1972) 727.
158. F. Vögtle, *Tetrahedron*, 25 (1969) 3231.
159. F. Vögtle and A.H. Effler, *Chem. Ber.*, 102 (1969) 3071.
160. F. Vögtle, *Tetrahedron Lett.*, 3623 (1968).
161. D. Hefelfinger and D.J. Cram, *J. Am. Chem. Soc.*, 93 (1971) 4767.
162. E. Weber, W. Wieder and F. Vögtle, *Chem. Ber.*, 109 (1976) 1002.
163. D. Parker, J-M, Lehn and J. Rimmer, *J. Chem. Soc., Dalton Trans.*, (1985) 1517.
164. K.Y. Novitski, G.T. Khachaturova, Y.K. Yurév and K. Geterotsikl, *Soedin.*, (1969) 406.
165. C.R. Lucas, S. Liu, M.J. Newlands, J-P. Charland and E.J. Gabe, *Can. J. Chem.*, 67 (1989) 639.

166. C.R. Lucas, S. Liu, M.J. Newlands and E.J. Gabe, *Can. J. Chem.*, **68** (1990) 1357.
167. C.R. Lucas, S. Liu, M.J. Newlands, J-P. Charland and E.J. Gabe, *Can. J. Chem.*, **66** (1988) 1506.
168. C.R. Lucas, S. Liu, M.J. Newlands, J-P. Charland and E.J. Gabe, *Can. J. Chem.*, **68** (1990) 644.
169. C.R. Lucas, S. Liu and L.K. Thompson, *Inorg. Chem.*, **29** (1990) 85.
170. S. Liu, C.R. Lucas, M.J. Newlands and J.P. Charland, *Inorg. Chem.*, **29** (1990) 4380.
171. B. de Groot and S.J. Loeb, *Inorg. Chem.*, **28** (1989) 3573.
172. B. de Groot, G.S. Hanan and S.J. Loeb, *Inorg. Chem.*, **30** (1991) 4644.
173. B. de Groot and S.J. Loeb, *Inorg. Chem.*, **29** (1990) 4084.
174. B. de Groot and S.J. Loeb, *J. Chem. Soc., Chem. Commun.*, (1990) 1755.
175. G.R. Giesbrecht, G.S. Hanan, J.E. Kickham and S.J. Loeb, *Inorg. Chem.*, **31** (1992) 3286.
176. W. Mansfeld, *Ber.*, **19** (1886) 696.
177. D. Gerber, P. Chongsawangvirod, A.K. Leung and L.A. Ochrymowycz, *J. Org. Chem.*, **42** (1977) 2644.
178. W.H. Carothers, *J. Am. Chem. Soc.*, **51** (1929) 2458, 2560.

179. W.H. Carothers, *J. Am. Chem. Soc.*, 52 (1930) 711, 3144, 3292.
180. W.H. Carothers, *J. Am. Chem. Soc.*, 55 (1933) 5031, 5203.
181. L.A. Ochrymowycz, C-P. Mark and J.D. Michna, *J. Org. Chem.*, 39 (1974) 2079.
182. J. Buter and R.M. Kellogg, *J. Chem. Soc., Chem. Commun.*, (1980) 466.
183. J. Buter and R.M. Kellogg, *J. Org. Chem.*, 46 (1981) 4481.
184. J. Buter and R.M. Kellogg, *Org. Synth.*, 65 (1987) 150.
185. G. Dijkstra, W.H. Kruizinga and R.M. Kellogg, *J. Org. Chem.*, 52 (1987) 4230.
186. D.H. Busch, *Record. Chem. Progr.*, 25 (1964) 107.
187. D.S.C. Black, *Rev. Pure & Appl. Chem.*, 25 (1965) 109.
188. D. Sellmann and L.S. Zapf, *Angew Chem. Int. Ed. Engl.*, 23 (1984) 807.
189. D. Sellmann and L.S. Zapf, *J. Organomet. Chem.*, 289 (1985) 57.
190. S.J. Loeb and G.K.H. Shimizu, 75th Canadian Chemical Conference, June 1991, Hamilton, Canada.
191. R.E. Wolf, J.R. Hartman, J.M.E. Storey, B.M. Foxman and S.R. Cooper, *J. Am. Chem. Soc.*, 109 (1987) 4328.
192. A.J. Blake, R.O. Gould and M. Schröder, *J. Organomet. Chem.*, 356 (1988) 389.

193. T. Yoshida, T. Adachi, T. Ueda, M. Watanabe, M. Kaminaka and T. Higuchi, *Angew Chem. Int. Ed. Engl.*, 26 (1987) 1171.
194. T. Adachi, N. Sasaki, T. Ueda, M. Kaminaka and T.J. Yoshida, *J. Chem. Soc., Chem. Commun.*, (1989) 1320.
195. A.J. Blake, G. Reid and M. Schröder, *J. Chem. Soc., Dalton Trans.*, (1989) 1675.
196. P.J. Blower, J.A. Clarkson, S.C. Rawle, J.R. Hartman, R.E. Jr. Wolf, R. Yagbasan, S.G. Bott and S.R. Cooper, *Inorg. Chem.*, 28 (1989) 4040.
197. J.A. Clarkson, R. Yagbasan, P.J. Blower and S.R. Cooper, *J. Chem. Soc., Chem. Commun.*, (1989) 1244.
198. M.T. Ashby and D.L. Lichtenberger, *Inorg. Chem.*, 24 (1985) 636.
199. W. Rosen and D.H. Busch, *J. Am. Chem. Soc.*, 91 (1969) 4694.
200. W.N. Setzer, C.A. Ogle, G.C. Wilson and R.S. Glass, *Inorg. Chem.*, 22 (1983) 266.
201. F.J. Rietmeijer, P.J.M.W.L. Birker, S. Gorter and J. Reedijk, *J. Chem. Soc., Dalton Trans.*, (1982) 1191.
202. C.E. Addison, N. Logan, S.C. Wallwork and C.D. Garner, *Q. Rev. Chem. Soc.*, 25 (1971) 289.

203. L. Chen, L.K. Thompson and J.N. Bridson, *Can. J. Chem.*, *71* (1993) 1086.
204. G. Bata and P. Mathur, *Inorg. Chem.*, *31* (1992) 1575.
205. B.E. Myers, L. Berger and S.A. Friedberg, *J. Appl. Phys.*, *40* (1969) 1149.
206. L. Chen, L.K. Thompson and J.N. Bridson, *Inorg. Chem.*, in press.
207. A. Hirsch and D. Orphanos, *Can. J. Chem.*, *43* (1965) 2708.
208. G.H. Robinson and S.A. Sangokoya, *J. Am. Chem. Soc.*, *110* (1988) 1494.
209. A. Domenicano, R. Spagna and A. Vaciago, *J. Chem. Soc., Chem. Commun.*, (1968) 1291.
210. L.E. Stoffels, W.G. Haanstra, W.L. Driessen and J. Reedijk, *Angew Chem. Int. Ed. Engl.*, *29* (1990) 1419.
211. F.B. Stocker, *Inorg. Chem.*, *30* (1991) 1472.
212. J.D. Ferrada, C. Tessier-Youngs and W.J. Youngs, *Inorg. Chem.*, *27* (1988) 2201.
213. H.L. Aalten, G.V. Koten, K. Goubitz and C.H. Stam, *J. Chem. Soc., Chem. Commun.*, (1985) 1252.
214. H.C. Kang, Y. Do, C.B. Knobler, M.F. Hawthorne, *J. Am. Chem. Soc.*, *109* (1987) 6530.

215. A. Muller, F.W. Baumann, H. Bogge, M. Romer, E. Krickemeyer and K. Schmitz, *Angew Chem. Int. Ed. Engl.*, 23 (1984) 632.
216. A.J. Blake, R.O. Gould, A.J. Holder, T.L. Hyde and M. Schröder, *Polyhedron*, 8 (1989) 513.
217. J.A. Clarkson, R. Yagbason, P.T. Blower, S.C. Rawle and S.J. Cooper, *J. Chem. Soc., Chem. Commun.*, (1987) 950.
218. H.J. Küppers, K. Wiegardt, Y.H. Tsay, C. Kruger, P. Nuber and J. Weiss, *Angew. Chem. Int. Ed. Engl.*, 26 (1987) 575.
219. A.J. Blake, R.O. Gould, R. Reid and M.J. Schröder, *J. Chem. Soc., Chem. Commun.*, (1990) 974.
220. B. De Groot and S.J. Loeb, *Inorg. Chem.*, 30 (1991) 3103.
221. Y. Kojima, T. Yamashita, Y. Ishino, T. Hirashima and K. Hirotsu, *Chem. Lett.*, (1983)453.
222. I.G. Danee, L.J. Fitzpatrick, A.D. Rae and M.L. Scudder, *Inorg. Chem.*, 22 (1983) 3785.
223. A. Guitard, A. Mari, A.L. Beauchamp, Y. Dartiguenave and M. Dartiguenave, *Inorg. Chem.*, 22 (1983) 1603.
224. N-O. Björk and A. Cassel, *Acta Chem. Scand.*, A30 (1976) 235.

Appendix. Crystal Data

Table 1. Crystal data for $[\text{Cu}_2(\text{PTPH})\text{Cl}_4] \cdot 2\text{CH}_3\text{OH}$ (1)

Parameter	Value
Empirical formula	$\text{Cu}_2\text{S}_2\text{N}_4\text{O}_2\text{C}_{20}\text{H}_{20}\text{Cl}_4$
Formula weight	681.42
Crystal color	green
Crystal dimensions (mm)	0.4x0.2x0.15
Crystal system	Monoclinic
Space group	C2/c (#15)
a (Å)	20.710(4)*
b (Å)	11.694(3)
c (Å)	15.509(4)
β (°)	133.85(1)
V (Å ³)	2709(2)
d_{calc} (gcm ⁻³)	1.671
Z	4
Abs. coeff., μ (cm ⁻¹)	21.47
Radiation, λ (Å)	MoK α , 0.71069
T(°C)	25
F_{000}	1368
Scan rate(degmin ⁻¹)	8.0
$2\theta_{\text{max}}$ (deg)	50.0
Data collected	2588
No. of unique data ($I > 3.00\sigma(I)$)	1393
No. of variables	154
Goodness of fit ^b	1.71
R^c	0.040
R_w^d	0.033

*Throughout this work, esd's are in parentheses and refer to the last digit printed.

^bGoodness of fit = $[\sum w(|F_o| - |F_c|)^2 / (\text{number of reflections} - \text{number of parameters})]^{1/2}$.

^c $R = \sum(|F_o| - |F_c|) / \sum|F_o|$.

^d $R_w = [(\sum w(|F_o| - |F_c|)^2) / \sum w(|F_o|)^2]^{1/2}$.

Table 2. Crystal data for [Cu₇(DPTD)Br₄] (4)

Parameter	Value
Empirical formula	Cu ₇ S ₃ N ₄ C ₁₀ H ₈ Br ₄
Formula weight	751.11
Crystal color	Dark green
Crystal dimensions (mm)	0.3x0.3x0.2
Crystal system	Monoclinic
Space group	C2/c (#15)
a (Å)	11.750(2) ^a
b (Å)	14.235(3)
c (Å)	12.243(3)
β(°)	107.53(2)
V (Å ³)	1952.6(7)
d _{calc} (gcm ⁻³)	2.555
Z	4
Abs. coeff., μ(cm ⁻¹)	106.09
Radiation, λ(Å)	MoKα, 0.71069
T(°C)	26
F ₀₀₀	1416
Scan rate(degmin ⁻¹)	8.0
2θ _{max} (deg)	50.0
Data collected	1876
No. of unique data (I > 2.00σ(I))	1319
No. of variables	115
Goodness of fit ^b	1.73
R ^c	0.031
R _w ^d	0.027

^aThroughout this work, esd's are in parentheses and refer to the last digit printed.

^bGoodness of fit = $[\sum w(|F_o| - |F_c|)^2 / (\text{number of reflections} - \text{number of parameters})]^{1/2}$.

^cR = $\Sigma(|F_o| - |F_c|) / \Sigma|F_o|$.

^dR_w = $[(\Sigma w(|F_o| - |F_c|)^2) / \Sigma w(|F_o|)^2]^{1/2}$.

Table 3. Crystal data for $[\text{Cu}_2(\text{PTPH})(\text{OH})(\text{NO}_3)_3(\text{H}_2\text{O})_2] \cdot 5$

Parameter	Value
Empirical formula	$\text{Cu}_2\text{S}_8\text{N}_{14}\text{O}_{22}\text{C}_{36}\text{H}_{30}$
Formula weight	1393.14
Crystal color	Light blue
Crystal dimensions (mm)	0.38x0.2x0.18
Crystal system	Triclinic
Space group	$\bar{1}$ (#2)
a (Å)	12.075(2)*
b(Å)	12.344(1)
c (Å)	8.728(2)
α (°)	97.78(1)
β (°)	96.70(1)
γ (°)	110.390(9)
V (Å ³)	1189.4(3)
d_{calc} (gcm ⁻³)	1.945
Z	1
Abs. coeff., μ (cm ⁻¹)	20.35
Radiation, λ (Å)	MoK α , 0.71069
T(°C)	25
F ₀₀₀	700
Scan rate(degmin ⁻¹)	16.0
2 θ_{max} (deg)	50.0
Data collected	4415
No. of unique data ($I > 3.00\sigma(I)$)	2768
No. of variables	362
Goodness of fit ^b	1.54
R ^c	0.035
R _w ^d	0.030

*Throughout this work, esd's are in parentheses and refer to the last digit printed.

^bGoodness of fit = $[\sum w(|F_o| - |F_c|)^2 / (\text{number of reflections} - \text{number of parameters})]^{1/2}$.

^cR = $\Sigma(|F_o| - |F_c|) / \Sigma|F_o|$.

^dR_w = $[\Sigma w(|F_o| - |F_c|)^2 / \Sigma w(|F_o|)^2]^{1/2}$.

Table 4. Crystal data for $[\text{Cu}_2(\text{PTPH})(\text{OH})(\text{NO}_3)_2(\text{H}_2\text{O})_2](\text{NO}_3)$ (6)

Parameter	Value
Empirical formula	$\text{Cu}_2\text{S}_2\text{N}_7\text{O}_{12}\text{C}_{13}\text{H}_{17}$
Formula weight	714.58
Crystal color	Deep blue
Crystal dimensions (mm)	0.3x0.25x0.15
Crystal system	Triclinic
Space group	$\bar{p}1$ (#2)
a (Å)	10.687(3) ^a
b (Å)	13.472(3)
c (Å)	9.638(2)
α (°)	103.03(2)
β (°)	90.75(2)
γ (°)	110.44(2)
V (Å ³)	1260.5(5)
$d_{\text{calc}}(\text{gcm}^{-3})$	1.883
Z	2
Abs. coeff., $\mu(\text{cm}^{-1})$	19.25
Radiation, $\lambda(\text{Å})$	MoK α , 0.71069
T(°C)	25
F_{000}	720
Scan rate(degmin ⁻¹)	16.0
$2\theta_{\text{max}}$ (deg)	50.0
Data collected	4697
No. of unique data ($1 > 3.00\sigma(I)$)	2238
No. of variables	369
Goodness of fit ^b	1.52
R^c	0.046
R_w^d	0.038

^aThroughout this work, esd's are in parentheses and refer to the last digit printed.

^bGoodness of fit = $[\sum w(|F_o| - |F_c|)^2 / (\text{number of reflections} - \text{number of parameters})]^{1/2}$.

^c $R = \sum(|F_o| - |F_c|) / \sum|F_o|$.

^d $R_w = [(\sum w(|F_o| - |F_c|)^2) / \sum w(|F_o|)^2]^{1/2}$.

Table 5. Crystal data for $[\text{Cu}_2(\text{PTPH})(\text{OH})\text{Cl}_3] \cdot 1.5\text{SCHCl}_3$ (9)

Parameter	Value
Empirical formula	$\text{Cu}_2\text{S}_2\text{N}_4\text{OC}_{19.5}\text{H}_{14.5}\text{Cl}_{7.5}$
Formula weight	777.96
Crystal color	Dark green
Crystal dimensions (mm)	0.3x0.3x0.3
Crystal system	Monoclinic
Space group	$P2_1/n$
a (Å)	11.065(2)*
b (Å)	12.907(6)
c (Å)	20.053(2)
β (°)	90.59(1)
V (Å ³)	2864(1)
$d_{\text{calc}}(\text{gcm}^{-3})$	1.804
Z	4
Abs. coeff., $\mu(\text{cm}^{-1})$	23.60
Radiation, $\lambda(\text{Å})$	MoK α , 0.71069
T(°C)	-80
F ₀₀₀	1540
Scan rate(degmin ⁻¹)	8.0
$2\theta_{\text{max}}$ (deg)	50.0
Data collected	5583
No. of unique data ($I > 3.00\sigma(I)$)	3869
No. of variables	344
Goodness of fit ^b	2.96
R ^c	0.052
R _w	0.054

*Throughout this work, esd's are in parentheses and refer to the last digit printed.

^bGoodness of fit = $[\sum w(|F_o| - |F_c|)^2 / (\text{number of reflections} - \text{number of parameters})]^{1/2}$.

^c $R = \Sigma(|F_o| - |F_c|) / \Sigma|F_o|$.

^d $R_w = [(\Sigma w(|F_o| - |F_c|)^2) / \Sigma w(|F_o|)^2]^{1/2}$.

Table 6. Crystal data for $[\text{Cu}_2(\text{PTP})(\text{OH})\text{Cl}_3] \cdot 2\text{CH}_3\text{CN}$ (11)

Parameter	Value
Empirical formula	$\text{Cu}_2\text{S}_2\text{N}_6\text{OC}_{11}\text{H}_{17}\text{Cl}_3$
Formula weight	630.94
Crystal color	Dark-green
Crystal dimensions (mm)	0.4x0.2x0.15
Crystal system	Monoclinic
Space group	$\text{P}2_1/\text{n}$ (#14)
a (Å)	12.104(1) ^a
b (Å)	11.014(4)
c (Å)	18.697(2)
β (°)	106.372(9)
V (Å ³)	2391.6(9)
d_{calc} (gcm ⁻³)	1.752
Z	4
Abs. coeff., μ (cm ⁻¹)	23.14
Radiation, λ (Å)	$\text{MoK}\alpha$, 0.71069
T(°C)	-100
F_{000}	1264
Scan rate(degmin ⁻¹)	8.0
$2\theta_{\text{max}}$ (deg)	50.0
Data collected	4675
No. of unique data ($I > 2.00\sigma(I)$)	3240
No. of variables	290
Goodness of fit ^b	1.64
R^c	0.033
R_w^d	0.033

^aThroughout this work, esd's are in parentheses and refer to the last digit printed.

^bGoodness of fit = $[\Sigma w(|F_o| - |F_c|)^2 / (\text{number of reflections} - \text{number of parameters})]^{1/2}$.

^c $R = \Sigma(|F_o| - |F_c|) / \Sigma|F_o|$.

^d $R_w = [(\Sigma w(|F_o| - |F_c|)^2 / \Sigma w(|F_o|)^2)]^{1/2}$.

Table 7. Crystal data for $[\text{Cu}_2(\text{PTPH})_2](\text{ClO}_4)_2 \cdot 2\text{CH}_3\text{CN}$ (12)

Parameter	Value
Empirical formula	$\text{Cu}_2\text{N}_6\text{O}_4\text{C}_{20}\text{H}_{15}\text{Cl}$
Formula weight	552.49
Crystal color	Deep red
Crystal dimensions (mm)	0.35x0.3x0.25
Crystal system	Triclinic
Space group	$\bar{p}1$ (#2)
a (Å)	11.220(4) ^a
b (Å)	11.397(3)
c (Å)	10.561(3)
α (°)	92.92(2)
β (°)	115.32(2)
γ (°)	108.22(2)
V (Å ³)	1132.4(7)
d_{calc} (gcm ⁻³)	1.620
Z	2
Abs. coeff., μ (cm ⁻¹)	12.98
Radiation, λ (Å)	MoK α , 0.71069
T(°C)	25
F_{000}	560
Scan rate(degmin ⁻¹)	16.0
$2\theta_{\text{max}}$ (deg)	52.1
Data collected	4703
No. of unique data ($I > 3.00\sigma(I)$)	2707
No. of variables	299
Goodness of fit ^b	2.24
R^c	0.046
R_w^d	0.043

^aThroughout this work, esd's are in parentheses and refer to the last digit printed.

^bGoodness of fit = $[\sum w(|F_o| - |F_c|)^2 / (\text{number of reflections} - \text{number of parameters})]^{1/2}$.

^c $R = \sum(|F_o| - |F_c|) / \sum|F_o|$.

^d $R_w = [(\sum w(|F_o| - |F_c|)^2) / \sum w(|F_o|)^2]^{1/2}$.

Table 8. Crystal data for $\{[\text{Cu}(\text{PTPO})_2\text{H}_2\text{O}][\text{Cu}(\text{PTPO})\text{Cl}_2][\text{CuCl}_4]\} \cdot 2.8\text{H}_2\text{O}$ (13)

Parameter	Value
Empirical formula	$\text{Cu}_3\text{S}_2\text{N}_9\text{O}_{6.8}\text{C}_{42}\text{H}_{37}\text{Cl}_6$
Formula weight	1276.15
Crystal color	Dark-green
Crystal dimensions (mm)	0.4x0.2x0.18
Crystal system	Monoclinic
Space group	$\text{P}2_1/\text{a}$ (#14)
a (Å)	13.95(2) ^a
b (Å)	25.248(7)
c (Å)	15.386(6)
β (°)	110.71(5)
V (Å ³)	5069(6)
d_{calc} (g cm ⁻³)	1.672
Z	4
Abs. coeff., μ (cm ⁻¹)	17.45
Radiation, λ (Å)	$\text{MoK}\alpha$, 0.71069
T (°C)	25
F_{000}	2573
Scan rate (deg min ⁻¹)	4.0
$2\theta_{\text{max}}$ (deg)	50.1
Data collected	9595
No. of unique data ($I > 2.50\sigma(I)$)	2784
No. of variables	460
Goodness of fit ^b	3.33
R^c	0.109
R_w^d	0.092

^aThroughout this work, esd's are in parentheses and refer to the last digit printed.

^bGoodness of fit = $[\Sigma w(|F_o| - |F_c|)^2 / (\text{number of reflections} - \text{number of parameters})]^{1/2}$.

^c $R = \Sigma(|F_o| - |F_c|) / \Sigma|F_o|$.

^d $R_w = \{[\Sigma w(|F_o| - |F_c|)^2 / \Sigma w(|F_o|)^2]\}^{1/2}$.

Table 9. Crystal data for $[\text{Cu}_2(\text{PTAPY})\text{Br}_2] \cdot 2\text{DMF}$ (15)

Parameter	Value
Empirical formula	$\text{Cu}_2\text{S}_7\text{N}_{10}\text{O}_2\text{C}_{18}\text{H}_{18}\text{Br}_2$
Formula weight	1187.69
Crystal color	Blue
Crystal dimensions (mm)	0.4x0.3x0.15
Crystal system	Triclinic
Space group	$\bar{P}1$ (#2)
a (Å)	14.037(3) ^a
b (Å)	14.941(4)
c (Å)	11.782(6)
α (°)	103.77(3)
β (°)	106.08(3)
γ (°)	84.59(2)
V (Å ³)	2305(2)
d_{calc} (gcm ⁻³)	1.711
Z	2
Abs. coeff., μ (cm ⁻¹)	44.90
Radiation, λ (Å)	MoK α , 0.71069
T(°C)	-125
F ₀₀₀	1184
Scan rate(degmin ⁻¹)	8.0
2 θ_{max} (deg)	50.0
Data collected	8474
No. of unique data ($1 > 2.00\sigma(I)$)	5866
No. of variables	524
Goodness of fit ^b	1.62
R ^c	0.036
R _w ^d	0.032

^aThroughout this work, esd's are in parentheses and refer to the last digit printed.

^bGoodness of fit = $[\sum w(|F_o| - |F_c|)^2 / (\text{number of reflections} - \text{number of parameters})]^{1/2}$.

^cR = $\Sigma(|F_o| - |F_c|) / \Sigma|F_o|$.

^dR_w = $[\Sigma w(|F_o| - |F_c|)^2 / \Sigma w(|F_o|)^2]^{1/2}$.

Table 10. Crystal data for $[\text{Cu}_2(\text{PTAPY})(\text{NO}_3)_2(\text{N}_3)(\text{H}_2\text{O})]_2(\text{NO}_3)_2 \cdot 1.2\text{CH}_3\text{OH}$ (17)

Parameter	Value
Empirical formula	$\text{Cu}_2\text{S}_2\text{N}_{14}\text{O}_{10.6}\text{C}_{32.53}\text{H}_{38.4}$
Formula weight	987.16
Crystal color	Blue
Crystal dimensions (mm)	0.4x0.35x0.1
Crystal system	Triclinic
Space group	$\bar{P}1$ (#2)
a (Å)	14.876(5) ^a
b (Å)	16.172(4)
c (Å)	10.068(2)
α (°)	95.45(2)
β (°)	108.40(2)
γ (°)	64.74(2)
V (Å ³)	2076(1)
d_{calc} (gcm ⁻³)	1.579
Z	2
Abs. coeff., μ (cm ⁻¹)	11.93
Radiation, λ (Å)	MoK α , 0.71069
T(°C)	25
F_{000}	1013
Scan rate(degmin ⁻¹)	8.0
$2\theta_{\text{max}}$ (deg)	49.3
Data collected	5682
No. of unique data ($I > 2.00\sigma(I)$)	3315
No. of variables	559
Goodness of fit ^b	2.44
R ^c	0.058
R_w ^d	0.051

^aThroughout this work, esd's are in parentheses and refer to the last digit printed.

^bGoodness of fit = $[\sum w(|F_o| - |F_c|)^2 / (\text{number of reflections} - \text{number of parameters})]^{1/2}$.

^cR = $\sum(|F_o| - |F_c|) / \sum |F_o|$.

^d $R_w = [(\sum w(|F_o| - |F_c|)^2) / \sum w(|F_o|)^2]^{1/2}$.

Table 11. Crystal data for $[\text{Cu}_3(\text{L}1)\text{Cl}_4] \cdot 2\text{CHCl}_3$ (18)

Parameter	Value
Empirical formula	$\text{Cu}_3\text{S}_{12}\text{N}_{12}\text{C}_{44}\text{H}_{30}\text{Cl}_{12}$
Formula weight	1747.76
Crystal color	Bluish-green
Crystal dimensions (mm)	0.25x0.15x0.08
Crystal system	Triclinic
Space group	$\bar{p}1$ (#2)
a (Å)	13.661(2)*
b (Å)	14.174(3)
c (Å)	9.412(2)
α (°)	101.08(2)
β (°)	96.94(2)
γ (°)	75.76(2)
V (Å ³)	3456.4(6)
d_{calc} (gcm ⁻³)	1.679
Z	1
Abs. coeff., μ (cm ⁻¹)	17.77
Radiation, λ (Å)	MoK α , 0.71069
T(°C)	26
F ₀₀₀	881
Scan rate(degmin ⁻¹)	4.0
2 θ_{max} (deg)	45.0
Data collected	4754
No. of unique data ($I > 3.00\sigma(I)$)	2080
No. of variables	373
Goodness of fit ^b	1.59
R ^c	0.056
R _w ^d	0.048

*Throughout this work, esd's are in parentheses and refer to the last digit printed.

^bGoodness of fit = $[\sum w(|F_o| - |F_c|)^2 / (\text{number of reflections} - \text{number of parameters})]^{1/2}$.

^cR = $\Sigma(|F_o| - |F_c|) / \Sigma|F_o|$.

^dR_w = $[\Sigma w(|F_o| - |F_c|)^2 / \Sigma w(|F_o|)^2]^{1/2}$.

Table 12. Crystal data for [Cu(L2)Cl₂] (19)

Parameter	Value
Empirical formula	CuS ₄ N ₄ C ₁₄ H ₁₆ Cl ₂
Formula weight	503.00
Crystal color	Greenish-blue
Crystal dimensions (mm)	0.2x0.15x0.05
Crystal system	Orthorhombic
Space group	Pnma (#62)
a (Å)	8.571(1) ^a
b (Å)	16.104(3)
c (Å)	13.961(2)
V (Å ³)	1927(1)
d _{calc} (gcm ⁻³)	1.734
Z	4
Abs. coeff., μ(cm ⁻¹)	18.39
Radiation, λ(Å)	MoKα, 0.71069
T(°C)	25
F ₀₀₀	1020
Scan rate(degmin ⁻¹)	8.0
2θ _{max} (deg)	50.0
Data collected	1979
No. of unique data (I > 3.00σ(I))	1070
No. of variables	125
Goodness of fit ^b	1.39
R ^c	0.040
R _w ^d	0.036

^aThroughout this work, esd's are in parentheses and refer to the last digit printed.

^bGoodness of fit = $[\sum w(|F_o| - |F_c|)^2 / (\text{number of reflections} - \text{number of parameters})]^{1/2}$.

^cR = $\Sigma(|F_o| - |F_c|) / \Sigma|F_o|$.

^dR_w = $[(\sum w(|F_o| - |F_c|)^2 / \sum w(|F_o|)^2)]^{1/2}$.

Table 13. Crystal data for $[\text{Cu}(\text{L}2)_2](\text{ClO}_4)_2 \cdot \text{CHCl}_3 \cdot \text{CH}_3\text{CN}$ (**22**)

Parameter	Value
Empirical formula	$\text{Cu}_5\text{N}_6\text{O}_8\text{C}_{21}\text{H}_{36}\text{Cl}_5$
Formula weight	1159.97
Crystal color	Brown
Crystal dimensions (mm)	0.3x0.25x0.15
Crystal system	Triclinic
Space group	$\bar{1}$ (#2)
a (Å)	12.888(4) ^a
b (Å)	17.462(6)
c (Å)	10.906(1)
α (°)	96.07(2)
β (°)	104.18(2)
γ (°)	94.51(2)
V (Å ³)	2352(1)
d_{calc} (gcm ⁻³)	1.638
Z	2
Abs. coeff., μ (cm ⁻¹)	11.47
Radiation, λ (Å)	MoK α , 0.71069
T(°C)	25
F ₀₀₀	1182
Scan rate(degmin ⁻¹)	16.0
2 θ_{max} (deg)	50.0
Data collected	8673
No. of unique data ($I > 3.00\sigma(I)$)	2941
No. of variables	545
Goodness of fit ^b	1.55
R ^c	0.053
R _w ^d	0.044

^aThroughout this work, esd's are in parentheses and refer to the last digit printed.

^bGoodness of fit = $[\sum w(|F_o| - |F_c|)^2 / (\text{number of reflections} - \text{number of parameters})]^{1/2}$.

^c $R = \sum(|F_o| - |F_c|) / \sum|F_o|$.

^d $R_w = [(\sum w(|F_o| - |F_c|)^2) / \sum w(|F_o|)^2]^{1/2}$.

Table 14. Crystal data for $[\text{Cu}_2(\text{L3})\text{Cl}_4]_x$ (23)

Parameter	Value
Empirical formula	$\text{Cu}_2\text{S}_2\text{N}_4\text{C}_{16}\text{H}_{20}\text{Cl}_4$
Formula weight	729.62
Crystal color	Brown
Crystal dimensions (mm)	0.3x0.2x0.15
Crystal system	Triclinic
Space group	$\bar{p}1$ (#2)
a (Å)	8.6204(8) ^a
b (Å)	9.850(1)
c (Å)	8.348(1)
α (°)	111.46(1)
β (°)	102.50(1)
γ (°)	71.818(9)
V (Å ³)	622.6(1)
d_{calc} (gcm ⁻³)	1.946
Z	1
Abs. coeff., μ (cm ⁻¹)	109.49
Radiation, λ (Å)	CuK α , 1.54178
T(°C)	25
F_{000}	366
Scan rate(degmin ⁻¹)	8.0
$2\theta_{\text{max}}$ (deg)	120.1
Data collected	1989
No. of unique data ($I > 3.0\sigma(I)$)	1312
No. of variables	179
Goodness of fit ^b	1.93
R^c	0.043
R_w^d	0.042

^aThroughout this work, esd's are in parentheses and refer to the last digit printed.

^bGoodness of fit = $[\sum w(|F_o| - |F_c|)^2 / (\text{number of reflections} - \text{number of parameters})]^{1/2}$.

^c $R = \sum(|F_o| - |F_c|) / \sum|F_o|$.

^d $R_w = [(\sum w(|F_o| - |F_c|)^2) / \sum w(|F_o|)^2]^{1/2}$.

Table 15. Crystal data for [Cu(L3)Cl₂] (24)

Parameter	Value
Empirical formula	CuS ₄ N ₄ C ₁₈ H ₂₀ Cl ₂
Formula weight	595.17
Crystal color	Pale green
Crystal dimensions (mm)	0.3x0.3x0.07
Crystal system	Triclinic
Space group	$P\bar{1}$ (#2)
a (Å)	11.001(1)*
b (Å)	12.888(2)
c (Å)	8.704(1)
α (°)	102.89(1)
β (°)	103.36(1)
γ (°)	75.84(1)
V (Å ³)	1145.8(3)
d_{calc} (gcm ⁻³)	1.725
Z	2
Abs coeff, μ (cm ⁻¹)	17.29
Radiation, λ (Å)	MoK α , 0.71069
T(°C)	26
F ₀₀₀	606
Scan rate(degmin ⁻¹)	8.0
2 θ_{max} (deg)	50.0
Data collected	4273
No. of unique data (I > 3.00 σ (I))	2059
No. of variables	262
Goodness of fit ^b	1.96
R ^c	0.056
R _w ^d	0.044

*Throughout this work, esd's are in parentheses and refer to the last digit printed.

^bGoodness of fit = $[\sum w(|F_o| - |F_c|)^2 / (\text{number of reflections} - \text{number of parameters})]^{1/2}$.

^cR = $\Sigma(|F_o| - |F_c|) / \Sigma|F_o|$.

^dR_w = $[\Sigma w(|F_o| - |F_c|)^2 / \Sigma w(|F_o|)^2]^{1/2}$.

Table 16. Crystal data for [Cu(L3)(NO₃)₂] (25)

Parameter	Value
Empirical formula	CuS ₆ N ₆ O ₆ C ₁₆ H ₂₀
Formula weight	648.28
Crystal color	Deep green
Crystal dimensions (mm)	0.4x0.35x0.2
Crystal system	Orthorhombic
Space group	P2 ₁ 2 ₁ 2 ₁ (#19)
a (Å)	15.148(2) ^a
b (Å)	15.562(3)
c (Å)	11.064(1)
V (Å ³)	2608.2(7)
d _{calc} (gcm ⁻³)	1.651
Z	4
Abs. coeff., μ(cm ⁻¹)	13.43
Radiation, λ(Å)	MoKα, 0.71069
T(°C)	25
F ₀₀₀	1324
Scan rate(degmin ⁻¹)	32.0
2θ _{max} (deg)	50.0
Data collected	2622
No. of unique data (I > 3.00σ(I))	1864
No. of variables	317
Goodness of fit ^b	1.48
R ^c	0.039
R _w ^d	0.034

^aThroughout this work, esd's are in parentheses and refer to the last digit printed.

^bGoodness of fit = [Σw(|Fo| - |Fc|)² / (number of reflections - number of parameters)]^{1/2}.

^cR = Σ(|Fo| - |Fc|) / Σ|Fo|.

^dR_w = [(Σw(|Fo| - |Fc|)² / Σw(|Fo|)²]^{1/2}.

Table 17. Crystal data for L6

Parameter	Value
Empirical formula	C ₁₅ H ₁₈ S ₄ N ₂
Formula weight	354.56
Crystal color	Colourless
Crystal dimensions (mm)	0.3x0.3x0.2
Crystal system	Monoclinic
Space group	P2 ₁ /n (#14)
a (Å)	8.827(2)*
b (Å)	11.461(2)
c (Å)	16.197(2)
β (°)	98.27(2)
V (Å ³)	1621.6(5)
d _{calc} (gcm ⁻³)	1.452
Z	4
Abs. coeff., μ(cm ⁻¹)	5.57
Radiation, λ(Å)	MoKα, 0.71069
T(°C)	25
F ₀₀₀	744
Scan rate(degmin ⁻¹)	8.0
2θ _{max} (deg)	50
Data collected	3231
No. of unique data (I > 2.00σ(I))	2021
No. of variables	245
Goodness of fit ^b	1.56
R ^c	0.033
R _w ^d	0.028

*Throughout this work, esd's are in parentheses and refer to the last digit printed.

^bGoodness of fit = $[\sum w(|F_o| - |F_c|)^2 / (\text{number of reflections} - \text{number of parameters})]^{1/2}$.

^cR = $\Sigma(|F_o| - |F_c|) / \Sigma|F_o|$.

^dR_w = $[(\Sigma w(|F_o| - |F_c|)^2) / \Sigma w(|F_o|)^2]^{1/2}$.

Table 18. Crystal data for [Cu(L5)Cl]₂ (29)

Parameter	Value
Empirical formula	Cu ₂ N ₂ C ₁₁ H ₁₆ Cl
Formula weight	403.50
Crystal color	Colourless
Crystal dimensions (mm)	0.35x0.35x0.1
Crystal system	Triclinic
Space group	$\bar{1}$ (#2)
a (Å)	9.410(2) ^a
b (Å)	10.291(2)
c (Å)	9.208(2)
α (°)	108.56(1)
β (°)	91.82(2)
γ (°)	68.04(1)
V (Å ³)	780.1(2)
d_{calc} (gcm ⁻³)	1.718
Z	2
Abs. coeff., μ (cm ⁻¹)	20.78
Radiation, λ (Å)	MoK α , 0.71069
T(°C)	25
F ₀₀₀	412
Scan rate(degmin ⁻¹)	16.0
2 θ_{max} (deg)	50.0
Data collected	2932
No. of unique data ($I > 3.00\sigma(I)$)	1856
No. of variables	173
Goodness of fit ^b	1.63
R ^c	0.035
R _w ^d	0.031

^aThroughout this work, esd's are in parentheses and refer to the last digit printed.

^bGoodness of fit = $[\Sigma w(|F_o| - |F_c|)^2 / (\text{number of reflections} - \text{number of parameters})]^{1/2}$.

^cR = $\Sigma(|F_o| - |F_c|) / \Sigma|F_o|$.

^dR_w = $[\Sigma w(|F_o| - |F_c|)^2 / \Sigma w(|F_o|)^2]^{1/2}$.

Table 19. Crystal data for [Cu(L5)Br]₂ (30)

Parameter	Value
Empirical formula	Cu ₂ S ₈ N ₄ C ₂₇ H ₃₂ Br ₂
Formula weight	895.90
Crystal color	Colourless
Crystal dimensions (mm)	0.25x0.25x0.2
Crystal system	Monoclinic
Space group	P2 ₁ /c (#14)
a (Å)	9.140(3) ^a
b (Å)	13.939(7)
c (Å)	13.115(5)
β (°)	106.77(4)
V (Å ³)	1600(1)
d _{calc} (gcm ⁻³)	1.860
Z	2
Abs. coeff., μ(cm ⁻¹)	43.32
Radiation, λ(Å)	MoKα, 0.71069
T(°C)	25
F ₀₀₀	896
Scan rate(degmin ⁻¹)	8.0
2θ _{max} (deg)	50.0
Data collected	3138
No. of unique data (I > 3.00σ(I))	2015
No. of variables	173
Goodness of fit ^b	1.49
R ^c	0.032
R _w ^d	0.029

^aThroughout this work, esd's are in parentheses and refer to the last digit printed.

^bGoodness of fit = $[\sum w(|F_o| - |F_c|)^2 / (\text{number of reflections} - \text{number of parameters})]^{1/2}$.

^cR = $\Sigma(|F_o| - |F_c|) / \Sigma|F_o|$.

^dR_w = $[\Sigma w(|F_o| - |F_c|)^2 / \Sigma w(|F_o|)^2]^{1/2}$.

Table 20. Crystal data for $[\text{Cu}_{1.5}(\text{L6})\text{Cl}_{1.5}]_x$ (31)

Parameter	Value
Empirical formula	$\text{Cu}_3\text{S}_2\text{N}_4\text{C}_{30}\text{H}_{36}\text{Cl}_3$
Formula weight	1006.12
Crystal color	Yellow
Crystal dimensions (mm)	0.4x0.2x0.2
Crystal system	Triclinic
Space group	$\bar{p}1$ (#2)
a (Å)	12.150(4) ^a
b (Å)	18.760(3)
c (Å)	8.700(3)
α (°)	91.27(2)
β (°)	107.69(2)
γ (°)	87.87(2)
V (Å ³)	1887.9(9)
d_{calc} (gcm ⁻³)	1.770
Z	2
Abs. coeff., μ (cm ⁻¹)	23.51
Radiation, λ (Å)	MoK α , 0.71069
T(°C)	25
F_{000}	1020
Scan rate(degmin ⁻¹)	16.0
$2\theta_{\text{max}}$ (deg)	50.0
Data collected	6983
No. of unique data ($I > 3.00\sigma(I)$)	4614
No. of variables	434
Goodness of fit ^b	1.83
R ^c	0.035
R_w ^d	0.034

^aThroughout this work, esd's are in parentheses and refer to the last digit printed.

^bGoodness of fit = $[\sum w(|F_o| - |F_c|)^2 / (\text{number of reflections} - \text{number of parameters})]^{1/2}$.

^cR = $\Sigma(|F_o| - |F_c|) / \Sigma|F_o|$.

^d $R_w = [(\Sigma w(|F_o| - |F_c|)^2 / \Sigma w(|F_o|)^2)]^{1/2}$.

Table 21. Crystal data for [Ag(L5)(ClO₄)₂]_x (32)

Parameter	Value
Empirical formula	Ag ₅ N ₂ O ₄ C ₁₁ H ₁₆ Cl
Formula weight	511.82
Crystal color	Colourless
Crystal dimensions (mm)	0.4x0.2x0.15
Crystal system	Monoclinic
Space group	P2 ₁ /n (#14)
a (Å)	9.382(4) ^a
b (Å)	19.274(4)
c (Å)	10.190(3)
β (°)	106.35(3)
V (Å ³)	1768(1)
d _{calc} (gcm ⁻³)	1.922
Z	4
Abs. coeff., μ(cm ⁻¹)	17.52
Radiation, λ(Å)	MoKα, 0.71069
T(°C)	25
F ₀₀₀	1024
Scan rate(degmin ⁻¹)	8.0
2θ _{max} (deg)	50.0
Data collected	3419
No. of unique data (I > 3.00σ(I))	1776
No. of variables	208
Goodness of fit ^b	1.34
R ^c	0.036
R _w ^d	0.029

^aThroughout this work, esd's are in parentheses and refer to the last digit printed.

^bGoodness of fit = $[\sum w(|F_o| - |F_c|)^2 / (\text{number of reflections} - \text{number of parameters})]^{1/2}$.

^cR = $\Sigma(|F_o| - |F_c|) / \Sigma|F_o|$.

^dR_w = $[(\Sigma w(|F_o| - |F_c|)^2) / \Sigma w(|F_o|)^2]^{1/2}$.



